Alma Mater Studiorum – Università di Bologna

DOTTORATO DI RICERCA IN

TECNOLOGIE DELL'INFORMAZIONE

Ciclo XX

Settore scientifico disciplinare di afferenza: ING-INF/06

ANALYSIS OF ION CHANNEL STOCHASTIC SIGNALS FOR BIOSENSING

Presentata da: Francesco Lodesani

Coordinatore Dottorato   **Relatore**

Prof. Riccardo Rovatti   **Prof. Marco Tartagni**

Esame finale anno 2008

Contents

INTRODUCTION

In recent years, we have assisted to an ever-increasing capability of electronic systems to detect extremely small signals in noisy environments. Following this trend, the capacity to electronically detect single molecular binding events could bring to a new, high performance class of biosensors. This represent a very interesting perspective: chemical and biological assays constitute, for example, one of the major area of interest in the diagnostic field, where it has been pointed out how, for several diseases, precocious diagnosis can be obtained only being able to reveal the presence of small concentrations of specific molecules in complex fluid mixtures like the blood.

In biological world, life of cells is guaranteed by their ability to sense and to respond to a large variety of internal and external stimuli: this is allowed by the action of many different molecular sensors located in the cytoplasm or embedded across the cell membranes. In particular, excitable cells, like muscle or nerve cells, produce quick depolarizations in response to electrical, mechanical or chemical stimuli: this means that they can change their internal potential through a quick exchange of ions between cytoplasm and the external environment. Since the membrane structure of the cells is basically formed by a bimolecular layer of phospholipids (lipid bilayer), essentially impermeable to polar molecules, ions can flow across cell membrane thanks to the presence of ion channels, proteins that span the lipid bilayer and act like switches, allowing ionic current to flow opening and shutting in a stochastic way. For a particular class of ion channels, ligand-gated ion channels, the stochastic properties of the gating processes are strongly influenced by binding between receptive sites located on the channel surface and specific target molecules. These channels, inserted in biomimetic membranes and in presence of a proper electronic system for acquiring and elaborating the electrical signal, could give us the possibility of detecting and quantifying concentrations of specific molecules in

1

complex mixtures from ionic currents across the membrane. In my research work, I investigated this possibility, as I will describe in this thesis. In particular, after a first, introductory chapter about the characteristics of the cell membranes and the ion channels, I will show the experiments I carried out in the ARCES section of the Laboratory of Cellular and Molecular Engineering of the University of Bologna-Campus of Cesena, focused on the creation and the characterization of artificial lipid membranes, the reconstitution of ion channels and the analysis of their electrical and statistical properties. Moreover, after a chapter about the basis of the modelling of the kinetic behaviour of ligand gated ion channels, I will propose a possible approach for the estimation of the target molecule concentration, based on a statistical analysis of the ion channel open probability. In the fifth chapter, it will be discussed the characterisation of the homomeric α_2 isoform of the glycine receptor, a ligand gated ion channel belonging to the Central Nervous System cells. Both experimental acquisitions and signal analysis, conducted in the Colquhoun lab of the Pharmacology Department of the University College of London, will be described. The six chapter represents the conclusions of this thesis, with some remark on the effective performance that may be achieved using ligand gated ion channels, such the ones analysed in chapter five, as sensing elements.

1   ION CHANNELS AND THEIR ENVIRONMENT

1.1   Cell membrane

The life of the living systems depends on the coordinated activity of several interconnected structures on different levels. The fundamental structural unit of this hierarchy is the cell. It's basically formed by the cytoplasm, a fluid matrix containing the nucleus and where all the organelles are suspended. The border of the cell, instead, is called cell membrane.

Cell membrane is not only a wall separating the cytoplasm from the external environment, but is also an active structure of the cell, which carries out several functions essential for the life. First of all, it is the gate between the cell and the external world, so it must represent a selective filter for all the chemical exchanges between the inner and the outer compartments, and a communication surface, which allows the transmission of the information with the neighbouring cells and the external world. It means that it picks and sends a large variety of stimuli (electrical, mechanical, of temperature, of light…) and mediates the interaction with the extracellular structures, performing also catalytic activities.

1.1.1 Phospholipids

All the chemical processes concerning with the cell life take place usually in liquid solution and the larger part of the structures of the cytoplasm are formed by soluble molecules, as well as the environment surrounding the cell. It means that the membrane, in order to preserve the integrity of the cell, must be basically constituted by an hydrophobic layer (a wall that can't be easily crossed by water and soluble molecules) made by phospholipids. They are long

3

molecules having a hamphipathic character, namely both hydrophobic and hydrophilic portions: they contain long lipid chains, but have polar (and, sometimes, electrical charged) head groups, which are therefore water soluble. In the membrane, the polar groups of the phospholipids are aligned towards the external parts, facing the inner and outer compartments; the apolar (not soluble) chains, instead, constitute the core of the membrane. This conformation is called "double layer" or, concisely , "bilayer", due to the bimolecular thickness of the layer. This kind of conformation is essentially due to a self assembling of the phospholipids, that orient them in an ordered structure to minimize the free energy, where the hydrophilic parts turn towards the water-based environment allowing the hydrophobic tales to avoid the contact with it. Obviously, the double layer must fold in a close shape (i.e. spherical), because otherwise it should have borders in which the apolar core is in touch with the water, becoming instable. Similar kinds of phospholipidic structures surround also the nucleus of the cell and a large part of the cell organelles. The bilayer self-assembling is mainly caused by hydrophobic interactions. Basically, molecules that doesn't contain ions or an asymmetrical distribution of the charge, aren't soluble in water, since they haven't a "bipolar momentum", and are defined hydrophobic. Covalent bonds between carbon atoms and hydrogen atoms are the most diffuse polar bond in the biological world. The force determining that the hydrophobic molecules (or, as in the case of the phospholipids, the hydrophobic parts of complex molecules) join together instead of dissolving into water, is called hydrophobic force. Actually, it's not a real binding force but it's instead determined by the energy that the system should need in order to put an hydrophobic molecule into water: an apolar molecule can't form hydrogen bonds with the water, and thus distorts the structure of the water molecules, which dispose them forming a "rigid cage" (supported by hydrogen bonds) around it. The presence of this rigid cages limits the free movements of the water molecules, originating a most ordered condition which, decreasing the system entropy, is energetically unfavourable. To join together the hydrophobic

4

molecules, creating a phase distinguished from the water phase, is the way for minimizing the limitation in the water free movements. Apolar molecules can also join, although weekly , thanks to van der Waals interactions.

When a suspension of phospholipids is spread in a water solution, it can form manly two different structures: liposomes (also said vesicles) and micelles. The difference between these two structures, is that in the first case a double layer includes a water compartment (like the cytoplasm in the cell), while in the second one the hydrophobic chains fill the centre excluding water molecules. The type of structure that tend to form depends mainly on the length of the phospholipid hydrophobic chains, their saturation degree, the temperature, the ionic composition of the water solution.
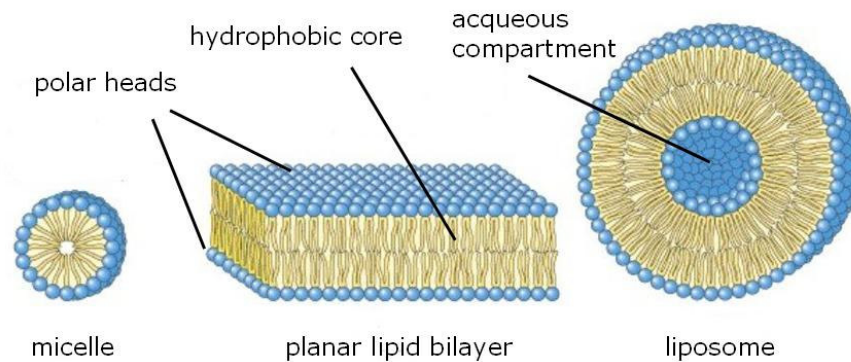
Figure 1.1   Different structures from phospholipids self-assembly

Hence, in liposomes, as well as in the cell, the lipid bilayer has an hydrophobic core about 3 nm thick, made by the aggregation of the carbon fatty acids composing the hydrophobic tales, stabilized by several van der Waals interactions and by the ionic and hydrogen bonds between the hydrophilic head

groups and the molecules of the water solution. In natural composed cell membranes, as well as in artificial bilayers made with a simpler mixture of phospholipids, each molecule can shift its position remaining in the layer, like in a two-dimensional fluid surface. It means that, for example, phospholipids can diffuse in their molecule sheet, keeping their polar heads facing the water solution and their hydrophobic tales inside the core of the bilayer. It can be effectively observed, using tagged phospholipids, that at a temperature of 37°C, each molecule diffuses with a velocity in the order of several micrometers per second, due to the thermal motion. Also the other molecules, like the great part of the proteins embedded in the cell membrane, can move laterally in the bilayer. This property of the lipid bilayers was described for the first time in 1972 by Singer and Nicolson; they proposed the model under the name of *fluid mosaic*.

1.1.2 Other membrane lipid components

In terms of lipid composition, phospholipids are the most abundant element in the cell membrane, but other classes of amphipathic lipids are present: glycolipids and steroids. The first are basically phospholipids in which the polar groups are associated with carbohydrate chains; they extend from the phospholipid bilayer into the aqueous environment outside the cell where act as recognition sites for specific chemicals as well as helping to maintain the stability of the membrane and attaching cells to one another to form tissues. Steroids carry out several function in the cells and in the membranes, in particular, their effect is to stabilize the structure and to modulate the fluidity of the fluid mosaic. In particular, in animal cell membranes the principal steroid is the cholesterol, while in fungal cells is the ergosterol.

6

1.2   Membrane proteins

Because of the oily core, the bilayer is ermeable to small hydrophobic solutes (such as chloroform or ethanol), but has a very low permeability to polar inorganic compounds and ionic molecules. For a cell, this means that even small molecules, such as sugars and salts, couldn't pass through the membrane, if it was composed only by lipids. Instead, lipids constitute only the scaffold of the cell membrane, where many other structures, especially protein-made, are embedded. Specific proteins embedded in the cell membrane can act as molecular signals that allow cells to communicate with each other. Protein receptors are found ubiquitously and receive signals from both the environment and other cells. These signals are transduced into a form that the cell can use to directly effect a response. Other proteins on the surface of the cell membrane serve as markers that identify a cell to other cells. The interaction of these markers with their respective receptors forms, for example, the basis of cell-cell interaction in the immune system. The capability of controlling the concentration of each ionic species is fundamental for the cell life, for several reasons. First of all, many physiological processes concerning with the maintenance and the homeostasis are strictly dependent on the concentrations of the various ions in the cytoplasm, and on the concentration differences between the extracellular and the intracellular medium. Moreover, animal cells must be protected from excessive osmotic forces by tight control of the osmolarity of the extracellular and intracellular media, which is first and foremost due to the ionic concentrations. Finally excitable cells, such as muscle or nerve cells, must produce quick depolarizations in response to electrical, mechanical or chemical stimuli: this means that they must change their internal potential through a quick flux of ions between cytoplasm and the external environment. For all these reasons, it's fundamental that the cell membranes enable ions to flow in an effective and selective way. Since the lipid bilayers are

basically impermeable to polar molecules, the flow of ions across the membrane is facilitated by specialised proteins, and in particular:

ion channels: proteins which span the lipid bilayer allowing ions to diffuse by forming an aqueous pore. Their characteristics will be pointed out in the section 1.3;

transporters: membrane proteins which aid movement of molecules across the membrane without forming pores. Between them, pumps transport molecules against their electrochemical gradient, exploiting energy provided by the breackdown of ATP to ADP on the cytosolic side of the membrane; co-transporters and exchangers transport, at the same time, ions against the gradient and other (of different species) following the gradient, so that they don't need external energy for their activity.

1.3 Ion channels

Ion channels are protein structures, present in the cell membrane but also in several organelles (for example, the endoplasmatic reticulum) which span the membrane bilayer, forming an aqueous path between its two sides. Their function is to pass, in a passive but selective manner, a large number of ions, in a short time. This capability is exploited by excitable cells to quickly change the transmembrane voltage, allowing for example the travelling action potential and the postsynaptic electrical response to chemical neurotransmission in nerve cells. Other cells and organelles exploit the capability of charge transport for ion homeostasis and osmolarity control. With the exception of the porins, ion channels must not to be intended as simple tunnels through the lipid bilayer: they act instead like switches, allowing ionic current to flow opening and shutting in a stochastic way. The conformational change between closed and

open state is called *gating*, and it is thought that it doesn't exist any stable or metastable conformation between these two conditions. It means that, even if the ion channel pores are basically formed by more subunits, all these parts change their conformation together and in a coordinated way (Monod et al., 1965). It's instead possible, for an ion channel, to have stable conformations leading to open conditions with different conductances. Channel gating is fundamentally a stochastic process whose behaviour is controlled by external factors. Ion channels can be classified according to which chemical or physical modulator controls their gating activity. Thus we have different groups of channels as summarized below:

- ligand gated channels (sensitive to chemical stimuli);

- voltage gated channels (sensitive to transmembrane potential);

- mechanosensitive channels (influenced by membrane strain);

- gap junctions (porins not gated and, usually, not selective for specific ions);

In many cases, anyway, ion channels show dependence on different stimuli; in particular, many ligand gated channels are also influenced by transmembrane voltage, and some voltage-gated channels can bind ionic molecules modifying their electrical behaviour (see, for example, *Ion Channels of Excitable Membranes* by B. Hille) . Moreover, all the ion channels are sensitive to other physical and chemical variables, like temperature and pH.
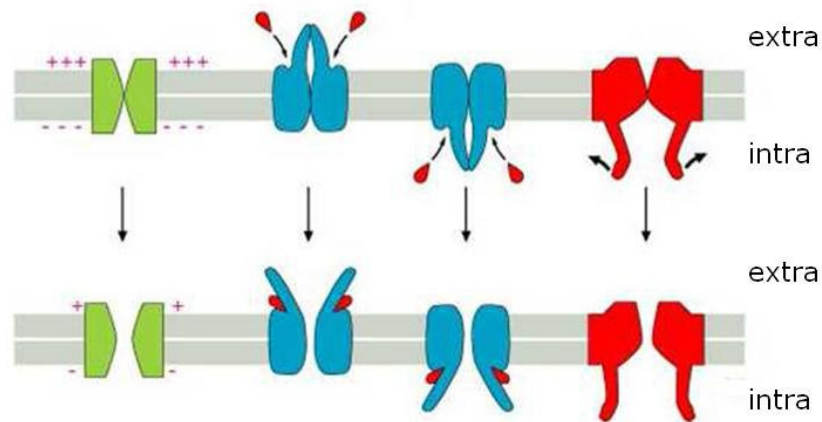
Figure 1.2 Examples of ion channel gating mechanisms: green channel gating is voltage dependent; blue channels are regulated by extra-cellular (left) or intra-cellular (right) ligand molecules; red channel is mechanosensitive.

1.3.1 Ligand gated ion channels

The capability to interact with the external world, as well as to propagate and process a large amount of information deriving from chemical stimuli, plays a leading role in the life, especially of the complex organisms. In multi-cellular organisms, in fact, cell-cell communication is essential for a large part of activities, in transmitter communication from pre- to post-synaptic cells, in the endocrine system, in development, in wound healing, in the immune response to foreign objects, etc. These functions are carried out by a series of highly specific molecular sensor systems, often based on the chemical binding of receptive sites with specific target molecules, usually defined agonists. Ligand gated ion channels (LGICs) constitute an important class of these systems;

10

since the receptor, which binds the activating molecule (the ligand) and the ion channel are part of the same nanomolecular protein complex, the transduction of the signal is fast, compared with other kinds of transducing mechanisms (enzymatic systems, G-protein coupled channels…). The LGICs are small highly specialized nanomolecular protein complexes, about 12 nm long and 8 nm in diameter, which span the 3-nm or so lipid bilayer membranes of the nerve or muscle cells. When the appropriate chemical neurotransmitter, the ligand, binds to the LGIC, which incorporates both the receptor and the ion channel, the ligand binding event can then cause the channel to open. The open channel selectively allows certain species of ions to pass from one side of the cell membrane to the other, through the channel. The resulting current (in both magnitude and sign) depends on the signs of the permeating ions and their electrochemical potential energy gradient across the membrane. For these properties, ligand gated ion channels play a critical role in the fast chemical transmission of electrical signals at the junction between nerve cells (a synapse) and between nerve cells and muscle cells. The arrival of an electrical signal at the synaptic terminal of a nerve causes the release of a chemical signal—a neurotransmitter molecule (the ligand, also referred to as agonist). The neurotransmitter rapidly diffuses across the very narrow 20–40-nm synaptic gap between the cells and binds to the LGIC in the membrane of the target (postsynaptic) cell and generates a new electrical signal in that cell. How this chemical signal is converted into an electrical one depends on the fundamental properties of LGICs.

2   EXPERIMENTS ON PLANAR ARTIFICIAL BILAYERS

2.1   Planar lipid bilayers

As it was described in Chapter 1, phospholipids forming the cell membrane tend spontaneously to create closed structures (liposomes, micelles) when inserted in an acqueous environment; alternatively, if spread on a water solution surface, they aligned their hydrophilic head groups towards the meniscus, leaving the hydrophobic tales in air. Another possible configuration, diffusely used in electrophysiological experiments (namely, for studying the electrical properties of the lipid membranes and the ion channels) is given by the planar lipid bilayers.

Planar lipid bilayers, also called black lipid membranes (BLMs), can be assembled across the hole in a septum made with a lipophilic, dielectric material, such as teflon (PTFE, FEP), delrin or polysulphone. The creation of planar bilayers is possible thanks to the characteristics of the septum material: the fatty acids, corresponding to the hydrophobic tales of the phospholipids, can easily link the borders of the aperture, fastening the bilayer suspended across the hole. The bilayer is then formed across an aperture which links two fluid filled chambers. Several techniques are reported in literature to create BLMs: most of them are suitable for laboratory experiments and need the presence of an experimenter, because of the poor reliability, also in controlled conditions. At present, no commercial systems are available for realising BLMs automatically, although new approaches developed in the last years are promising and will probably bring to it in the next future (see, for example, Trojanowics, 2003). The fundamental problem in obtaining BLMs in an easy way and with a satisfactory rate of success is that, in any case, bilayers must be created for self assembling, and the structure that lipids should form is highly organized and

very unstable: a layer 3 nm thick, over holes having diameters in the order of hundreds of micrometers.

The three main techniques for realizing BLMs[1] are the Montal-Mueller technique, the BLM on patch pipette technique and the painted lipid technique.

The **Montal-Mueller technique** (Montal and Mueller, 1972) is based on the apposition of two lipid monolayers, each formed on the meniscus of a water solution. The set up is formed by two chambers, each connected to a pomp, separated by a drilled septum. Firstly the desired experimental solution is added to both chambers to a level below the hole in the septum, and a phospholipid monolayer is formed at the solution-air interface; the bilayer is then formed by increasing the level of the solution, first in one and then in the other chamber so that each monolayer is raised to cover the hole and the two monolayer hydrophobic tales link together forming the BLM.

The **BLM on patch pipette technique** was introduced by Wilmsen and colleagues (Wilmsen *et al.* 1983; Hanke *et al.* 1984). Bilayers are formed at the end of conventional patch-clamp pipettes (like the ones used in patch clamp experiments, see Chapter 5) with tip diameters in the range 0.5-5 µm. The tip of the pipette is immersed in the experimental solution in a compartment and a phospholipid monolayer is formed at the air-water interface .

[1]   These techniques refer only to suspended BLMs, namely, planar lipid membranes created between two aqueous compartments. BLMs can be also realised on solid or gel-like polymer supports, as it will be breafly described in section 2.5.

A portion of the monolayer is transferred to the pipette tip by raising the pipette into the air. The polar head groups of the phospholipids orientate so that they interact with the aqueous pipette-filling solution and the glass wall of the pipette. The hydrophobic chains of the molecules face the air. A bilayer is constructed by re-immersion of the pipette in the bath solution. In fact, as the tip of the pipette crosses the monolayer at the air solution interface, a second region of monolayer interacts with the monolayer in the pipette to form a bilayer. This technique has an yield lower than the other two described methods, but allows to create very stable bilayers, characterized by a low value of noise, thanks to the limited dimension of the membrane.

The **painted BLM technique** was first described by Mueller and colleagues (Mueller *et al.* 1962; Mueller and Rudin, 1969). Bilayers are formed from a dispersion of either one or a mixture of purified phospholipids in a non-polar solvent such as n-decane. Prior to bilayer formation, the hole on which the bilayer is to be formed is "primed", namely coated with a small quantity of the phospholipid dispersion. After the pre-coating, chambers are filled with the desired experimental solution, and then other phospholipid dispersion is spread across the hole using a stick (for example, in we used a borosilicate rod). As described by White (1986), at the outset, the film spread across the hole is several micrometers thick and in equilibrium with an annulus (Plateau-Gibbs border) formed as the lipid dispersion "wets" the septum. The film then thins spontaneously: phospholipids tend to self assemble in a bilayer structure while the solvent spreads in the solution. As the film thins, van der Waals attraction between the aqueous phases on either side of the film contributes an additional driving force. This technique is very commonly used, mainly because it represents the easiest way for creating a bilayer, whose formation can be easily observed through the thinning of the membrane (see section 2.4). The main drawbacks are that this technique needs a large septum hole (larger than 100 um), and only the central part of the aperture is covered by a bilayer, while on

14

the border part there is a thick and not organised structure of lipids and solvent. These things determine a bilayer inclined to mechanical oscillations and then quite noisy. Another possible drawback is that the painted bilayers are not volatile-free, namely, molecules of solvent are entrapped between their hydrophobic tales, changing the bilayer thickness and structure and, therefore, potentially changing the functionality of the inserted ion channels. Anyway, bilayer solvent does not appear to have significant adverse effects (Labarca *et al.* 1980; Latorre, 1986; Moczydlowski *et al.* 1984).

2.2   Set-up for bilayer experiments

The experimental set up used for the bilayer creations and the ion channel insertions   is mainly formed by the Bilayer Workstation, produced by Warner Instruments (Hamden, USA). It includes:

- an anti-vibration plane, to minimise mechanical interferences which could break the membranes and introduce noise to the signal;

- a grounded Faraday cage to minimise noise from electrical interference;

- an apparatus for the creation of the membranes (with painted BLM technique);

- a stirplate system;

- a two-syringes based perfusion system.

Moreover:

- a patch-clamp amplifier (mod. Axopatch 200B, Axon Instruments, USA);
- a Personal Computer;
- an analog to digital converter, connected to the PC (DIGIDATA 1322, Axon Instruments, USA);
- a signal generator(HP 33120A, Hewlett-Packard , USA);
- an oscilloscope (TDS 3034B, Tektronix, USA).

2.2.1 Apparatus for the formation of painted bilayers

Planar lipid bilayers are formed, using painting technique, inside the apparatus illustrated in figure 2.1. It consists of a black delrin block (A) into which is cut a circular chamber (the *trans* chamber) connected to a second circular chamber which holds the bilayer cup (B), made with delrin or polysulphone. The cup contains a well (volume 1.2 ml - the *cis* chamber). The face of the cup adjacent to the well is machined to form a thin (approximately 250 um) septum through which is drilled a hole that, once the cup is located in the block, connects the two chambers. The painted bilayer is formed across this hole. Beside the two main chambers, other two small compartments are dug in the black block. They can be filled by the same solution of the two main compartments and used to contain the Ag/AgCl electrodes, once connected to the trans and cis chambers with agar bridges. Agar bridges are borosilicate tubes, with an internal diameter of 1.5 mm, heated with a flame, bent and filled with a boiling, highly conductive saline solution (we used 3 M KCl) including also a 4% volume of Agar (Sigma-Aldrich, USA). This solution, at room temperature, becomes a gel, due to the agar presence. Agar bridges usefulness is to avoid the presence of Ag^+ ions in

16

contact with the membrane, coming from the electrodes, which could generate contamination. There are three available sizes for the cup holes: diameters of 150 um, 200 um, 250 um. As said before, using holes with smaller dimension (under 100 um), the rate of success in self assembling of bilayers could be very low. On the other hand, bigger is the hole, bigger are the mechanical noise and the fragility of the membrane. In any case, not all the hole surface is covered by a bilayer, but the real bilayer is encircled by a lipidic, not ordered, structure. The amplitude of the bimolecular sheet can be estimated using a microscope or, in a rougher but more practical manner, from the capacitance of the membrane, as it will be shown in section 2.4.
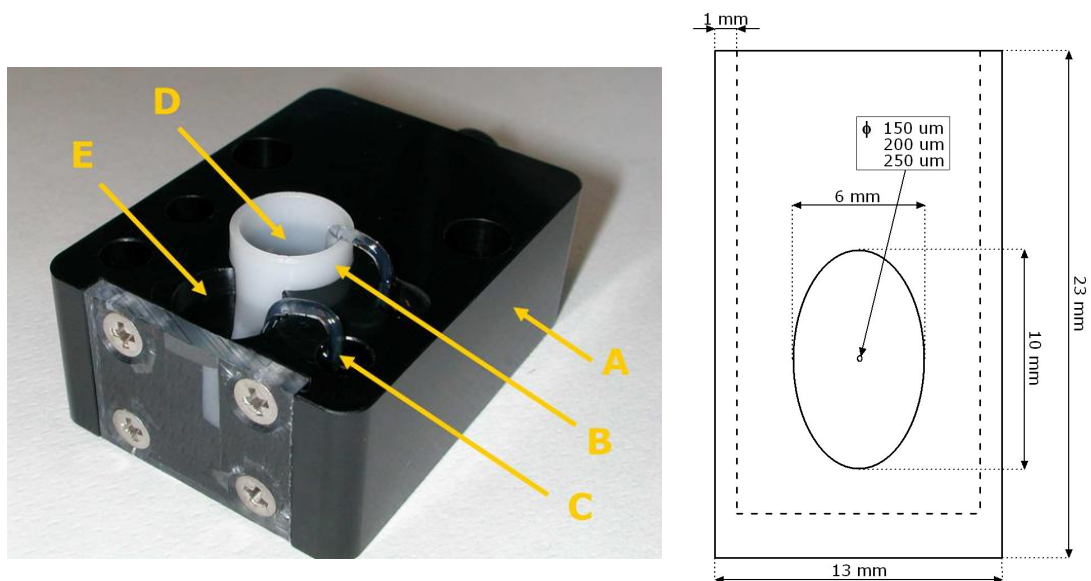
Figure 2.1   Left. Apparatus for the creation of painted BLMs. In particular, it is possible to note: (A) the black delrin block; (B) the bilayer cup; (C) the agar solution-filled bridges; (D) the *cis* chamber; (E) the *trans* chamber. Right. A drawing of the bilayer cup, reporting its measures.

The perfusion system is formed by two syringes mounted on a support, set inside the Faraday cage and magnetically fixed on the anti-vibration plane. The two syringes are connected to tubes, both inserted in the trans chamber at different depths, thanks to a prop: one is full of the new solution to insert while the second one is used to extract the old solution. It was changed, during a perfusion, a volume equal to, at least, five time the volume of the chamber. All metallic objects inside the cage were hearted to a single point that was connected to the amplifier hearth, to eliminate loops.

2.2.2 Headstage and amplifier

Axopatch 200B is an analog amplifying system designed for cellular electrophysiology and, in particular, for ultra-low noise patch-clamp measurements, suitable for single-channel and whole-cell voltage or current clamping. It includes a 4-pole Bessel filter with an adjustable bandwidth from 1 kHz to 100 kHz. The first stage of the amplifier is called headstage (model CV-203BU, Axon Instruments) and is a cooled probe containing a current-to-voltage converter. The feedback element of the first stage can be set in order to have a resistor feedback or a capacitive feedback. Figure 2.2 shows the resistive headstage diagram, whose overall transfer function is the one reported in equation (2.1).

$$V_{Out} = \frac{R_f}{Z} V_P \, .$$

(2.1)

It is possible to switch between two feedback resistors obtaining two different transresistance values (0.05 mV/pA and 0.5 mV/pA). Because of the virtual short circuit at the input of the op-amp, the voltage applied to the DUT (in our case the BLM) is the desired voltage V_p (the pipette voltage, which is the command voltage V_{cmd} after series resistance and pipette (probe) offset compensations have been applied). Then, a subtractor removes V_p from the output of the converter. In figure 2.2 is also visible a parasitic stray capacitance (on the order of 0.1 pF) in parallel of the feedback resistors. This capacitance has a big influence on the bandwidth of the system; in fact, it causes the introduction of an undesired pole (at f = $1/2\pi R_f C_{Rf} \approx$ 30 kHz for R_f = 50 MΩ and f ≈ 3 kHz for R_f = 500 MΩ). This pole must have to be compensated, and this is the reason for the introduction of the High Frequency Boost, which operates a zero-pole cancellation and then extend the bandwidth.
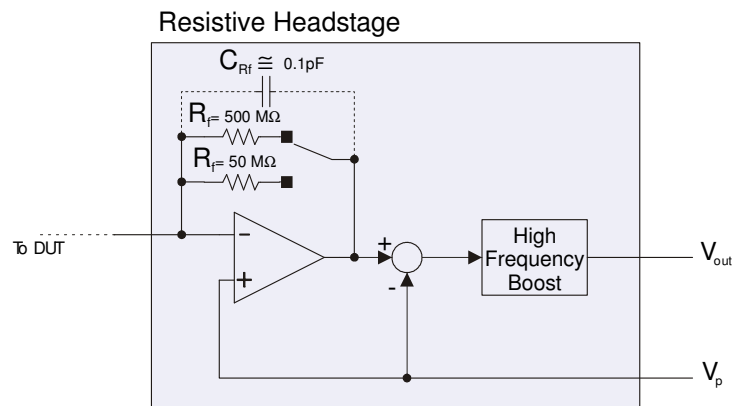
Figure 2.2   Headstage circuit in resistive-feedback configuration.

When the headstage is configured for use a capacitor as feedback element (figure 2.3), it becomes an integrator. Therefore, a differentiator following the this integrating stage is needed (and also a differential amplifier, like in the resistive headstage ,to subtract V_p) to retrieve a voltage output proportional to the current input. With the capacitive headstage scheme, the overall transfer function is the one reported in equation (2.2).

$$V_{Out} = (\frac{C_d \, R_d}{C_f \, Z})V_P.$$

(2.2)

The most important advantages of the capacitive headstage are the improved bandwidth and the reduced noise respect to the resistive headstage scheme. On the other hand, there is a major disadvantage: when the current input has an average value different to zero, or in presence of a spike, the integrator can saturate. For this reason, the capacitive headstage is combined with a reset circuit: when the output of the integrator goes out of the range $-10V \div +10V$, C_f is discharged by switching on a MOS transistor placed in parallel to the capacitor. During this operation, the output value is held by a Sample and Hold. The total time needed for the reset is about 50 us and during this time a "data not valid" signal goes high, for signalling bad samples in the output data. The capacitive headstage can be then used only in single channel recording, where the measured current is in the range of the pA. For greater current values, saturation should occur very frequently, so the resistive configuration should be preferred.
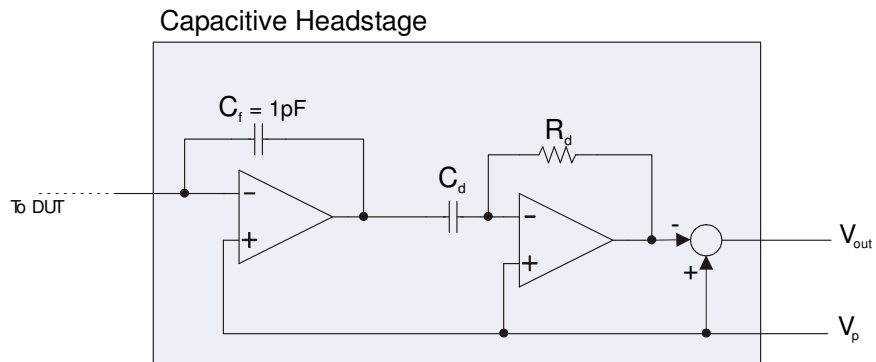
Figure 2.3   Headstage circuit in capacitive-feedback configuration.

2.3   Lipid mixture creation

For the creation of the BLMs with painting technique, several lipid composition were tested, in order to achieve large and stable bilayers. The one which guaranteed the best performance, being then used for all the following experiments concerning ion channels introduction, is composed by a mixture of Phosphatidylcholine (PC) and Phosphatidylethanolamine (PE) with a weight ratio 7:3, in a solution of n-decane (15-20 mg/ml). Phospholipids were purchased by Sigma-Aldrich, in chloroform stock solutions (10 mg/ml). Stocks were warmed to room temperature before opening, to reduce fluid condensation on the cold fluid surface. Phospholipids were then dried under a stream of nitrogen in glass tubes and resuspended in n-decane (Fluka, USA). The substitution of the apolar solvent, from the chloroform of the initial stocks to the n-decane of the mixture used in painted bilayers creation, is due to their different volatility. Chloroform is poorly volatile, and then suitable for preserving

lipids; instead, for the same reason, it shouldn't be used in bilayer self-assembly. In fact, it doesn't allow an efficacious thinning of the membranes (see section 2.4), because it tends to remain bound with the hydrophobic tales of the phospholipids. The highly volatile solvent n-decane is then preferred.

2.4   Capacitance test

Using painted BLM technique, the self assembling of the bilayer occurs progressively, after the deposition, upon the cup hole, of a thick film of lipids in an apolar solvent. This process, called thinning of the membrane, can last a time variable from few seconds to several minutes, depending on the of the used lipid mixture (types and quality), on the used solvent, on the characteristics of the cup (material, hole size and thickness of the border), on the temperature. The thinning process, and the area of the effective bilayer, can be monitored both in an optical and an electrical way. The optical way is based on the observation of the lipid structure through a low-power microscope (10 to 40x) in reflected white light conditions. The thinning of the membrane is evidenced by changing in the interference colours which finally reaches to black where the thickness of the membrane is close to 3 nm (the bilayer thickness); the area of the bilayer can be thus estimated from the surface of the "black zone" (this is the reason why planar lipid bilayers are also called black lipid membranes; see, for example, Tien 1974, cap. IV).

The electrical way, instead, is based on the properties of the BLMs, which behave as capacitors, due to their apolar core. In a working range of frequencies (1-10000 Hz), the system between the electrodes, before the lipid addition, can be represented as in figure 2.4.A (the part inside the frame), where $2 \times R_e$ includes the resistance of the solution and the resistances due to

the interfaces between the solution and the electrodes, C_s is the capacitance of the dielectric septum, R_h is the resistance due to the septum aperture. When a lipid film occludes the hole, the capacitance C_b appears in series with R_h, as shown in figure 2.4.B (inside the frame). During the thinning of the membrane, the value of the capacitance C_b increases (it's basically a plane capacitor in which the dielectric layer is getting thinner). The final value of C_b is practically the one of the bilayer, which will be largely greater than the one of the Plateau-Gibbs border. In order to observe the formation of the bilayer and to estimate its area, a capacitance test was made before starting every further experiment. It consists in applying a triangular wave (1-10 kHz, 1-10 mV), generated by the signal generator and then brought to the headstage and imposed as an input signal. Before the lipid painting, since the low frequency values of the triangular wave, there is a pure resistive path between the two electrodes. The output signal is then simply a scaled version of the input. After the painting, in presence of a lipid mixture occluding the hole, the system behaves practically as a capacitor, given by the parallel between C_s and C_b.

The output signal, in this case, is a square wave, whose amplitude increases during the thinning process, being proportional to the capacitance value. In fact, the capacitance value can be estimated, from the output current value, simply using the I-V relation for a plane capacitor:

$$I \simeq C \frac{\Delta V}{\Delta t} \Rightarrow C \simeq \frac{\Delta t}{\Delta V} I \qquad (2.3)$$

where ΔV is the amplitude of the input signal, Δt is half period of the triangular wave.
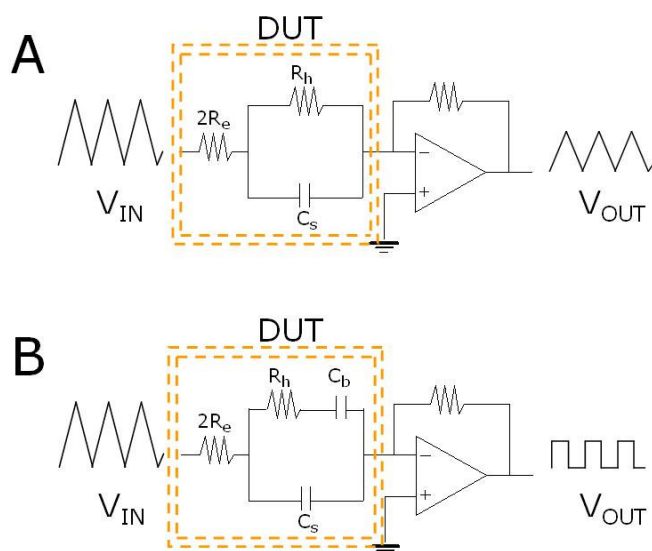
Figure 2.4   System response to a triangular voltage input. (A)The electrode resistance (2R$_e$) is in parallel with the apparatus, which, in absence of lipids covering the hole, can be schematised by the parallel between the hole resistance R$_h$ and the septum capacitance C$_s$. (B) In presence of a membrane, the lipid structure covering the hole introduces the capacitance C$_b$.

The specific capacitance of a natural bilayer, which doesn't include solvent, is about 0.8 uF/cm^2 (White, 1986; Montal *et al.* 1986). This value is so large mainly because of the extreme membrane thinness. In the case of painted bilayers, it is reduced by the presence of solvent, and is in the region of 0.4 uF/cm^2 (Alvarez, 1986), depending on the used lipid mixture and solvent. This means that, for a cup hole diameter of 200 um, if the effective bilayer covers half of the hole surface, the expected capacitance value is $c_b \times A_b = 63\ pF$, where c$_b$ is the specific capacitance (0.4 uF/cm^2) and A$_b$ is the bilayer area

($A_b = \pi(100\,\mu m)^2 \,/\, 2 = 0.5 \times \pi \times 10^{-4}\,cm^2$). A good membrane should be, at least, half of the hole size; for lower values, the insertion of complex channels through vesicle fusion becomes difficult (see section 2.6). As said before, when viewed optically, a thick torus of amorphous lipid surrounds the bilayer formed in the centre. For a 'good' membrane, this torus is much smaller than in a 'bad', poorly formed membrane. In any case, the capacitance values of the torus and the septum, which should be added to the bilayer one, are negligible.

2.5   Other kinds of artificial lipid bilayers

Since the BLMs are intrinsically fragile, being suspended between two liquid compartments, other techniques were studied for increasing their stability. The basic idea is to create bilayers laid on scaffolds, in order to reduce the mechanical oscillations which cause their breaking down. The two main categories are the following:

Supported BLMs (s-BLMs): are BLMs covering an electrode patterned on a substrate (Tien et al., 1989; Martynski and Tien, 1991). The advantage, as said before, is that they can last for a long time before rupturing. The major drawback of this method is that only a thin water layer (in the nm order) separates the membrane and the substrate. In these conditions no complex ion channels (like the LGICs) can be properly embedded, because there is no space enough for their transmembrane domains. Furthermore, it is only possible to control the solution on the side of the membrane that is not in contact with the electrode. A further development was the creation of spacers molecules, namely phospholipids having molecular chains connecting their polar heads with the electrode, allowing greater distances between the bilayer

and the substrate (see, for example Lang et al., 1992; Koper, 2007). In any case, at present, this approach seems to be incompatible with the insertion of functional complex ion channels, and only porins have been successfully used in combination with this technique (Gritsch et al., 1998; Steinem et al., 1997; Bailay and Cremer, 2001).

Polymer-cushioned BLMs: this technique is a combination of the suspended-BLM and the supported-BLM approaches. Electrodes are patterned over a surface and a polymer (typically a cellulose hydrogel or a gel of agarose) is coated on top of the electrodes. This polymer stabilises the membrane and acts as a spacer from the solid substrate complex. Also in this case, the possibility of having ligand gated channels properly inserted and working has been not demonstrated yet.

2.6   Channels insertion

Reconstitution of ion channels into planar lipid bilayers is a powerful technique to study their properties (i.e. ion selectivity, conductance, kinetics, voltage dependence) in a controlled and easy to handle system, but getting the channels into the bilayer is often a big challenge. Some channels insert spontaneously into the bilayer when they are added into the solution surrounding it. Channels that insert spontaneously, for example, gramicidin and alamethicin, are easier to study and have been well characterised (see, for example, Andersen et al., 2005). However, many ion channels are not soluble in solution and do not insert spontaneously into bilayers. All the most complex channels, including all the ligand gated ion channels, fall within this category. One method to place these channels into bilayers is to isolate them in

liposomes and induce the liposomes to fuse with a bilayer. Usually, it means fracturing the cell membrane into small pieces, which spontaneously form liposomes, and then delivering the liposomes near the bilayer with the right fusion conditions. Sometimes, to assure the fusion with the BLM, it's enough to have liposomes with a controlled size (about 100 um of diameter) and an osmotic gradient between the two compartments of the bilayer apparatus. In other cases it's not enough, because not all channels induce fusion. At present, it's not clear what are the properties which an ion channel must have for producing the fusion of the liposomes ; as a consequence, it's not generally possible to know if a particular channel-containing liposome is also capable of fusing. In the early ninetieth, Dixon Woodbury developed the Nystatin/Ergosterol method for reconstituting ion channels into BLMs: the great achievement of this method is that allows the insertion of all kinds of channels into bilayers, making fusigenic the liposomes. In the following sections, experiments will be described, concerning all these possible approaches for inserting ion channels in planar lipid membranes.

2.7   Gramicidin channel

The first ion channel we inserted in BLMs is the gramicidin A channel, an antibiotic product by Bacillus Brevis, formed by just 15 amino acids. In membranes, gramicidin A forms channels that are specific for monovalent cations (Hladky and Haydon, 1972). Actually, in normal conditions, it is not a common ion channel, which spans entirely the membrane, but is a dimeric channel. This means that gramicidin conducting channels are formed by two nonconducting subunits, each embedded in one of the two molecular sheets forming the bilayer. Every subunit is entirely composed by hydrophobic

residues, and tend to insert itself between the fatty acids chains, locally bending the monolayer around it. Following the fluid mosaic model, gramicidin subunits can freely spread in their monolayer because of Brownian forces; when two subunits belonging to different monolayers are near enough, they align themselves, thanks to hydrogen bonds, forming a conductive pore having a diameter of 4 Å and a length of about 25 Å (Finkelstein and Andersen, 1980). This open pore lasts till the breaking of the bonds: the channel lifetime is then dependent on temperature, pH, compositions of the solution and of the bilayer (in particular, it depends on the membrane thickness). Every subunit can place itself spontaneously in the BLM, getting in the monolayer facing the aqueous compartment where it's inserted. In order to obtain the formation of the gramicidin channels, solution containing monomers was added in both cis and trans chambers of the apparatus, after the BLM creation.

2.7.1 Experimental set-up

For the gramicidin experiments, we used mainly the following solution (mimicking the extracellular fluid composition) containing (mM): 150 NaCl, 8 HEPES, 50 EGTA. Solution pH was adjusted to 7.2 with NaOH. During the first experiments, we used also a simple KCl 500 mM solution, without adjusting the pH. We didn't characterize conductance and kinetics of the dimeric channels in this case but, qualitatively, the bilayer stability and the capacity of the pores to open were preserved. All chemical reagents were purchased from Sigma-Aldrich, USA. Milli-Q ultrapure water was used.

Purified gramicidin A, purchased in a powder stock by Sigma-Aldrich, was dissolved in ethanol with a 1ng/ml concentration. After the creation of the bilayer, a volume of gramicidin solution of 2-10 ul was added in each chamber.

It's highly improbable, for a gramicin monomer, to cross a lipid monolayer: in fact, no channel formations have been seen inserting gramicidin solution in only one of the two compartments. Current signal was recorded, with a clamped potential, starting at least five minutes after gramicidin addition (in order to achieve equilibrium conditions). Signal was acquired analogically filtering at 1 kHz. Data were directly digitized, recorded and monitored using the specific software tool pCLAMP 9 (Axon Instruments, USA) , with a sapling rate of 500 kHz. Examples of recorded channel activities are reported in figure 2.5.
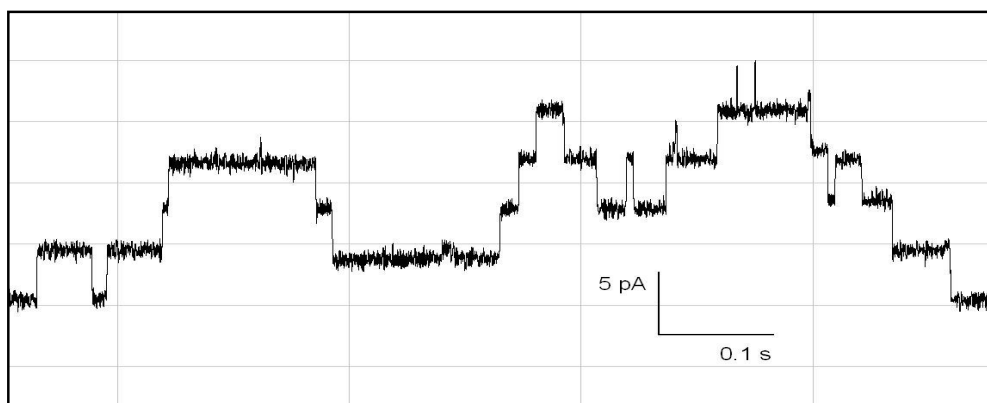
Figure 2.5   Signal recording from gramicidin dimeric channels inserted in BLM. 200 mV applied, 1 kHz filtered.

2.7.2 Conductance analysis

Data records were used for an estimation of the single channel conductance and its lifetime distribution. For the channel conductance analysis, data records

were firstly idealised through a threshold-based Matlab routine. This routine compares the difference between two consecutive data points and a threshold value. When this threshold is exceeded, the current amplitude jump is estimated, through the difference between the average of the data points preceding and the ones following the jump. These current values are inserted in a vector, and their average value represents the channel current amplitude in correspondence of the imposed voltage. In figure 2.6 is then reported the gramicidin I-V characteristic, for applied potential between -140 mV and +140 mV. Mean values and standard deviation were calculated using, at least, one hundred values for each point. As expected, it's well fitted by a line which virtually cross the axes origin (the exact intersection is in correspondence of I=-0.0462 pA), in agreement with the symmetry of the channel-bilayer complex. The estimated conductance value is 22 pS, in agreement with literature data (Rostovtseva et alii, 1998).
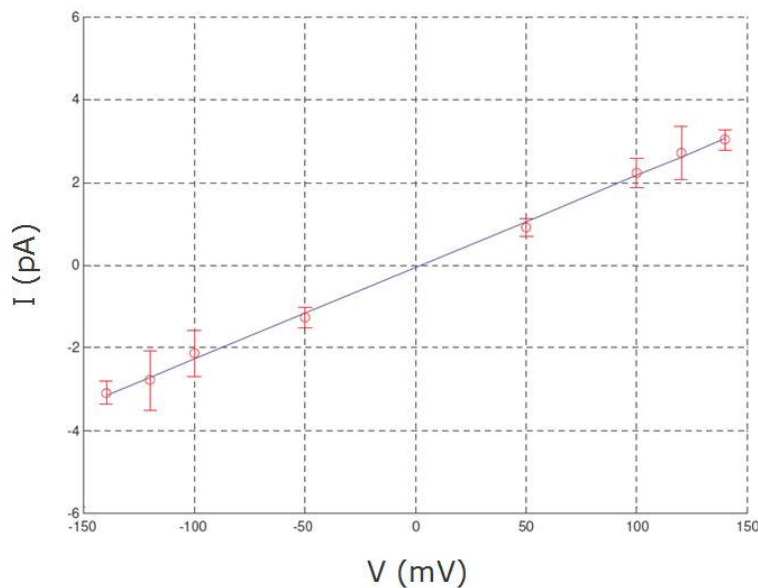
Figure 2.6   I-V curve of gramicidin ion channels.

2.7.3 Channel lifetime estimation

As described before, gramicidin channel is formed by the coaxial bond between two subunits. The chemical relation describing the pore formation is then:

$$A + A \underset{K_R}{\overset{K_D}{\rightleftharpoons}} A_2$$
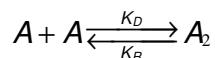
where A is the single monomer molecule, A_2 is the dimeric structure. K_D, the direct transition rate, practically expresses how easily the monomers meet and bind. It doesn't depend on the strength of their bond but only on how they move in the fluid mosaic. In any case, it's impossible to estimate this rate without knowing the monomers concentration in the monolayers, which could only be achieved from an analysis of the equilibrium between the molecules in solution and the molecules embedded in the membrane. The reverse transition rate K_R, instead, depends on the binding force between the monomers (and also on temperature, pH, applied voltage, membrane composition…); it can be estimated through the distributions of the gramicidin open channel lifetime. In order to do it, acquisition were made, inserting a small volume of gramicidin solution in the chambers (0.5 ul), so that the probability of observing multiple openings (more than one channel open at the same time) was minor (and, in these case, multiple channels weren't considered for the lifetime evaluation). Data elaboration was made using Clampfit software (Axon Instruments, USA), analysing 250 openings from four records, all made with an applied voltage of 100 mV . The histogram below reports these open lifetimes. In accord with the theory (see Chapter 3), histogram is well fitted by a single exponential. The probability density function of the open lifetime is expressed by (2.4).

$$f(t) = K_D \, e^{K_D t} \, . \tag{2.4}$$

Normalising the histogram (imposing a unit subtended area), we obtained K_D=8 transition/second, corresponding to a mean channel open lifetime of 125 ms.
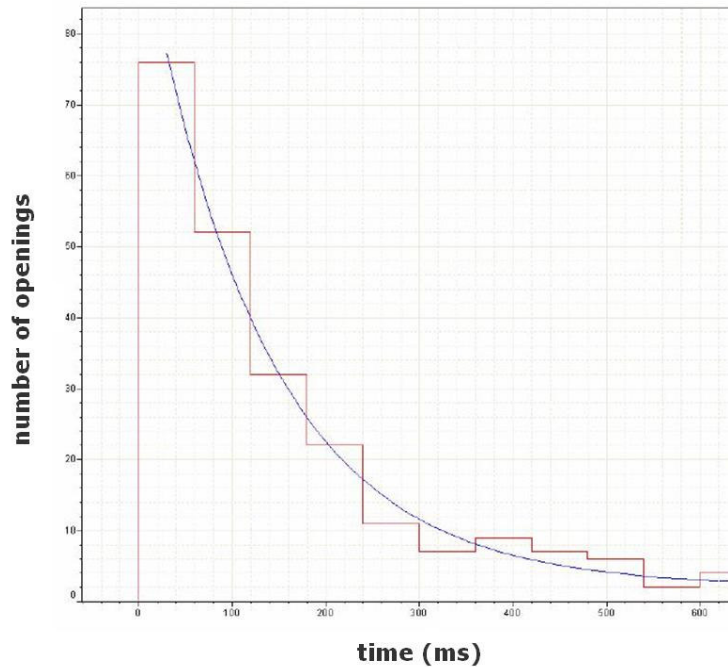
Figure 2.7   Histogram of the gramicidin open lifetimes (red) fitted by a single exponential curve (blue).

2.8   Insertion of fusigenic liposomes

Only few channels, usually characterised by a simple structure, can be effectively incorporated in an artificial bilayer directly inserting them in the

solution chambers. In particular, this is not the case of ligand gated ion channels, with few rare exceptions, like the ryanodine receptor-channel proteins (Imagawa *et al.* 1987; Lai *et al.* 1988). This is basically due to their complex structure: LGICs are formed by several subunits, and each of them crosses the bilayer several times, not only in its pore-forming portion. As a consequence, each subunit is made by several hydrophobic residues, to anchor the bilayer's core, alternated with hydrophilic residues, to face the extremities of the BLM and the aqueous compartments. It is then energetically unlikely the spontaneous insertion of the channel subunits, because it should involve the passage of the hydrophobic residues through the apolar core of the membrane. Therefore, the standard method for the incorporation of both native and purified channel proteins into pre-formed planar lipid bilayers involves the fusion of a channel-containing membrane vesicle with the bilayer, a procedure first described by Chris Miller in his studies of the sarcoplasmic reticulum K+-selective channel (Miller and Racker, 1976; Miller, 1978). Several experimental studies were conducted, leading to empirical protocols and rules for optimizing the vesicle fusion processes. For example, if either the planar bilayer or membrane vesicle contain a proportion of negatively charged phospholipids, the occurrence of the pre-fusion binding can be encouraged by the inclusion of millimolar concentrations of divalent or trivalent cations in the experimental solutions (Cohen, 1986; Hanke, 1986). Moreover, vesicles only fuse when they are induced to swell (Finkelstein *et al.* 1986). Vesicle swelling is most commonly induced by forming an osmotic gradient across the bilayer, so that the osmotic pressure of the solution in the chamber to which the membrane vesicles are added (*cis*), is greater than the one on the other side of the bilayer (*trans*). In this case, osmotic gradients created with salt solutions will be particularly effective if the liposomes contain ion channels permeable to one or both of the ions composing the used salt (Cohen, 1986). The efficiency of vesicle-bilayer fusion can also be influenced by other factors. Greater is the area of the bilayer, more likely the membrane vesicles will come into pre-fusion contact and hence

greater will be the likelihood of fusion. For this reason, in the case of a painted BLM, the dimension of the effective bilayer is crucial: a small bilayer, surrounded by a thick, large Plateau-Gibbs border, will be reached by liposomes with difficulty. Another factor which can help the vesicle fusion is the stirring, thanks to the presence in the chambers of rotating magnets which agitate the solutions. As said before, vesicles will fuse with planar bilayers in presence of an osmotic gradient if vesicles contain a permeability pathway for the solute: in fact, vesicles containing channels fuse more readily than channel-free vesicles (Woodbury and Hall, 1988; Cohen *et al.* 1989) and not all the ion channels help equally the fusion process. Woodbury and Miller (1990) have described a method for maximising vesicle fusion with planar bilayers, where nystatin is incorporated into membrane vesicles in presence of ergosterol. Also this last method will be briefly discussed, in the last part of this chapter.

2.9   Example of spontaneously fusigenic vesicles: crude membranes from N1E115 cells

For testing the insertion methods of ion channels embedded in fusigenic vesicles, we used the immortalised cell line N1E-115 (ATCC number: CRL-2263). This line was established in 1971 by T. Amano, E. Richelson, and M. Nirenberg by cloning the C-1300 spontaneous mouse neuroblastoma tumor, C-1300. Cells were cultured and maintained in Dulbecco's modified Eagle medium containing 10% (v/v) foetal bovine serum, 1% (v/v) penicillin streptomycin solution (100000 units/ml penicillin and 10 mg/ml streptomycin (from Sigma-Aldrich) and 1% (v/v) L-glutamine (from Cambrex Corporation, USA) at 37°C in a 95% air 5% CO_2 incubator, and passaged every 2-3 days.

2.9.1 Experimental set-up.

Vesicle formed by N1E115 cells were realised, extracting cell membranes patches through a gradient sucrose method. In particular, our experimental protocol followed the one described by Benos et alii (2003), adapted for our cell line and instrumentation. It was composed by the following steps:

1. Rinse cells (from 3-4 petri dishes) with 300 ul of high-K+ buffer containing 400 mM KCl, 5 mM PIPES, 300 mM sucrose, supplemented with a protease inhibitor cocktail (phenylmethylsulfonilfluoride, 100 uM; pepstatin, 1 uM; aprotinin, 1 ug/ml; leupeptin 1ug/ml; DNAse I, 1 ug/ml). pH 6.8.

2. Homogenize cells for 5 min through sonication.

3. Gently layer the homogenate on a discontinuous sucrose gradient (50% on bottom 20% on the top in high K+ buffer plus protease inhibitors). For this purpose, 1.5 ml test tubes were used.

4. Centrifugate at 23,500 g for 30 min.

5. Eliminate the top layer, and collect the interface (white cloudy layer) which contains vesicles from membrane patches.

6. Dilute threefold with high K+ buffer.

7. Centrifugate at 23,500 g for 30 min.

8. Collect the pellet, and resuspend it in a final volume of 100 µl of buffer including (mM): 300 sucrose, 100 KCl, 5 MOPS, pH 6.8.

Vesicles were than aliquoted and stored at -80°C. They were always used within 10 days after creation.

Since vesicles were formed by patches of N1E115 cells, they contained a large number of different membrane proteins and ion channels, although with a particular abundance of potassium channels. During bilayer experiments, the basic solution we used in both cis and trans chambers was composed only by KCl, 100 mM ,and HEPES, 10 mM; pH was adjusted to 7.2 with KOH. As a consequence of this choice, all the currents from channels specific for ions other than K^{+} and Cl^{-} were avoided.

Bilayers were realised following the procedure described before (sections 2.2, 2.3, 2.4); an osmotic gradient was created, replacing 300 ml of solution, in the cis chamber, with 300 ml of a 3 M KCl solution. In this way, the final salt concentration in the cis chamber was increased to about 650 mM. After the creation of the osmotic gradient, 3 ul of liposome solution were added in the cis chamber, and magnetic stirring was activated. After applying a constant transmembrane potential (40 mV), a vesicle-fusion event could be revealed by a sudden increasing of the current output (due to the activation of the channels belonging to the vesicle). Stirring was then suspended and the solution in the cis chamber was changed with the basic solution, in order to re-establish symmetry conditions at the two sides of the bilayer. A volume not less than five times the one of the cis chamber was substituted during perfusion in every case. During acquisitions, signal was directly stored in Axon binary files using pClamp tool (Axon Instruments, USA); a sampling frequency of 100 kHz was used; signals were filtered at 2 kHz using the 4-pole Bessel filter of the Axopatch amplifier. An example of single channel signal is reported in figure 2.8, corresponding to a clamped potential of 60 mV.

When a single channel activity was seen, an input voltage protocol was imposed by the software. The imposed waveform was a sequence of steps ranging from -60 mV to + 60 mV. Each step was 20 seconds long, and had 20 mV of amplitude.

10 pA

200 ms
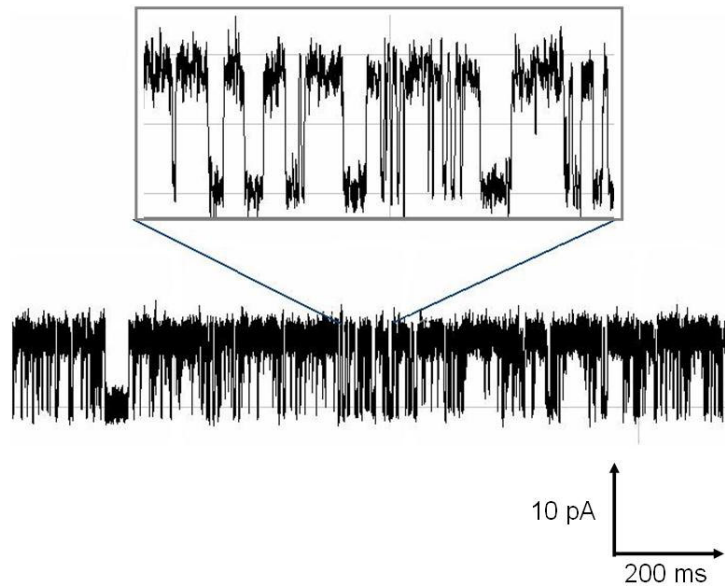
Figure 2.8   Single cannel activity.

In some cases, at the end of the experiments, 50 ul of a solution containing KCl (100 mM) and TEA (2 mM, purchased by Sigma-Aldrich), were added both in cis and trans chambers, for testing the specificity of the observed channels for K^+ ions. In fact, as described before, the solution used for creating the vesicles and for filling the bilayer apparatus chambers contained only KCl salt: as a consequence, registered channel activities could derive only from potassium channels or chloride channels. Tetraethylammonium (TEA) ion is a potassium-selective ion channel blocker, commonly used in neurophysiology experiments

to block the voltage activated potassium channels. The fact that, in every case, ion channel activity ceased after adding TEA bolus, demonstrated the specificity of the observed channels for potassium ions. This selectivity for potassium ions was also suggested by the big conductance values observed, as it will show hereafter (chloride channels are usually less conductive).

2.9.2 Channel conductance characterization

In order to determine the conductance of the ion channel populations which made fusigenic the vesicles and were therefore incorporated in the planar lipid bilayer, for every value of voltage applied in the acquisitions, and for every acquisition, an amplitude histogram was made, showing the number of samples having an amplitude that falls between the limits specified on the abscissa. An example is reported in figure 2.9. As it clear from this example, histograms are well fitted by the composition of two Gaussian bells: one has its peak in correspondence with zero (or close to zero), and collects the shut-channel samples; the other tallies with the open channel condition and its centre is the mean value of the open state current. The standard deviations of the two bells are similar: for the shut-channel corresponding bell is, in this case, 0.48 pA, while for the open-channel corresponding bell is 0.50 pA. It means that the noise not dependent on channel activity, due to instrumentation, thermal motion, mechanical fluctuations of the BLM, not perfect seal between the BLM and the septum, preponderates on the one due to channel activity.

The signals of twenty single channels were recorded, but just in three cases all the protocol was entirely applied, without observing channel rundown (deactivation of the channel) and BLM breaking. In other nine cases, data are available for only two voltage values (+40 mV and +60 mV). In the last eight

cases, data refer only to one potential value. Basically the system can be represented by the electrical model shown in figure 2.10.
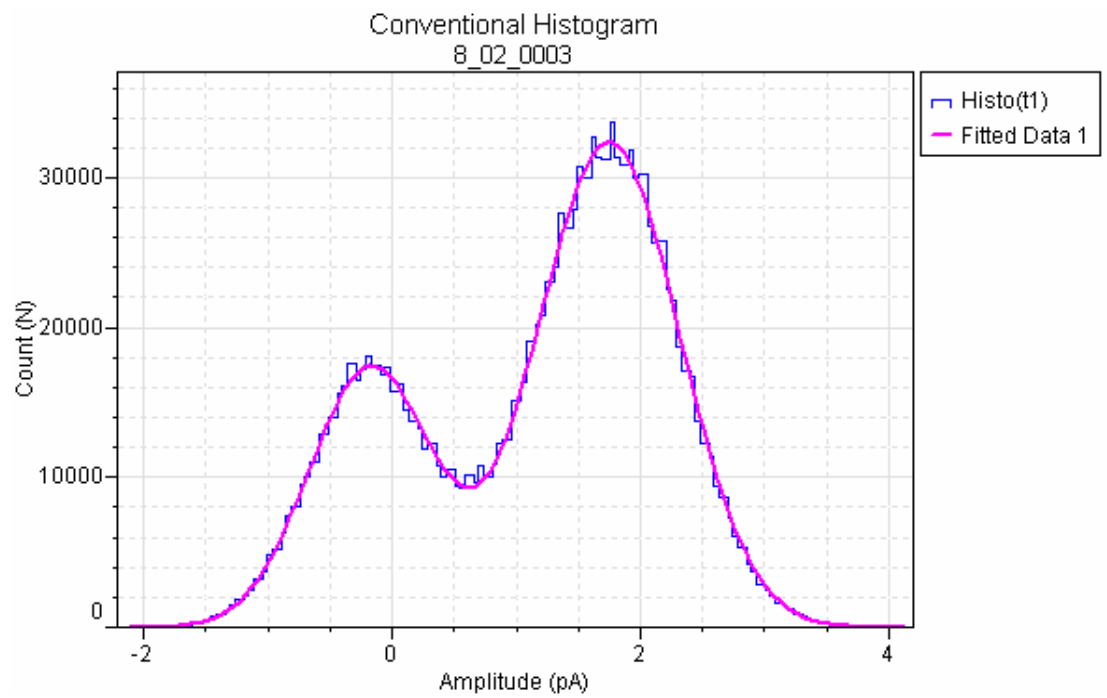
Figure 2.9 Amplitude histogram of the samples recorded during a single channel acquisition.
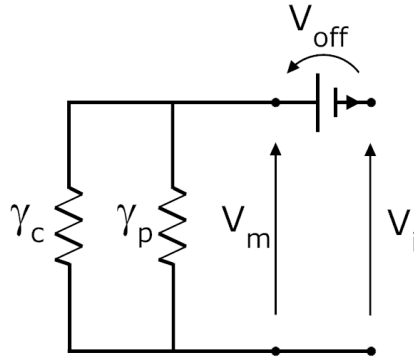
Figure 2.10 Electrical model of a single ion channel inserted in a BLM.

In the scheme, V_i is the applied input potential, V_{off} is an offset potential, mainly due to electrochemical effects at the interfaces of the electrodes, γ_C is the ion channel conductance (obviously, this term is different from zero only when the channel is open), γ_p is the conductance of the membrane leakage (namely, due to the not perfect seal between membrane and septum); V_m is the ddp effectively applied to the membrane. In the hypothesis of having a constant offset potential and an ohmic behaviour of the leakage, the currents, in correspondence of a clamped voltage V_i are, in open (*O*) and close (*C*) channel conditions, the ones reported in equations (2.5).

$$I_{Oi} = (\gamma_c + \gamma_p)(V_i + V_{off})$$
$$I_{Ci} = \gamma_p(V_i + V_{off})$$

(2.5)

It follows, from 2.5

$$\Delta I_i = I_{Oi} - I_{Ci} = \gamma_c(V_i + V_{off})$$

(2.6)

not dependent on the leakage. The values of the currents I_{Oi}, I_{Ci} are obtained from the peak values of the respective Gaussian bells in the amplitude histogram. If we consider two consecutive step values of the applied potential (for example, V_i = 60 mV and V_j = 40 mV), and the channel conductance doesn't vary a lot between these input values, we can estimate it as:

$$\gamma_{c,ij} = \frac{\Delta I_i - \Delta I_j}{V_i - V_j}.$$
(2.7)

Offset potentials resulted, in any case, smaller than 4 mV in modulus. The whole VI curves, between -60 mV and +60 mV, were drawn for three of the analysed channels. These are reported in figure 2.11, were the offset potentials were neglected.
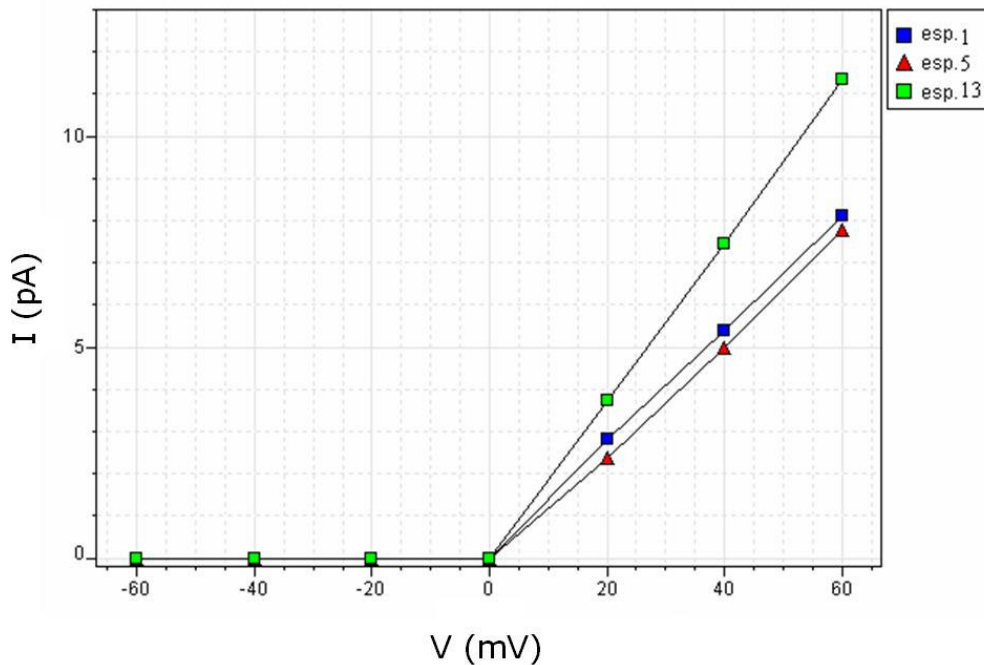
Figure 2.11   I-V curves derived from three single ion channel acquisitions.

Observing these curves, it is directly possible to bring out two different behaviours: the channels relating to acquisitions 1 and 5 have more or less the same conductance, smaller than the one of the number 13. However, in all cases the qualitative trend is the same: channel characteristics are strongly asymmetrical. Channels are active only in presence of positive potential applied, and there they have a nearly ohmic behaviour. Conductance values are reported in the table 2.1.

Acquisition number	Conductance 20-40 mV	Conductance 40-60 mV
1	132 pS	138 pS
5	129 pS	136 pS
13	185 pS	195 pS

Table 2.1   Conductance values from the I-V curves reported in figure 2.11.

For other nine acquisitions, where data were available for the two voltage values +40 mV and +60 mV, conductance 40-60 mV was calculated, obtaining that the channels can be shared in two populations, on the basis of their conductance, as reported in table 2.2.

Group	mean±std (pS)	min-max (pS)	Number of channels
Less conductive	137.21±2.00	135-140.5	7
More conductive	189.30±6.97	177.5-195	5

**Table 2.2**   Conductance values.

2.10   Nystatin/Ergosterol method

In the previous section, it was described the method for inserting complex ion channels in planar lipid bilayers, through the fusion of liposomes incorporating the membrane proteins, under particular fusion conditions (osmotic gradient, stirring…). It was also said that liposomes are made fusigenic exactly by the ion channels embedded in them, and that not all ion channels assure this property. Hence, it could be important to have a versatile technique, able to guarantee the insertion of all ion channel species in the BLM. This is important also because it can avoid misleading. In fact, the only way for getting ion channels is to obtain them from cells, eventually overexpressing them in heterologous systems, namely in cells which naturally haven't a big channels density on their surface. If we make liposomes from this transfected cells, we will obtain a large amount of liposomes basically including only the transfected channel species, but also few (in comparison) vesicles containing endogenous, contaminating channels. If these endogenous-containing vesicles are more fusigenic than the other, they will fuse easier. The risk is than to insert channels different from the ones we want to study or to use. The nystatin/ergosterol technique, developed by Woodbury and Miller (1990), avoid this problem, making all the vesicles equally fusigenic.

For nystatin/ergosterol-induced fusion, nystatin (an antibiotic) and ergosterol (a sterol present specially in moulds and yeasts membranes) are added to the vesicle membrane. These components combine to form ion channels that induce fusion in presence of a salt gradient. Channels are formed of about 10 nystatin monomers in a barrel-state arrangement with ergosterol apparently required as a glue to hold the monomers together (Marty and Finkelstein, 1975). When the glue is removed, the channels fall apart. Thus, if ergosterol-rich vesicles fuse into an ergosterol-free bilayer, nystatin channels will turn off after ergosterol dissociates from the channel complex and diffuses away into the huge excess of bilayer lipid. Therefore, if vesicles contain, besides

nystatin/ergosterol complexes, other ion channels, after the fusion and the subsequent nystatin barrels dissociations, these channels will remain the only ones active in the bilayer.

Another interesting property of the nystatin/ergosterol-containing vesicle is that its fusion can be easily revealed, because it causes a current spike if a voltage is applied across the planar lipid bilayer. It is then possible to monitor the number of fusions, stopping the process simply by switching off the stirring system. The reason of the current spikes is that, immediately after the fusion, nystatin/ergosterol pores are open, producing a sudden current; after that, ergosterol spreads in the BLM breaking the channels, so the current decreases progressively up to zero.
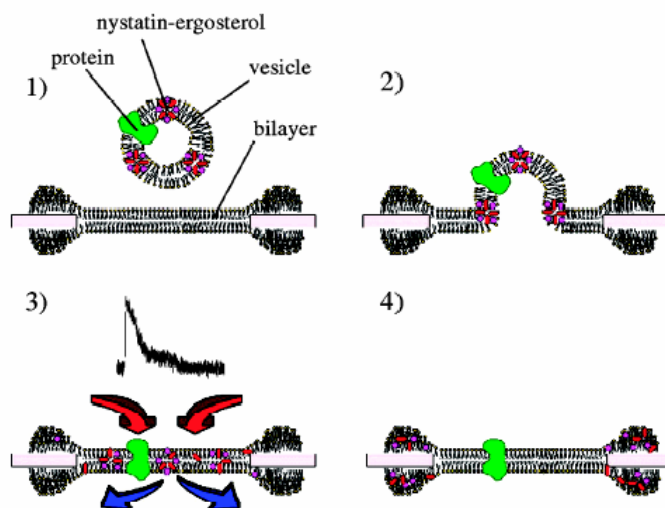
Figure 2.12 Schematic representation of the N/E technique. (1) Vesicles contain the channel proteins and several N/E complexes; (2) N/E complexes allow the fusion of the vesicles; (3) A current spike is observed, due to N/E channels: current signal progressively decreases, because of the N/E complexes breaking; (4) after the breaking of all the N/E complexes, it is possible to study the channel protein (green) without interferences.

In our experiments, we set up the technique for creating nystatin/ergosterol-containing vesicle, following the Woodbury protocol (Woodbury, 1998). Lipid composition of the vesicles which assured the best fusing performance was: 20% ergosterol, 20% Phosphatidylserine (PS), 20% Phosphatidylcholine (PC), 40% Phosphatidylethanolamine (PE). Percentages refer to molar concentrations; all products were purchased from Sigma-Aldrich. 10 mg/ml stocks of lipids (with the right ratios) in chloroform were created and used within 7 days. Compared to the BLM composition, which is the one described before (section 2.3), vesicles included also ergosterol and PS. In particular, PS was used since the presence of charged phospholipids can help their fusion, as exposed in section 2.8. Lyophilized nystatin (Sigma-Aldrich) were dissolved in methanol creating 2.5 mg/ml stocks. In order to create the vesicles for one day of experiments, 150-200 ul from lipid stock and 5 ml from nystatine stock were dried together in a glass test tube under a stream of nitrogen, rotating the tube for avoiding lipid accumulation on the bottom. The dried mixture was then resuspended in 250 ul of a solution containing (mM): NaCl, 150; HEPES, 8 (pH:7.2). Mixture was then vortexed for 10 minutes, becoming cloudy. At this point, lipids were assembled in the water solution in mono or multi-lamellar liposomes: they were then dimensioned using an extruder (Avanti Polar Lipids, Alabaster, USA), an instrument that forces the passage of the lipid solution through a polycarbonate filter (with 100 nm diameter pores). The other experimental conditions (creation of the bilayer, osmotic gradient, stirring) are the same used in N1E115-deriving vesicles experiments. No other channels than nystatin/ergosterol complexes were included in the vesicles. An example of trace, containing multiple current spikes due to liposomes fusion, is reported in figure 2.13.
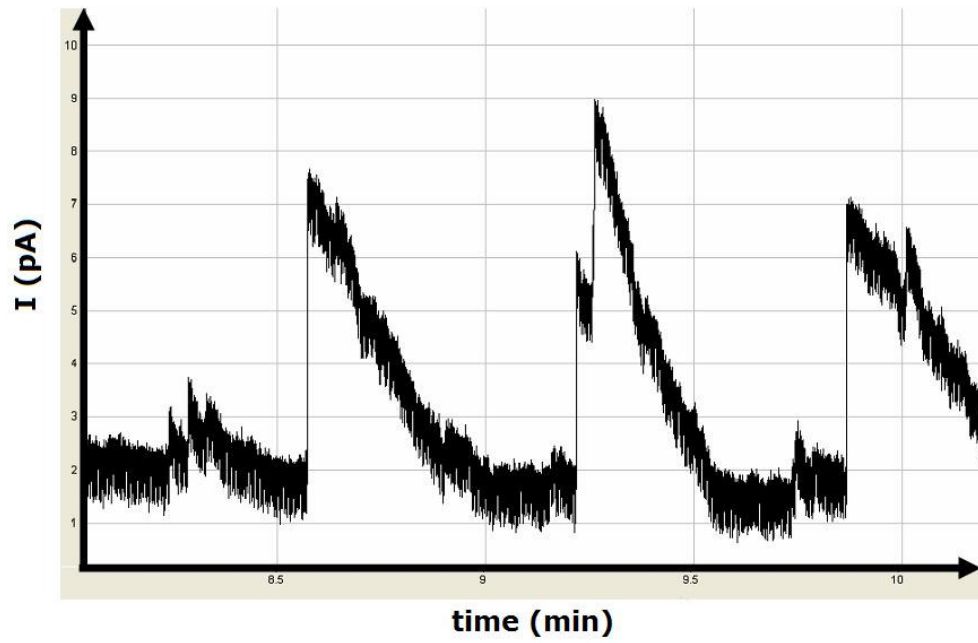
Figure 2.13   Multiple fusion of vesicles containing N/E channels.

3   ION CHANNEL MODELS

3.1   Basic concepts in ion channel modelling

The law of mass action states that the rate of any reaction is directly proportional to the product of reactant concentration. It implies that the lifetime of each chemical species present a memoryless random variable that does not depend on the age of the species. Therefore, future states of the system depend only on the present state, and not on how that state was reached. Supposing that the concentration of all the molecular species that could interact with an ion channel remain constant and also the other influence factors (as temperature, pH, transmembrane voltage) don't change, the system can be treated as a homogeneous Markov process with discrete states (a finite number of channel stable and metastable conformations) in continuous time. The probabilities of transition between one state and another can be considered constant (not time dependent).
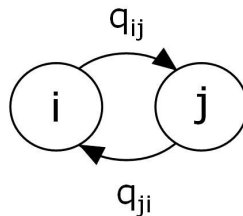
Figure 3.1   Two connected states in a Markov chain

Given two different states i, j in a Markov chain, we can define $p_{i,j}(\Delta t)$ as:

$$p_{ij}(\Delta t) = \text{Prob}(state\ j\ at\ time\ t + \Delta t\ |\ state\ i\ at\ time\ t).\qquad(3.1)$$

Transition rate constant $q_{i,j}$ is then given by:

$$q_{ij} = \lim_{\Delta t \to 0} \left[p_{ij}(\Delta t) / \Delta t \right].$$

(3.2)

The simplest possible representation for an ion channel is given by a two-state Markov chain: it's formed by a shut state S (corresponding to the condition of zero current through the channel), and an open state O (corresponding to a channel protein conformation which allows ions to flow through).

$$S \underset{\alpha}{\overset{\beta}{\rightleftarrows}} O$$

(3.3)

where α and β are, respectively, the shutting and the opening rates of the process. In this case, the probability of having a shutting during Δt is:

$$\text{Prob(channel shuts between t and } t + \Delta t \mid \textit{was open at time t}) = \alpha \Delta t + \circ(\Delta t)$$

(3.4)

where $\circ(\Delta t)$ is a quantity which tend to zero for small Δt and describes the possibility of having several transitions occurring during Δt. We are interested in the length of time in which the system stays in a particular state, i.e. in the open state *O*. The lifetime of a channel, that is the interval in which the channel is open between two consecutive shuttings, is a continuous random variable, so its behaviour can be described through its probability density function *f(t)*. It can be found by differentiating the cumulative distribution function *F(t)*, which express the probability that the lifetime is equal or less than t:

$$f(t) = \lim_{\Delta t \to 0} \left[\text{Prob}\left(\textit{lifetime between t and } t + \Delta t \right) / \Delta t \right].$$

(3.5)

48

In order to obtain the expression of the probability density function $f(t)$, we can start considering $R(t)$, the probability of having a lifetime equal or longer than t (clearly R(t)=1-F(t)):

$$R(t) = \text{Prob}(channel\ open\ between\ 0\ and\ t). \qquad (3.6)$$

The expression of the cumulative probability function R, at the time $t+\Delta t$ is given by:

$$
\begin{aligned}
R(t+\Delta t) &= \text{Prob}\big(channel\ open\ between\ t\ and\ t+\Delta t\big) = \\
&= \text{Prob}\big(open\ between\ 0\ and\ t\big) \times \\
&\quad \times \text{Prob}\big(open\ between\ t\ and\ t+\Delta t\ |\ open\ between\ 0\ and\ t\big)
\end{aligned}
\qquad (3.7)
$$

where the decomposition of the time course in two intervals (between *0* and *t* and between *t* and *t+Δt*) and the product between the two probabilities are due to the fact that the lifetime in a state is a memoryless variable, so the two probabilities refer to independent events. Another consequence of the memoryless nature of the lifetime variable is that:

$$
\begin{aligned}
&\text{Prob}\big(open\ throughout\ t,t+\Delta t | open\ throughout\ 0,t\big) = \\
&= \text{Prob}\big(open\ throughout\ t,t+\Delta t | open\ at\ t\big) = 1 - \alpha\Delta t - \circ(\Delta t).
\end{aligned}
\qquad (3.8)
$$

Thus:

$$\frac{dR(t)}{dt} = \lim_{\Delta t \to 0} \frac{R(t+\Delta t)-R(t)}{\Delta t} = \lim_{\Delta t \to 0}\big\{-R(t)[\alpha - \circ(\Delta t)]\big\} = -\alpha R(t). \qquad (3.9)$$

As long as α is constant, the solution of equation (3.9) is:

$$R(t) = e^{-\alpha t} \qquad\qquad (3.10)$$

being $R(0)=1$ (the channel can't move from the open state in zero time).
The cumulative distribution function $F(t)$ is given by $1-R(t)$:

$$F(t) = \text{Prob}(open\,lifetime \leq t) = 1 - R(t) = 1 - e^{-\alpha t}. \qquad (3.11)$$

The probability density function $f(t)$ can be now drawn from differentiating $F(t)$:

$$f(t) = \frac{dF(t)}{dt} = \alpha e^{-\alpha t}, \qquad t \geq 0. \qquad (3.12)$$

Hence, open lifetime distribution is exponential, and its mean is $1/\alpha$. In fact:

$$E = \int_0^{+\infty} t f(t) dt = \int_0^{+\infty} \alpha t e^{-\alpha t} dt = \frac{1}{\alpha}. \qquad (3.13)$$

Clearly, using an analogous argumentations, it can be shown that also the shut time distribution is exponential with mean $1/\beta$. The case just considered is the simplest one, having only two states. In this case, we found that both open and shut states have lifetime exponentially distributed and the mean values of their distribution are the inverses of the transition rates from the states. In general, for more complex mechanisms, counts the following rule.

Lifetime in every single state is exponentially distributed with mean

=1/(sum of transition rates that lead away from the state).

We aspect besides (and it will be demonstrated in section 3.4.6) that all the distributions of quantities such as open and shut times, and in general all the lifetimes in subsets of the Markov chain, will be mixtures of exponentials. The general form of their p.d.f (probability density function) is then:

$$f(t) = \sum_{i=1}^{n} a_i \, \lambda_i \, e^{-\lambda_i t} \qquad (3.14)$$

where $\sum_{i=1}^{n} a_i = 1$.

3.2 Agonist binding

Let's consider now a generic ligand-gated ion channel *Ch* whose behavior is influenced by the interaction with a specific ligand molecule *L*. The Markov Chain representing the behavior of *Ch* is characterized by the presence of at least one couple of states like the one reported in figure 3.2, where (*Ch*) is the state representing the not bound channel, (*ChL*) the state representing the channel bound to a molecule *L*.
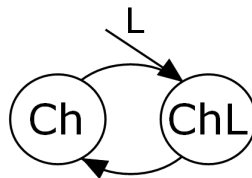
Figure 3.2   Two connected states in a Markov chain with a molecule binding.

Cutting off this couple of states from the rest of the chain pinpointing channel's behaviour, we obtain the following reversible chemical reaction:

$$L + Ch \xrightleftharpoons[k_I]{k_D} ChL \qquad (3.15)$$

where k_D is the velocity constant of the direct reaction, k_I of the inverse reaction. At the equilibrium, the system can be described by this relation:

$$K_{EQ} = \frac{k_D}{k_I} = \frac{[ChL]}{[Ch][L]} \Rightarrow [ChL] = K_{EQ}[Ch][L] \qquad (3.16)$$

where K_{EQ}, the equilibrium constant of the reaction, is the ratio between the molar concentration of the complex ChL and the product of the concentrations of the free (not bound) reagents Ch and L.

In the case of ion channels embedded in a membrane, if we consider negligible the rundown of channels (the possibility of having inserted channels deactivating during the acquisition), the total number of channels N is constant. Since V, the volume of solution surrounding the membrane in which molecules L are inserted and bind the channels, is constant, we can write equation (3.16) in terms of number of molecules taking part in the reaction:

$$\frac{n}{V \times A} = K_{EQ} \frac{N-n}{V \times A} \frac{n_L}{V \times A} \qquad (3.17)$$

where n is the mean number of bound channels, n_L is the number of target molecules, A is Avogadro's number. Note that equation (3.17) doesn't distinguish between total number of target molecules and number of not bound

52

target molecules: this approximation is possible because the total number of target molecules is strongly larger than N. Starting from equation (3.17):

$$n = K_{EQ}(N-n)\frac{n_L}{V \times A} = K_{EQ}(N-n)[L] = \frac{N \times K_{EQ} \times [L]}{1 + K_{EQ} \times [L]}. \qquad (3.18)$$

Since K_{EQ} is constant (for the Le Châtelier's principle), the mean number of bound channels depends on ligand molecule concentration following a not decreasing relation like the one represented in figure 3.3. In particular, this is the relation between the number of bound channels and the ligand molecule concentration, when a specific receptorial site is considered.
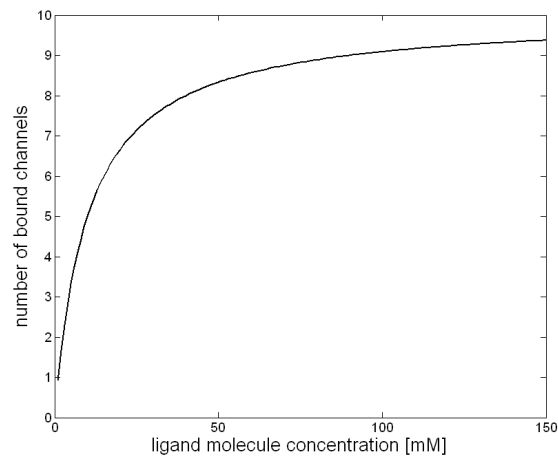
Figure 3.3   number of bound channels as a function of ligand concentration

3.3   Del Castillo-Katz model

An important step in single ion channel modelling was the del Castillo-Katz model (1957), in which a possible mechanism of a ligand gated ion channel was described by a three-state chain, like the one reported in (3.19). In this case, the opening of a channel follows the interaction between the receptor and a single ligand molecule. Using this model, let's consider the case of a channel activated by the agonist and in which the binding and the dissociation steps are fast enough compared with the subsequent conformation change: the vacant state *R* and the occupied state *AR* (where "*A*" indicates the ligand molecule bound) can be considered close to equilibrium at all times. Therefore, vacant and occupied states would behave as a single (shut) state.

$$\underbrace{R \underset{k_I}{\overset{k_D}{\longrightarrow}} AR}_{shut\,"state"} \underset{\alpha}{\overset{\beta}{\longrightarrow}} AR^* \tag{3.19}$$

where the superscript "*" symbolize the open channel condition. From the equilibrium between the vacant and the occupied shut states, the following relation can be drawn:

$$P_R \times k_D \times [A] = P_{AR} \times k_I \tag{3.20}$$

where

P_R is the probability of being in the dissociated (vacant) state;

P_{AR} is the probability of being in the bound shut state;

[A] is the ligand molecule concentration.

In this case, the system behaves basically like the simpler two-states model described by relation (3.3), while the two shut states on the left in (3.19) collapse in a single one. This does not affect the way we look at the shutting reaction, with rate constant α; instead, the transition rate from shut to open can no longer be taken as β, because the "shut state" spends part of its time without ligand bound and, while the receptor is not occupied, opening is impossible. The total shut channel probability is $P_S = P_R + P_{AR}$. Introducing the dissociation constant $K_{DISS} = k_I / k_D$, we have:

$$P_R = P_{AR} \frac{K_{DISS}}{[A]}$$

$$P_S = P_R + P_{AR} = P_{AR} \frac{[A] + K_{DISS}}{[A]} \qquad (3.21)$$

$$\Rightarrow P_{AR} = P_S \frac{[A]}{[A] + K_{DISS}} \Rightarrow \beta' = \beta \frac{[A]}{[A] + K_{DISS}}.$$

Using β' in place of β, the three-state mechanism becomes then formally identical to the two-state mechanism before considered.

3.4 General theory

The general theory for the modelling of the single channel kinetic behaviour was firstly proposed by David Colquhoun and Alan G. Hawkes during the seventies, before the introduction of the patch clamp technique (Neher and Sackmann 1981), which led to the recording of single channel current signals. The complete theory was basically formalised in the first eighties (see, in particular, Colquhoun and Hawkes, 1982). The work of these two scientists strong

influenced the electrophysiology in the last thirty years, giving a general method, applicable to any mechanism, for deriving the distribution of the length of time spent in any specified subset of states.

Given any n-state Markov chain representing a channel mechanism, its mass action transition rate constants can be conveniently specified in a n × n Matrix, denoted Q. The entry in the ith row, jth column, denoted q_{ij}, represent the transition rate from state i to stat j (whenever $i \neq j$), namely

$$q_{ij} = \lim_{\Delta t \to 0} \left[Prob\left(in\, state\, j\, at\, time\, t + \Delta t \mid in\, state\, i\, at\, time\, t \right) / \Delta t \right], \quad i \neq j. \qquad (3.22)$$

The element q_{ij} is obviously set to zero if there is no link from i to j. Diagonal elements ($i = j$) of the matrix, instead, are chosen so that the sum of the elements of every row of Q is zero:

$$q_{ii} = -\sum_{\substack{j=1 \\ j \neq i}}^{n} q_{ij}, \qquad i = 1,...,n. \qquad (3.23)$$

3.4.1 Definition of burst

The states composing the Markov chain can be conveniently divided into subsets, as follows:

1. Subset $\mathscr{A}$ comprises the open states ($k_{\mathscr{A}}$ in number);
2. Subset $\mathscr{B}$ comprises the short-lived shut states ($k_{\mathscr{B}}$ in number);
3. Subset $\mathscr{C}$ comprises the long-lived shut states ($k_{\mathscr{C}}$ in number).

56

Obviously, the distinction between states belonging to subsets $\mathscr{B}$ and $\mathscr{C}$ is basically due to the values of their lifetimes, exponentially distributed around a mean which is, for every state, inversely proportional to the sum of transition rates that lead away from the state. The choice of the limit value for the mean open lifetime is arbitrary, but in practice follows from the qualitative analysis of the single-channel record. Let's consider the signal from a single channel in steady state conditions: all the macroscopic variables which can change its electrical response, such as ligand molecule concentration, transmembrane voltage, pH…are fixed, so that the channel kinetic rates don't change during the acquisition. If the channel is ligand-gated and, in particular, agonist-activated (that is, it can't open if it's not bound with, at least, a ligand molecule) and the ligand concentration is far from saturating , usually openings appear in bursts. A burst is therefore a sequence of openings which appears grouped in the trace, intercalated between shuttings which are greatly shorter than the inter-burst shuttings. The simplest case in which it's possible to observe bursts is the del Castillo-Kats model (3.19), where the binding constant rate is $k_D \times [A]$, and $[A]$ is the ligand concentration. When $[A]$ is very low, the lifetime of the unbound state R is very long, having mean given by $1/(k_D \times [A])$. It can be considered belonging to $\mathscr{C}$. Bursts of openings will be then possible, if k_I is not to high compared to β: they will be formed by the transitions between states AR, belonging to $\mathscr{B}$, and AR^*; belonging to $\mathscr{A}$. It is also possible to note from this example, that the division of states into the subsets defined before is not only, for ligand-dependent ion channels, a characteristic of the reaction mechanism: it depends on the particular values of the rate constants and drug concentrations that are specified.

It can be useful to order the rate constants in a Q matrix so that the lowest $k_{\mathscr{A}}$ indexes correspond to the states of $\mathscr{A}$, while the highest $k_{\mathscr{C}}$ indexes correspond to the elements of $\mathscr{C}$. In this case, according to the subset just

defined, Q matrix can be intended as composed by nine submatrixes as shown in (3.24):

$$Q = \begin{bmatrix} Q_{\mathscr{AA}} & Q_{\mathscr{AB}} & Q_{\mathscr{AC}} \\ Q_{\mathscr{BA}} & Q_{\mathscr{BB}} & Q_{\mathscr{BC}} \\ Q_{\mathscr{CA}} & Q_{\mathscr{CB}} & Q_{\mathscr{CC}} \end{bmatrix}. \tag{3.24}$$

In fact, for ligand-gated channels, there is at list a couple of states like the ones drawn in figure 3.2, where, in presence of a binding between ligand molecule and channel receptive site, the direct reaction constant rate is proportional to the ligand concentration. If the binding is a necessary condition for the channel to open, for low agonist concentrations long shut periods will be observed.

It's possible to define the *n×n* matrix *P(t)*, with elements given by the transition probabilities between the states of the chain:

$$p_{ij}(t) = \text{Prob(state } j \text{ at time } t \mid \text{ state } i \text{ at time zero).} \tag{3.25}$$

So, every element of the Q matrix is given by

$$q_{ij} = \lim_{\Delta t \to 0} \frac{p_{ij}(\Delta t)}{\Delta t}. \tag{3.26}$$

If a system is in any state *i*, the probability that the next transition will be to state *j*, regardless of when the transition occurs, can be denoted π_{ij} and is given by:

$$\pi_{ij} = -\frac{q_{ij}}{q_{ii}} \tag{3.27}$$

where the denominator $-q_{ii}$ is the sum of all the transition rates that lead away from the state *i*.

3.4.2 Probability of staying within a subset

We want now to draw the expressions of the probabilities analogous with $p_{ij}(t)$, but such that the system remains within a specified subset of states, for example $\mathscr{A}$. This approach is useful, because usually receptors are characterised by models containing several open states, all having the same conductance value. In the same way, all the shut states have, obviously, zero conductance. If we observe an opening or a shutting in a record, it's then generally impossible to know if the system sojourned in only one state, or more. It's then important to realise a statistical analysis of the groups of indistinguishable states. First of all it can be defined $p_{ij}^{\mathscr{A}}(t)$ as

$$p_{ij}^{\mathscr{A}}(t) = Prob(system\ remains\ within\ \mathscr{A}\ throughout\ (0,t)$$
$$and\ is\ in\ state\ j\ at\ time\ t\ |\ in\ state\ i\ at\ time\ 0),\qquad i,j \in \mathscr{A}. \qquad (3.28)$$

The same probability, evaluated at time $t+\Delta t$, can be expressed as the probability that the system has to stay in $\mathscr{A}$ in whole the interval $(0,t+\Delta t)$, being in j at time $t+\Delta t$, if it is in *i* at time zero. Obviously, at time *t* the system can be in any state $k \in \mathscr{A}$.

$$p_{ij}^{\mathscr{A}}(t+\Delta t) = \sum_{k \in \mathscr{A}} \{ Prob[system\ remains\ within\ \mathscr{A}\ throughout\ (0,t)$$
$$and\ is\ in\ state\ k\ at\ time\ t\ |\ in\ state\ i\ at\ time\ 0] \times \qquad (3.29)$$
$$\times Prob(state\ j\ at\ t+\Delta t\ |\ in\ state\ k\ at\ t)\},\qquad i,j \in \mathscr{A}.$$

So, it's possible to write out $p_{ij}^{\mathscr{A}}(t+\Delta t)$ as a sum of terms, each formed by two factors. The first factor is, according to (3.28), $p_{ik}^{\mathscr{A}}(t)$. When $k \neq j$, the second one is (similarly to (3.4)), $q_{kj}\Delta t + o(\Delta t)$; instead, for $k = j$, it results *1-Prob(leave k)*, that is $1 + q_{kk}\Delta t + o(\Delta t)$, since q_{kk} is the opposite of the sum of the rates that lead away from *k*. Thus, in matrix notation we have

$$P_{\mathscr{A}}(t+\Delta t) = P_{\mathscr{A}}(t)[I + Q_{\mathscr{A}}\Delta t + o(\Delta t)]. \tag{3.30}$$

In fact, the sums $\sum p_{ik}(t)q_{kj}\Delta t, i,k,j \in \mathscr{A}$ form the matrix product $P_{\mathscr{A}}(t)Q_{\mathscr{A}}\Delta t$, and a unity is added to the elements of the diagonal by the identity matrix. Therefore

$$\frac{dP_{\mathscr{A}}(t)}{dt} = \lim_{\Delta t \to 0}\frac{P_{\mathscr{A}}(t+\Delta t) - P_{\mathscr{A}}(t)}{\Delta t} = P_{\mathscr{A}}(t)\,Q_{\mathscr{A}}. \tag{3.31}$$

As $P_{\mathscr{A}}(0) = I$ (no transitions are possible in zero time), the solution of (3.31) is

$$P_{\mathscr{A}}(t) = exp(Q_{\mathscr{A}}t). \tag{3.32}$$

These results were drawn for the subset $\mathscr{A}$ but, clearly, analogous relations apply to all the other subsets, and also for the whole system.
The Laplace transform of $P_{\mathscr{A}}(t)$, that will be used afterwards, is

$$P_{\mathscr{A}}^{*}(s) = \mathscr{L}\{P_{\mathscr{A}}(t)\} = (sI - Q_{\mathscr{A}})^{-1}. \tag{3.33}$$

We aim now to obtain a practical way for calculating the transition probabilities matrixes, like the one defined in (3.32). This can be done by using the spectral expansion of $Q_{\mathscr{A}\mathscr{A}}$ (see appendix A): this rate constant matrix can be expressed by

$$Q_{\mathscr{A}\mathscr{A}} = \sum_{i=1}^{k_{\mathscr{A}}} A_i\, \rho_i \qquad (3.34)$$

where the scalars ρ_i are the eigenvalues of $Q_{\mathscr{A}\mathscr{A}}$ (and they are usually, for ion channel models, all distinct and not positive) and the matrices A_i can be obtained from the eigenvectors of $Q_{\mathscr{A}\mathscr{A}}$. Calling λ_i the eigenvalues of $-Q_{\mathscr{A}\mathscr{A}}$ (therefore, $\lambda_i = -\rho_i, \quad i = 1,...,k_{\mathscr{A}}$), we have

$$P_{\mathscr{A}\mathscr{A}}(t) = \sum_{i=1}^{k_{\mathscr{A}}} A_i\, e^{-\lambda_m t} \qquad (3.35)$$

which demonstrates that all the transition probabilities are formed by a mixture of exponential terms.

3.4.3 Equilibrium state occupancies

An important thing to know, for the following analysis, is the fraction of molecules in each state at equilibrium: in order to do it, we shall denote the occupancy of state i at time t as $p_i(t)$, and $p(t)$ the $1 \times n$ vector including the occupancies for each of the n states. The corresponding vector of derivatives is given by (3.36).

$$\frac{dp(t)}{dt} = \left[\frac{dp_1(t)}{dt} \quad \frac{dp_2(t)}{dt} \quad ... \frac{dp_n(t)}{dt} \right].$$

(3.36)

The kinetic equations that describe the system state occupancies can be written as

$$\frac{dp(t)}{dt} = p(t)Q$$

(3.37)

in fact, equation (3.37) states that each element of the derivative vector is given by

$$\frac{dp_i(t)}{dt} = \sum_{j=1}^{n} p_j(t)q_{ji}, \qquad i = 1,...,n$$

(3.38)

namely, the sum of the probabilities of being, at time t, in each state of the system, multiplied for the frequencies of the transitions to i state, as follows from the law of mass action. When $i=j$, the addend is negative, and its modulus is the probability of being in i state, multiplied for the sum of the rates leading away from i. Since in steady state the derivative terms must be zero, the equilibrium values must satisfy the system (3.39).

$$\begin{cases} p(\infty)Q = 0 \\ \sum_{i=1}^{n} p_i = 1 \end{cases}$$

(3.39)

where the last equation is due to the fact that the probability of being in one of the states of the system must clearly be 1. The system, therefore, has n+1 equations and only n unknowns (in fact, the determinant of the Q matrix is zero). Several "tricks" for obtaining the $p(\infty)$ vector for any mechanism in a straightforward way are available: for example, it can be directly calculated by adding a unit column (with all values set to 1) on the right end of the Q matrix. Calling S this $n\times(n+1)$ matrix, vector $p(\infty)$ can be calculated as

$$p(\infty) = u_n (SS^T)^{-1}.$$ (3.40)

where u_n is a row vector with n elements.

3.4.4 Transition from a subset to another

It should be interesting to obtain the expression of the density that describes the probability of staying within the subset of states $\mathscr{A}$ for the time t and then leaving it for a state outside (for example, in subset $\mathscr{B}$). We start then defining it:

$$g_{ij}(t) = \lim_{\Delta t \to 0} [Prob(stay\ in\ \mathscr{A}\ throughout\ (0,t), and\ move\ to\ j$$
$$between\ t\ and\ t + \Delta t\ |\ in\ state\ i\ at\ time\ 0)\ /\ \Delta t\,], \qquad i \in \mathscr{A}, j \in \mathscr{B}.$$ (3.41)

It means to consider all the possible paths between *i* and *j* which go out from the subset $\mathscr{A}$ through each possible state $r \in \mathscr{A}$

$$g_{ij}(t) = \sum_{r \in \mathscr{A}} p_{ir}^{\mathscr{A}}(t) q_{rj}, \qquad i \in \mathscr{A}, j \in \mathscr{B}$$ (3.42)

that is, in matrix notation (and remembering (3.32))

$$G_{\mathscr{AB}}(t) = P_{\mathscr{AA}}(t)Q_{\mathscr{AB}} = exp(Q_{\mathscr{AA}} t)Q_{\mathscr{AB}}.$$ (3.43)

The elements $g_{ij}(t)$ can't be properly considered probability density functions, because they haven't a unitary subtended area: thus, in order to obtain the *p.d.f*s, they must be shared by a normalizing term, namely their area, given by

$$\int_0^\infty g_{ij}(t)dt = Prob(exits\ to\ j\ |\ starts\ in\ i), \qquad i \in \mathscr{A}, j \in \mathscr{B}$$ (3.44)
$$= g_{ij}^*(0)$$

where $g_{ij}^*(0)$ is the Laplace transform of $g_{ij}(t)$ for s=0. It can be easily calculated from the Q matrix: in fact, the transform of $G_{\mathscr{AB}}(t)$ (as expressed in 3.43) results, remembering 3.33

$$G_{\mathscr{AB}}^*(s) = P_{\mathscr{AA}}^*(t)Q_{\mathscr{AB}} = (sI - Q_{\mathscr{AA}})^{-1}Q_{\mathscr{AB}}.$$ (3.45)

It can be useful to define the constant matrix $G_{\mathscr{AB}}$, as

$$G_{\mathscr{AB}} \equiv G_{\mathscr{AB}}^*(0) = -Q_{\mathscr{AA}}^{-1}Q_{\mathscr{AB}}.$$ (3.46)

Its elements will be denoted $g_{ij} \equiv g_{ij}^*(0)$. Note that, if the subset $\mathscr{A}$ is composed by just one state *i*, g_{ij} corresponds to the previous defined π_{ij} (expression (3.27)), because there aren't possible transitions inside $\mathscr{A}$, so the first transition from *i* is the one leading to *j*. We can now define a probability

density function for the lifetime of sojourn in $\mathscr{A}$, given the starting and the exit states, as

$$f_{ij}(t) = \frac{g_{ij}(t)}{g_{ij}^*}.$$
(3.47)

The corresponding distribution function is then

$$F_{ij}(t) = \int_0^t f_{ij}(t)\,dt = Prob(life\,in\,\mathscr{A} \leq t \mid exits\,to\,j\,and\,starts\,in\,i), \quad i \in \mathscr{A},\,j \in \mathscr{B}.$$
(3.48)

Since now we described the way in which a sojourn in $\mathscr{A}$ ends, specifying the state in $\mathscr{B}$ where the system moves going out from the subset $\mathscr{A}$. Obviously, if the subset $\mathscr{A}$ is composed by more than one state, this kind of distribution can't completely define the system. It will be then defined an alternative distribution, by specifying the state in $\mathscr{A}$ from which exit from the subset occurs, without caring about the state of $\mathscr{B}$ in which the system enters the new subset. First of all, it can b defined $h_{ij}(t)$ as

$$h_{ij}(t) = \lim_{\Delta t \to 0}[Prob(stay\,in\,\mathscr{A}\,from\,time\,0\,to\,time\,t, and\,leave\,\mathscr{A}\,from$$
$$state\,j\,between\,t\,and\,t + \Delta t \mid in\,state\,i\,at\,time\,0)\,/\,\Delta t], \qquad i,j \in \mathscr{A}.$$
(3.49)

with Laplace transform, for s=0, given by

$$h_{ij}^*(0) = \int_0^\infty h_{ij}(t)\,dt = Prob(exits\,from\,j \mid starts\,in\,i), \qquad i,j \in \mathscr{A}.$$
(3.50)

65

So, every element $h_{ij}(t)$ is given by all the possible routes such that the system remains in $\mathscr{A}$ throughout *(0,t)*, starting from $i \in \mathscr{A}$, and then go out from the subset from $i \in \mathscr{A}$ to any state $r \in \mathscr{B}$:

$$h_{ij}(t) = p_{ij}^{\mathscr{A}}(t) \sum_{r \in B} q_{jr}, \qquad i, j \in \mathscr{A} \qquad (3.51)$$

that is, in a matrix form

$$H_{\mathscr{A}\mathscr{A}}(t) = P_{\mathscr{A}\mathscr{A}}(t) D_{\mathscr{A}} \qquad (3.52)$$

where $D_{\mathscr{A}}$ is a diagonal matrix with elements $\sum q_{jr}$. It is possible to define now, in analogous to (3.47), the probability density function

$$f_{ij}'(t) = h_{ij}(t)/h_{ij}^{*}(0) \qquad i, j \in \mathscr{A}. \qquad (3.53)$$

But factor $d_{jj} = \sum_{r \in \mathscr{B}} q_{jr}$ is present both in the numerator and in the denominator; therefore, it cancels (as long as it's not zero) and the expression becomes

$$f_{ij}'(t) = p_{ij}^{\mathscr{A}}(t)/p_{ij}^{\mathscr{A}*}(0) \qquad i, j \in \mathscr{A} \qquad (3.54)$$

which corresponds to the distribution function

$$\int_{0}^{t} f_{ij}'(t)\, dt = Prob(life\, in\, \mathscr{A} \leq t \mid exits\, from\, j\, and\, starts\, in\, i), \qquad i, j \in \mathscr{A}. \qquad (3.55)$$

66

3.4.5 Burst analysis

Let's consider a sort of problem in which we are interested only in the probability of having a particular sequence of transitions, and not in the time spent in each state. For example, it could be interesting to know the probability of having a burst including a certain number of openings. In the simplest possible case, namely $k_{\mathscr{A}} = k_{\mathscr{B}} = 1$, the probability of starting from the state $1 \in \mathscr{A}$, going to $2 \in \mathscr{B}$ and coming back is $\pi_{12}\,\pi_{21}$ or, equally, $g_{12}\,g_{21}$. Instead, if $\mathscr{A}$ is composed by two states (1 and 2) and also $\mathscr{B}$ is formed by two states (3 and 4), we need to know, in order to calculate the probability of going from $\mathscr{A}$ to $\mathscr{B}$ and coming back, the probabilities of starting from state 1 and from state 2. Calling $\Phi_b = [\phi_1\ \phi_2]$ the $k_{\mathscr{A}}$ column vector, where ϕ_1 is the probability of starting from state 1, ϕ_2 the one of starting from state 2 (with $\phi_1 + \phi_2 = 1$), we find that the probability of an $\mathscr{A} \to \mathscr{B} \to \mathscr{A}$ transition that ends in state 1 is

$$\phi_1\left(g_{13}\,g_{31} + g_{14}\,g_{41}\right) + \phi_2\left(g_{23}\,g_{31} + g_{24}\,g_{41}\right) \tag{3.56}$$

which is the first element of the $(k_{\mathscr{A}} \times 1)$vector

$$\Phi_b\, G_{\mathscr{A}\mathscr{B}}\, G_{\mathscr{B}\mathscr{A}} \tag{3.57}$$

whose second element is the probability of a $\mathscr{A} \to \mathscr{B} \to \mathscr{A}$ transition starting in state 1 and ending in state 2. The result expressed in (3.57) is valid for every value of $k_{\mathscr{A}}$ and $k_{\mathscr{B}}$. The overall probability of the $\mathscr{A} \to \mathscr{B} \to \mathscr{A}$ transition is the sum of the elements of the vector (3.57), given by (3.58).

$$\Phi_b\, G_{\mathscr{AB}}\, G_{\mathscr{BA}}\, u_{\mathscr{A}} \qquad\qquad (3.58)$$

where $u_{\mathscr{A}}$ is simply a unit $k_{\mathscr{A}} \times 1$ vector. So ,if $\mathscr{A}$ includes more than one state, the characterization of bursts implies the knowledge of the initial state probabilities vector Φ_b. The period before the beginning of a burst is characterized by at least one sojourn in $\mathscr{C}$; so, we can take as a starting point the fraction of channels that is in each state of $\mathscr{C}$ at equilibrium, forming the $k_{\mathscr{C}}$ column vector $p_{\mathscr{C}}(\infty)$ (it can be obtained from (3.40)). A burst starts when the system reaches the subset $\mathscr{A}$ from subset $\mathscr{C}$: it can happen with a direct transition $\mathscr{C} \to \mathscr{A}$ or through $\mathscr{B}$. The frequency of transitions directly from $i \in \mathscr{C}$ to $j \in \mathscr{A}$ is given by $p_i(\infty)q_{ij}$; instead, the number of transitions $\mathscr{C} \to \mathscr{B} \to \mathscr{A}$ per unit time is

$$p_i(\infty)\sum_{k\in\mathscr{B}} q_{ik}\, g_{kj}, \qquad i\in\mathscr{C}, j\in\mathscr{A}. \qquad\qquad (3.59)$$

The result, in matrix notation, is that the vector Φ_b of the initial state probabilities is

$$\Phi_b = \frac{p_{\mathscr{C}}(\infty)(Q_{\mathscr{CB}}\, G_{\mathscr{BA}} + Q_{\mathscr{CA}})}{p_{\mathscr{C}}(\infty)(Q_{\mathscr{CB}}\, G_{\mathscr{BA}} + Q_{\mathscr{CA}})u_{\mathscr{A}}} \qquad\qquad (3.60)$$

where the denominator is simply a scalar term for normalising Φ_b (since the sum of its elements must be one). The end of a burst, instead, is when there is a transition, directly or through $\mathscr{B}$, from $\mathscr{A}$ to $\mathscr{C}$. It' is possible to define a

68

$k_{\mathscr{A}} \times 1$ vector, e_b (the subscript stands for "burst"), whose elements are the probabilities of ending a burst having the elements of $\mathscr{A}$ as the last open state:

$$e_b = (G_{\mathscr{A}\mathscr{C}} + G_{\mathscr{A}\mathscr{B}}\, G_{\mathscr{B}\mathscr{C}}\,)u_{\mathscr{C}}\,. \qquad (3.61)$$

The postmultiplication by the unit vector $u_{\mathscr{C}}$ sums the probabilities over all $\mathscr{C}$ states, because arrival in any long-shut state ensures the end of the burst. It can also be demonstrated, starting from (3.61), that

$$e_b = (I - G_{\mathscr{A}\mathscr{B}}\, G_{\mathscr{B}\mathscr{A}}\,)u_{\mathscr{A}}\,. \qquad (3.62)$$

This result is intuitive: in fact, (3.61) expresses the overall probabilities of moving from each state of $\mathscr{A}$ to the subset $\mathscr{C}$, that are the probabilities of finishing a burst. To exit from the burst is obviously the complementary event of not to exit from it, therefore the sum of the two complementary events must be one and is represented by the identity matrix.

3.4.6 Distribution of the open time

It is now possible to define the time distribution of the latency in a subset of states, for example, the open state subset $\mathscr{A}$. Calling $\mathscr{F}$ the subset including all the shut states ($\mathscr{F} = \mathscr{B} \cup \mathscr{C}$), the matrix $G_{\mathscr{A}\mathscr{F}}$ describe the time from the start of an opening, through any number of transitions within open states (subset $\mathscr{A}$), until eventually exit to any of the shut states (subset $\mathscr{F}$). The distribution function of the open length can be then written, using an expression of $G_{\mathscr{A}\mathscr{F}}$ analogous to the one in (3.43), in the form (3.63).

$$f_{\mathscr{A}}(t) = \Phi_0\, G_{\mathscr{AF}}\, u_{\mathscr{F}} = \Phi_0\, exp(Q_{\mathscr{AA}}\, t) Q_{\mathscr{AF}}\, u_{\mathscr{F}} = \Phi_0\, exp(Q_{\mathscr{AA}}\, t)(-Q_{\mathscr{AA}})\, u_{\mathscr{A}} \qquad (3.63)$$

where Φ_0 is the $1 \times k_{\mathscr{A}}$ initial vector giving the probability of each opening starting in a specified open state. It is clearly given by:

$$\Phi_0 = \frac{p_{\mathscr{F}}(\infty) Q_{\mathscr{FA}}}{p_{\mathscr{F}}(\infty) Q_{\mathscr{FA}}\, u_{\mathscr{A}}} \qquad (3.64)$$

where, similarly to (3.60), the denominator is simply a normalisation term, while the numerator expresses the probability of being in each state of $\mathscr{F}$, multiplied for the probability of transition to an open state. The matrix relationship

$$Q_{\mathscr{AA}}\, u_{\mathscr{A}} + Q_{\mathscr{AF}}\, u_{\mathscr{F}} = 0 \qquad (3.65)$$

follows from the fact that the rows of the overall transition matrix Q must add to zero. The matrix exponential can be practically computed using the spectral expansion (see appendix A). Note that expression (3.63) shows that the permanency in each subset of states of the Markov chain as a distribution given by a mixture of exponential terms.

3.4.7 Number of openings per burst

The probability of starting a burst from each of the states of $\mathscr{A}$ is Φ_b (3.60), while the probability of ending a burst having each of the states of $\mathscr{A}$ as the last open state is e_b (3.62). Inside the burst, every opening is due to a double

passage $\mathscr{A} \to \mathscr{B} \to \mathscr{A}$, having probabilities $G_{\mathscr{AB}} G_{\mathscr{BA}}$. Therefore, the probability of a burst with r openings ($r = 1,...,\infty$) is

$$P(r) = \Phi_b (G_{\mathscr{AB}} G_{\mathscr{BA}})^{r-1} e_b = \Phi_b (G_{\mathscr{AB}} G_{\mathscr{BA}})^{r-1} (I - G_{\mathscr{AB}} G_{\mathscr{BA}}) u_{\mathscr{A}} \qquad (3.66)$$

and the probability of a burst containing, at least, r openings, is

$$P(r \geq i) = \Phi_b (G_{\mathscr{AB}} G_{\mathscr{BA}})^{i-1} u_{\mathscr{A}} \qquad (3.67)$$

where, compared to (3.66), the factor $(I - G_{\mathscr{AB}} G_{\mathscr{BA}})$, forcing the shutting, has disappeared. The mean number of openings per burst is

$$E = \Phi_b \left[\sum_{r=1}^{\infty} r (G_{\mathscr{AB}} G_{\mathscr{BA}})^{r-1} \right] (I - G_{\mathscr{AB}} G_{\mathscr{BA}}) u_{\mathscr{A}} \qquad (3.68)$$

Since it can be demonstrated that $\sum_{r=1}^{\infty} r H^{r-1} = (I - H)^{-2}$ we have

$$E = \Phi_b (I - G_{\mathscr{AB}} G_{\mathscr{BA}})^{-1} u_{\mathscr{A}}. \qquad (3.69)$$

The distribution P(r), defined in (3.66), can be written as a sum of exponential terms: in fact, the $k_{\mathscr{A}}$ square matrix $G_{\mathscr{AB}} G_{\mathscr{BA}}$ can be written in the form of its spectral expansion:

$$G_{\mathscr{AB}} G_{\mathscr{BA}} = \sum_{i=1}^{k_{\mathscr{A}}} A_i \rho_i \qquad (3.70)$$

where it can be demonstrated that the eigenvalues of the matrix $G_{\mathscr{A}\mathscr{B}} G_{\mathscr{B}\mathscr{A}}$, ρ_i, are all between zero and one. The matrixes A_i can be found from the eigenvector of the same matrix (see appendix A). The distribution P(r) can be then written in the form

$$P(r) = \Phi_b \sum_{i=1}^{k_{\mathscr{A}}} \left(A_i \, \rho_i^{r-1} \right) e_b = \sum_{i=1}^{k_{\mathscr{A}}} w_i \, \rho_i^{r-1} \tag{3.71}$$

where the terms w_i, weight of a $k_{\mathscr{A}}$ geometric distribution, are given by

$$w_i = \Phi_b \, A_i \, e_b . \tag{3.72}$$

3.4.8 Burst length

In the last section, the probabilities regarding the number of openings per burst were drawn, without considering the length of time spent in the burst. In order to extract the probability density function of the burst time length, the expression describing all the possible routes through the Markov chain, inside a burst, must be considered. It can be carried out from equation (3.66), which states the probability of having a certain number r of openings. A burst can cover every possible number of openings ($r = 1, 2, ..., \infty$): therefore, all these probabilities must be added. Equation (3.66) was calculated considering the Laplace transforms of the G matrices, setting $s=0$; in this case, instead, we are looking for a time distribution: s is not set to zero for the periods spent in the burst. The Laplace transform of the required p.d.f. is, considering that $\sum_{r=1}^{\infty} H^{r-1} = (I - H)^{-1}$

72

$$f^*(s) = \sum_{r=1}^{\infty} \Phi_b \left[G^*_{\mathcal{AB}}(s) G^*_{\mathcal{BA}}(s) \right]^{r-1} \left[G^*_{\mathcal{AB}}(s) G_{\mathcal{BC}} + G^*_{\mathcal{AC}}(s) \right] u_{\mathcal{C}}$$

$$= \Phi_b \left[I - G^*_{\mathcal{AB}}(s) G^*_{\mathcal{BA}}(s) \right]^{-1} \left[G^*_{\mathcal{AB}}(s) G_{\mathcal{BC}} + G^*_{\mathcal{AC}}(s) \right] u_{\mathcal{C}} \qquad (3.73)$$

where the end of burst vector e_b is expressed in the form shown in eq. (3.61) and matrix $G_{\mathcal{BC}}$ is kept with $s=0$ because it describes the final transition $\mathcal{B} \rightarrow \mathcal{C}$, not included in the burst. This transform can be inverted, leading to the p.d.f. expression:

$$f(t) = \Phi_b \left[exp(Q_{\mathcal{EE}} t) \right]_{\mathcal{AA}} (-Q_{\mathcal{AA}}) e_b = \Phi_b \left[exp(Q_{\mathcal{EE}} t) \right]_{\mathcal{AA}} (Q_{\mathcal{AB}} G_{\mathcal{BC}} + Q_{\mathcal{AC}}) u_{\mathcal{C}} \quad (3.74)$$

where subset $\mathcal{E}$ is defined as $\mathcal{E} = \mathcal{A} \cup \mathcal{B}$ (namely, it includes the open and the short-lived shut states). The expression $\left[exp(Q_{\mathcal{EE}}(t)) \right]_{\mathcal{AA}}$ indicates the submatrix obtained from $exp(Q_{\mathcal{EE}}(t))$ considering only the rows and columns corresponding to the states in $\mathcal{A}$.

3.4.9 Total open time per burst

This case is similar to the total burst length case, but now we are interested only in the time spent in states belonging to $\mathcal{A}$. Laplace transform is the same as in (3.73), but now in the term $G^*_{\mathcal{BA}}(s)$, s is set to zero because the time spent in $\mathcal{B}$ mustn't be considered:

$$f_{open}^*(s) = \Phi_b \left[I - G^*_{\mathcal{AB}}(s) G_{\mathcal{BA}} \right]^{-1} \left[G^*_{\mathcal{AB}}(s) G_{\mathcal{BC}} + G^*_{\mathcal{AC}}(s) \right] u_{\mathcal{C}} \qquad (3.75)$$

73

The inverse transform of (0.75) is:

$$f_{open}(t) = \Phi_b \, exp(V_{AA} \, t)(Q_{AB} \, G_{BC} + Q_{AC})u_C \qquad (3.76)$$

where $V_{AA} = Q_{AA} + Q_{AB}G_{BA}$.

3.4.10 Practical definition of burst

From the empirical point of view, we can approximate a burst as any series of openings separated by gaps shorter than some specified duration, say t_{crit}. It's than clear that is important (and not always so easy) to define a correct value for t_{crit}, such that the number of bursts picked out from an experimental record is insensitive to the exact number chosen. If we suppose that the distribution of all shut periods in the record can be described by a probability density function that is the sum of several exponential terms (see (3.35))

$$f(t) = \sum w_i \, e^{-\lambda_i t} \qquad (3.77)$$

then the number of burst will be, the number of interburst shut times minus one; the number of interburst shut times coincide with the number of shut times lasting more than t_{crit}. Calling $N+1$ the number of openings in a record (while N is the number of gaps), the number of interburst gaps will be N_I given by:

$$N_I = N \, Prob(shut \, period \geq t_{crit}) = N \int_{t_{crit}}^{\infty} f(t) \, dt$$
$$= N \sum (w_i / \lambda_i) e^{-\lambda_i \, t_{crit}} \qquad (3.78)$$

74

The equation above shows that N_l is a monotonically decreasing function of t_{crit} (since all the eigenvalues λ_i are non negative); an adequate separation into bursts will be then possible only if the time constant of the exponentials in (3.78) are well separated, so that, once the faster components have died away, the components remaining are so slow that, on the relevant time scale, the function derivative is close to zero.

3.4.11 Definition of cluster

As it was described defining the burst, long lived shut states belonging to $\mathscr{C}$ are usually states describing the binding of target molecules. In particular, if a channel has more than one receptive site, and it can open only when at least n of these sites are occupied, all the states corresponding to a number of bound ligand molecules m<n belong to $\mathscr{C}$, for low values of agonist concentration. Bursts can be observed, and the inter-burst shuttings occur when not enough agonist molecules are bound with the channel. Intuitively, if the agonist concentration is increased, the inter-burst period will become progressively shorter, because the binding probability of each channel receptive site will increase. In saturating conditions, in practice, all the receptive sites are always bound: therefore, we shouldn't observe long shuttings but only a continuous, fast flipping of the channel current level. Instead, records usually continue to show long shut periods, even longer than the inter-bursts shuttings. This have been modelled inserting in the Markov chains very long-lived shut states, often connected to the open ones: they were called desensitized states. In the example reported in figure 5.13, which refers to the homomeric α_2 glycine receptor model characterised in this thesis, D_1 and D_2 are desensitized states: they can be reached only from the open states, but these passages are infrequent, because the rates leading to D1 and D2 are greatly smaller than the

rates α_3. The long sojourns in D_1 and D_2 states delimited periods of intense channel activities, called clusters. All the clusters analysis is similar to the burst one, eventually introducing a fourth subset of states, including the desensitized states. For intermediate values of the agonist concentration, things become more complicated, because both bursts and clusters appear, as it was firstly observed by Sakmann et al. (1980). In model used for single channel analysis, desensitized states usually aren't considered, because it's impossible to characterize their connecting rates, as it will be discussed in Chapter 5.

4 SINGLE CHANNEL OPEN PROBABILITY ESTIMATION

4.1 Introduction

In this chapter, it will be shown a possible approach for estimating the single channel open state probability directly from signal records. In particular, this approach refers to the signal derived from a BLM in which is inserted a limited number of active ligand gated ion channels (up to 20, say). The number of inserted channels is a random variable, since the methods for inserting the channels into a BLM don't allow to fix it (see section 2.6). The open state probability was chosen, as a parameter to relate to the ligand molecule concentration, because the curve representing the relationship between ligand concentration and open state probability is usually monotonically increasing in a wide range (see for example the case of the heteromeric glycinergic receptor, reported in figure 6.4).

4.2 Signal analysis

A single ion channel can be modelled by a continuous time Markov chain in which any state represent a possible conformations of the protein: some of these are "open" states (allowing current to flow), the other ones are "shut" states, as discussed in Chapter 3. In many cases, all open states are characterized by the same conductance: the electrical signal deriving from a single ion channel is then similar to a random telegraph signal, that is a purely random signal which may assume two distinct values: "0", corresponding to the shut channel condition, and "1", the open channel condition. Their levels can be represented, at a given time, as a Bernoulli random variable with open probability p and shut probability $1-p$. For N ion channels of the same type

inserted in a biomimetic membrane, behaving independently from one another, the number of open channels can be represented, at a given time, as a binomial random variable N_{OPEN}, with N and p as parameters. The instantaneous current I_1 from a single open channel, instead, can be intended as a Gaussian random variable, characterized by a mean value $<I>_1$ and a variance σ^2 due to both instrumentation error (σ^2_{instr}) and intrinsic channel current variance (σ^2_{ch}). The probability density function (p.d.f.) for the current intensity provided by N channels of the same type embedded in a membrane is then (in absence of leakage currents):

$$f(I) = \sum_{j=0}^{N} w_j \frac{1}{\sqrt{2p}\,\sigma_j} exp\left\{-\frac{\left(I-<I>_j\right)^2}{2\sigma_j^2}\right\}$$ (4.1)

where:

$\sigma_j^2 = \sigma_{instr}^2 + j\,\sigma_{ch}^2$ is the overall variance of the jth Gaussian bell;

$<I>_j = j<I>_1$ is the mean current amplitude in correspondence of j open channes;

$w_j = \binom{N}{j} p^j (1-p)^{N-j}$ is the weight of the jth Gaussian bell.

In practice, it's a sum of N + 1 Gaussian variables, each relating to the condition of having a certain number N_{OPEN} of open channels (between 0 and N); w_i is the probability of having N_{OPEN}=j , given by the expression of the binomial random variable

The histogram reporting the number of signal samples for given discrete-amplitude current bins can be described by a succession of couples: C_m=(I_m,

78

h_m), where m=1,2,…N_{BIN} (N_{BIN} is the number of bin used for discretise the current axis), I_m is the nominal current value for the mth bin and h_m is the number of samples in the bin.
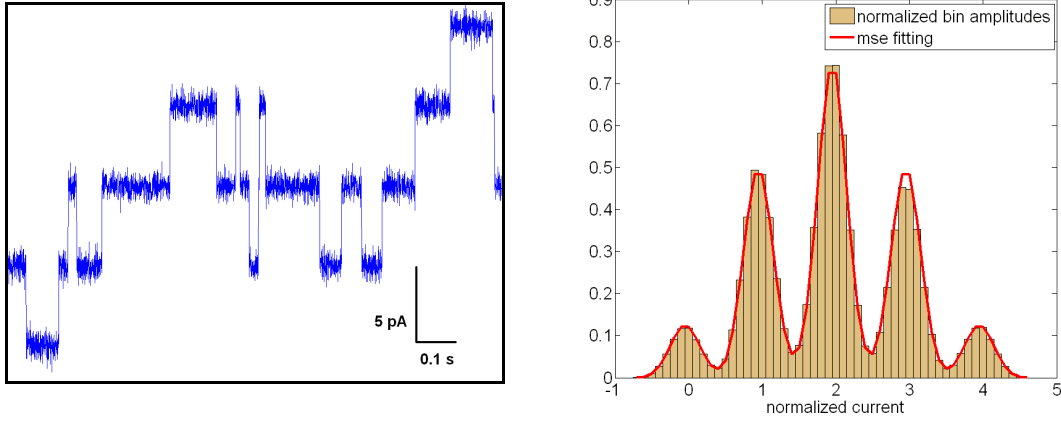
Figure 4.1   Time varying signal and statistical distribution of four ion channels. Left, ionic current versus time with added Gaussian noise having $\sigma_{instr} = 0.1 \times < I >_1$ and $\sigma_{ch} = 0.03 \times < I >_1$. Right, statistical distribution used for PDF fitting. Current values were normalized sharing them for <I>$_1$.

The succession of values, normalized in order to have a unitary subtended area, becomes: $\tilde{c}_m = (I_m, \tilde{h}_m)$, where

$$\tilde{h}_m = \frac{h_m}{\Delta I \sum_{m=1}^{N_{BIN}} hm}, \quad \forall m = 1, 2, ..., N_{BIN} \qquad (4.2)$$

where ΔI is the bin width.

The normalized values of simulated ion current $\tilde{c}_m$, are well-fitted by the current probability density function f(I).

On the hypothesis that the number N of active channels correctly implanted in the membrane does not change during data recording (namely, there is no rundown during the acquisition), and assuming that the standard deviation of the superimposed instrument-related Gaussian noise σ_{instr} is known from a previous calibration and that σ_{ch} is known from the knowledge of the channel's behaviour, it's possible to estimate p and N by fitting the distribution of normalized experimental data with the probability density function f(I), according to equation (4.1). The fitting is achieved by a numerical procedure through a minimization of the square error function Θ(p,N) where:

$$\Theta(p,N) = \sum_{m=1}^{N_{BIN}} \left[f(I) - \tilde{h}_m \right]^2 \tag{4.3}$$

The algorithm estimates the single channel open state probability for each value of the number of inserted channels not greater than a maximum considered number of channels (N_{MAX}) and stores such probability values in a vector with dimension N_{MAX}. The value of the vector corresponding to the minimum square error is actually the correct value of p (and its position corresponds to the correct number of channels). For ligand-gated ion channels, a sigmoidal relationship occurs between open probability and ligand concentration, at least until deep saturation conditions are not achieved. Thus, in a wide range, single channel open probability depends on ligand concentration by a monotonic function. Therefore, by using a known relationship it is possible to determine the concentration value from the knowledge of the model of the ion channel's behaviour and the estimated value of p.

4.3   Simulation results

In order to test the algorithm, a Monte Carlo simulator was realized: it simulates the signal produced by a limited number (not greater than 20) of ion channels of the same type. Each of these channels was modelled by a Del Castillo Katz model, with a dissociation constant of $1.7 \times 10^{-6} M^{-1} s^{-1}$ and an efficacy $E = \beta / \alpha = 1.2$. In particular, these data refer to a muscarinic acetylcholine receptor (Noma, Osterrieder, 1980), whose opening, actually, is mediated by a G protein coupling. Used simulator added a noise due to instrumentation as large as the single channel mean current ($\sigma_{instr} = 0.5 \times < I >_1$) and intrinsic channel current variability ($\sigma_{ch} = 0.05 \times < I >_1$).
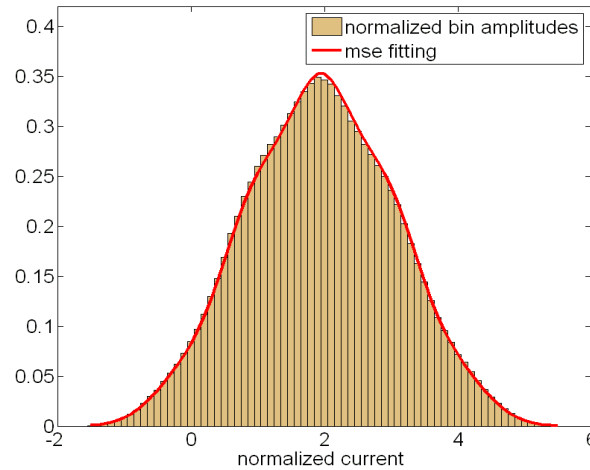
Figure 4.2   Time varying signal and statistical distribution of four ion channels, in correspondence of an added noise equal to the one used for simulations ($\sigma_{instr} = 0.5 \times < I >_1$).

A comparison between the a priori known open state probability value and the estimated one was realized, as described by the scheme in figure 4.3.
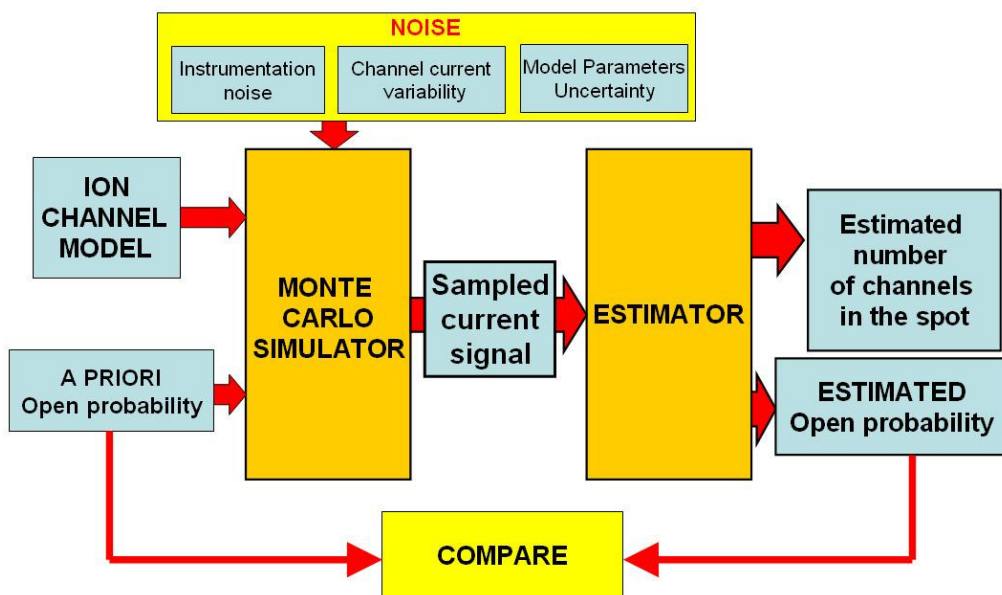
Figure 4.3   Block diagram. A Monte Carlo simulator produce a signal mimicking the stochastic electrical behaviour of an unknown (but limited) number of ion channels embedded in the same BLM, in correspondence of a given agonist molecule concentration. The single channel open state probability (and the number of inserted channels) are then estimated.

Open State Probability	Mean Percentage Error
0.001	21.20%
0.005	2.93%
0.01	3.02%
0.05	0.86%
0.1	0.58%
0.5	0.15%

Table 4.1   Results of the estimation of p. 20 simulations per group were performed, each with a number of inserted channels between 1 and 12.

Results obtained from simulated records (lasting 2 hours, 20 records for each concentration value, each containing a number of channels between 1 and 12) are reported in the table 1. In particular, mean percentage error were calculated as:

$$mean\ percentage\ error = \left(\frac{\langle |expected\ value - estimated\ value| \rangle}{expected\ value} \right) \times 100 \qquad (4.4)$$

Considering an array approach, in which a large number of spots, each containing a planar artificial membrane with a limited number of ligand-gated embedded ion channels and an electronic interface for collecting the data, algorithm performance could significantly improve: simple averaging among values of p derived from single spots analysis produces an error reduction as high as the square root of the number of spots. Moreover, interpolating data could allow to produce a right estimation also of very low values of p. In fact, for example, when the number of channels N of a single spot is overestimated (it happens in correspondence of low values of p), p is underestimated and vice versa; usually, when a spot contains only one channel, estimation of N is correct. Having a great number of spots and setting the channels inserting procedures in order to have a low mean number of channels per spot (also if it means to have some empty spots), could virtually assure to have some spots containing only one channel. These spots will be recognize because they will register the lower probability p between the spots with an estimated N equal to one, and they will report the correct value of p.

5 SINGLE CHANNEL CHARACTERIZATION

5.1 Introduction

Ligand gated ion channels are natural transducers, giving an appreciable current response (in the order of the pA) related to the binding of specific target molecules (called ligand molecules, or agonist, when they increase the channel electrical activity). If we want to exploit their properties and use them to create chemical sensors, the knowledge of their behaviour is essential. In particular, it's mandatory to understand what is the relationship between the agonist concentration and their electrical response. It was said, in Chapter 1, that the gating of ligand gated ion channels is a stochastic process, and the interaction with the ligand molecules affects the channel kinetics, not the conductance. In this chapter, it will be discussed the characterisation of the homomeric α_2 isoform of the glycine receptor, a ligand gated ion channel belonging to the Central Nervous System cells. Both experimental acquisitions and signal analysis will be described.

5.2 Glycine receptors

Glycine receptors (GlyR) are membrane proteins that belong to an important class of synaptic ion channels, the nicotinic superfamily, which comprises also ACh muscle and neuronal nicotinic, GABA (A and C) and 5-HT3 receptors. GlyR channels mediate fast synaptic transmission in the Central Nervous System, in which they have an inhibitory function, and periphery; in particular, they are predominantly expressed in the spinal cord and brain stem. Like the other members of the nicotinic superfamily, glycine receptors are pentameric. They are formed of some combination of $\alpha 1$- $\alpha 4$ and β subunits, arranged

84

quasi-symmetrically in a circular order around the channel pore. The channel pore of glycine receptor is selective for chloride ion flow. In mammalian, the adult form of the GlyR is the heteromeric $\alpha_1\beta$ receptor, and is believed to have a stoichiometry (proportion) of three α_1 subunits and two β subunits (Kuhse et al., 1993; Burzomato et al., 2003). Immature nerve cells are known, instead, at least in the spinal cord, to express α_2 homomeric GlyRs, progressively replaced by the adult $\alpha_1\beta$ form during the two first postnatal weeks in rodents (Akagi and Miledi, 1988; Malosio et al., 1991). Structural information on nicotinic receptors comes basically from two sources: the advanced cryo-electron microscopy of *Torpedo* muscle-type nicotinic receptors (closed and, at lower resolution, open) (Unwin, 2003; Miyazawa et al., 1999) and the atomic resolution crystal structures of *Lymnea* acetylcholine binding protein (Brejc, 2001; Celie, 2004), which is supposed to be homologous to the extracellular domain of the receptors (see, for example, Cascio 2004). Despite these recent advances, the information in these structures has several limitations: first of all there is no direct evidence about the structure of glycine receptors, so structural inferences are based solely on analogy with nicotinic receptors, and the dynamic of the process of activation remains somewhat uncertain and is subject of intense study. Binding of the ligand in the extracellular domain produces a wave of conformational change that spreads to the transmembrane domains that form the channel and causes it to open. The other source of information for ion channels is functional, through single-channel kinetics, which aims at establishing a mechanism that accurately models the activation of the channel.

5.2.1 Heteromeric $\alpha_1\beta$ form

The $\alpha_1\beta$ form is the most intensively studied one between glycine receptors, because it is the dominant form in adult mammalian central nervous system. It appears to have a structure that alternates α and β type subunits, with three

agonist binding sites located in the interface between neighbouring subunits (two between α_1 and β subunits, one between two α_1 subunits) (Kulhse et al., 1993). The receptor can be activated by a range of simple amino acids including glycine, β-alanine and taurine, and can be selectively blocked by the high-affinity competitive antagonist strychnine. The kinetics of the heteromeric $\alpha_1\beta$ form has been modelled, in the last years, principally through two different schemes: one derived from GABA receptor model (Jones & Westbrook ,1995), the other proposed by Burzomato et al. (2004): they are represented, respectively, in figures 5.1.A and 5.1.B. In particular, Burzomato et al. (2004) have demonstrated that the mechanism can be equally well fitted by the two schemes, but the second one includes a lower number of free parameters (14 instead of 18) and doesn't need to postulate the presence of cooperativity (an increase of the affinity for binding to the shut states when other binding sites have already been occupied by glycine). In fact, in this case, the increase of the open efficacy is explained through the presence of "flip states" (AF, A_2F and A_3F), conformational protein changes preceding the openings.
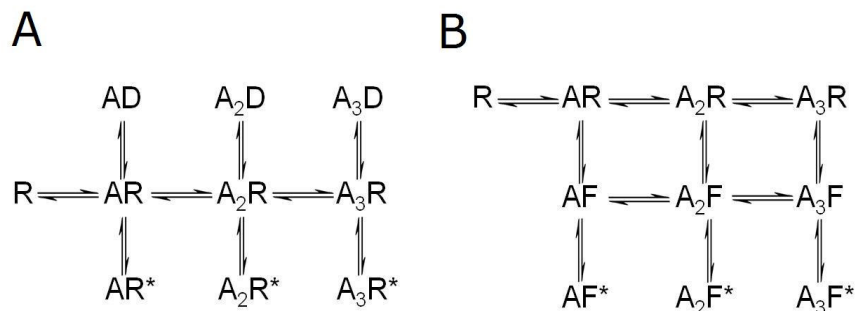
Figure 5.1   Kinetic schemes used for modelling the heteromeric $\alpha_1\beta$ glycine receptor. (A) Model with cooperativity; (B) Flip model (no cooperativity between binding sites). In both cases (and in all the other Markov chains drawn in this chapter), the prefix 'A_x' indicates that x agonist molecules are bound; the superscript '*' marks the open states.

5.2.2 Homomeric α2 form

The only homomeric ion channel to have been analyzed in detail by single-channel methods is the glycine α1 receptor (Beato et al., 2002; Beato et al., 2004; Legendre et al., 2002). It seems likely that this homomeric pentamer would be symmetrical, and therefore that the five binding sites would be identical in the resting state, although crystallographic evidence is thin because of the paucity of protein structures with no ligand bound. Equally good fits have been obtained by Beato et al. (2004) by postulating either three or five binding sites, and these two cases could not be distinguished. It follows that, if there are indeed five binding sites, it must be supposed that the gating reaction "saturates" after three agonist molecules are bound. The apparent interactions have been then explained by a pre-opening conformation change of the sort postulated for the heteromeric receptor (Figure 5.1.B), as reported in Burzomato et al. (2004). No single channel steady-state characterization has been done, instead, on homomeric α_2 form. Mangin et al. (2003) have proposed a Markov model (Figure 5.2), estimating the rates constant from whole cell recording and fast glycine applications on outside out patches. This model postulates a couple of binding states (but the authors admit that the question is controversial) and only one open state, related to the fully bound condition. In a further paper by the same group (Shi-Wang et al., 2007) the number of binding states has been raised to three.

$$AD \qquad A_2D$$
$$\Updownarrow \qquad \Updownarrow$$
$$R \rightleftharpoons AR \rightleftharpoons A_2R \rightleftharpoons A2R^*$$
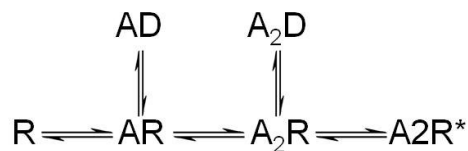
Figure 5.2   Two ligand-sites Markov chains used for modelling the homomeric α_2 glycine receptor.

5.3   Patch Clamp Technique

In chapter one were described that excitable cells, such as muscle or nerve cells, produce quick depolarizations in response to electrical, mechanical or chemical stimuli, changing their internal potential through a quick flux of ions between cytoplasm and the external environment. This is, in fact, the most widespread and important method used by cells for transmitting and elaborating information. The coordinated electrical behaviour of the specific excitable cells forming a tissue are the basis, for example, for every motor and brain activity. Electrophysiology is basically the branch of physiology that studies the relationship between electric phenomena and bodily processes. It involves measurements of voltage change or electrical current flow on a wide variety of scales from single ion channel proteins to whole tissues like the heart.

The capability of recording the electrical activity of a single cell membrane date back to the half of the XX century (Graham and Gerard, 1946; Cole, 1949; Hodgkin and Huxley, 1952). In these first studies, a sharp electrode was inserted in the cell whilst the ground electrodes was put in the fluid surrounding the cell. Electrical activity of excitable membranes was usually recorded using two main techniques: voltage clamp and current clamp. In voltage clamp technique, the voltage is externally clamped and the deriving current through the cell membrane is recorded; contrariwise, in current clamp, the current between the electrodes is set by the experimenter and the transmembrane potential is the output.

The patch-clamp technique (Neher and Sackmann 1981) is a further development of the previously described ones (for details see *Single Channel Recording*, 2nd ed. Eds: Sakmann, B., Neher, E. Plenum Press, New York), which allows to record currents from single ion channels. The innovation is that, while conventional intracellular recording involves impaling a cell with a fine electrode; patch-clamp recording uses an electrode composed by a glass micropipette with a relatively large tip hole diameter (in the order of the um),

containing an Ag/AgCl wire and sealed onto a patch of the cell surface. The interior of the pipette is filled with a saline solution so that the metal electrode, in contact with this solution, conducts the electrical changes to a voltage clamp amplifier. The patch clamp pipette is pressed against a cell membrane and suction is applied to the inside to pull the cell's membrane inside the tip of the electrode. The suction causes the cell to form a tight seal with the pipette, with a resistance between 1-100 $G\Omega$. This high seal resistance allows to resolve membrane currents in the pA range. This means that is possible to record small currents across the membrane of small cells and even the current through a single open channel pore. The high seal resistance is achieved by direct interaction between the surface of the glass pipette and the cell membrane on atomic dimensions. Most likely interactions are salt bridges between negative charges on the glass and the membrane surface mediated by divalent cations and hydrogen bonds between O-Groups on the glass surface and O- or N-Groups of the phospholipids forming the membrane as well as van der Waals interactions. Depending on pipette size, cell type, and channel density, the electrically isolated membrane patch can contain one or several channels proteins. Opening and closing of the channels results in sudden current changes that can be recorded under voltage clamp. Once realised the gigaseal, four different configurations can be achieved: whole cell, inside-out, cell attached and outside-out. Between them, the last two configurations are mainly useful for the analysis of the kinetics of single ligand gated ion channels and will be briefly described below.

Cell-attached configuration: The electrode remains sealed to the patch of membrane (Figure 5.3). This allows the recording of currents through single ion channels in that patch of membrane under relatively natural condition, with the integrity of the cell maintained. For ligand-gated channels or channels that can be activated or blocked through the action of drug

molecules, the drug of choice is usually included in the pipette solution. Thus, it is not possible to change the drug concentration during the acquisition, because the pipette solution can't be prefunded: the technique is limited to one point in a dose response curve per patch. Moreover, there is no access to both the fluid compartments at the opposite hands of the membrane, since the parch is attached to the cell, in contact with the cytoplasm. Another limitation is that this configuration doesn't allow to set the effective transmembrane potential: in fact, since the membrane patch under investigation is not excided from the cell, the transmembrane potential is given by the sum of the clamped potential between the electrodes, and the potential of the inner side of the cell. Since cell potential is usually, in resting conditions, electronegative compared to the external fluid (during the experiments, a bathing solution is used, whose composition mimic the cellular external environment), the total transmembrane potential is greater than the one externally imposed.

"Outside-out" patch: In this configuration, the patch is pulled out from the cell with a particular procedure (briefly described in section 5.10; for more details see, for example, Molleman 2003). The final result is that the patch reforms as a ball of membrane on the end of the pipette, where the outside of the membrane corresponds to the external surface of the ball, and the internal part of the membrane is in touch with the intrapipette solution (Figure 5.4). Huge advantage of this configuration is that the experimenter can perfuse the same patch with different solutions since the binding sites of the ligand-gated channels are mainly located on the extracellular side of the proteins. Outside-out patching doesn't give the experimenter the opportunity to examine the properties of an ion channel in contact with its usual

environment. Since the membrane patch is detached from the cell, the composition of the intracellular side is lost. In particular, there is a washout of the cytosolic factors (substituted by the intra-pipette solution) and the distruption of the cytoskeletal structure. Several studies in the last years, pointed out that this "not physiological conditions" alter the electrical behaviour of the ion channels, both in terms of conductance and kinetics. However, this configuration is largely used whenever a chemical stimulus (i.e. a change in drug concentration) must be applied. The composition of the intra-pipette solution should be as similar as possible to the fluid composing the intra-cellular environment. Using pipettes of the same dimension, the surface of the patch of membrane under investigation, in the outside-out configuration, is greater then the one of the cell-attached configuration (approximately ten times).
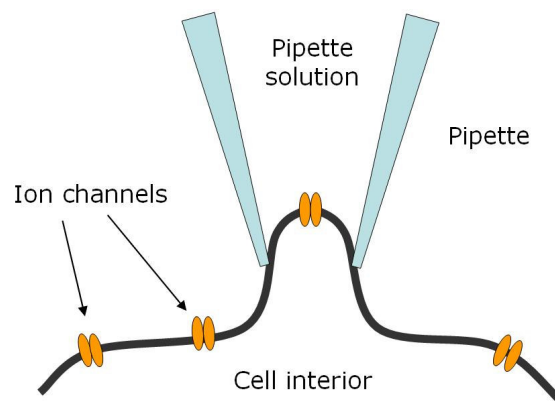
Figure 5.3   Cell-attached configuration.
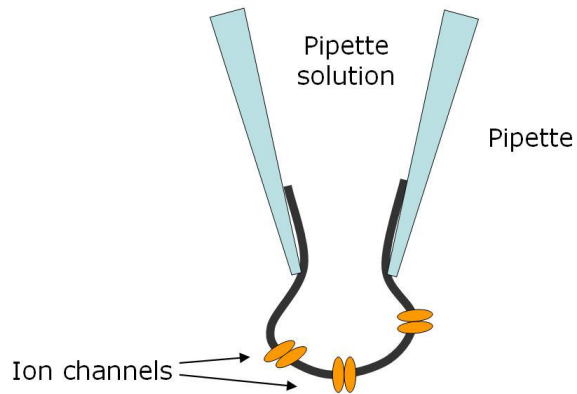
Figure 5.4   Outside-out configuration.

5.4   Patch Clamp experiments

Basically, patch clamping involves the placement of a glass micropipette, filled with saline solution and an Ag/AgCl electrode wire, onto a cell forming a tight seal. Therefore, the set up of the experiments needs first of all the culture of the cells, eventually their transfection, the creation of the patch pipettes, the preparation of the solutions used to fill the pipettes and to bath the cells. In the experiments described in the following part of this chapter, homomeric α_2 glycine receptors were transfected in an heterologous system, namely cells belonging to not excitable tissues. In such a way, it was possible to study the target channels limiting the interferences due to the presence of other kinds of channels (endogenous channels).

5.5 Cell culture and transfection

Glycine receptors were heterologously expressed in Human embryonic kidney (HEK293), an immortalised cell line obtained from the American Type Culture Collection (ATCC). These cells contains only a low density of endogenous ion channels, usually characterised by a very low conductance (less then 5 pS), not comparable to the glycine receptors one (over 50 pS); furthermore, they are very easy to grow and transfect very readily. For these reasons, they are widely use in cell biology and, in particular, they are good candidates for constituting an heterologous system for electrophysiological studies.

Cells were cultured and maintained in Dulbecco's modified Eagle medium containing 10% (v/v) foetal bovine serum and 1% (v/v) penicillin streptomycin solution (100000 units/ml penicillin and 10 mg/ml streptomycin; all from Gibco, UK) at 37°C in a 95% air 5% CO_2 incubator, and passaged every 2-3 days, up to 40 times. Before experiments, cells were plated onto polylysine-coated coverslips and transfected using a calcium phosphate co-precipitation method (Groot-Kormelink et al., 2002). For the amplification and cloning pcDNA3.1 plasmids were used (Invitrogen, The Netherlands), containing inserts encoding the rat glycine receptor subunits α2 (GenBank accession number X61159), enhanced green fluorescent protein (eGFP, Clontech, UK) and non-coding plasmid pcDNA3.1. Several different mixtures of DNA were used for the cell transfection, including a percentage of glycine subunit receptor encoding DNA between 3% and 20%; the percentage of eGFP encoding DNA was 18%. EGFP is a protein, originally isolated from the Aequorea jellyfish, that fluoresces green when exposed to blue light. Once expressed in a cell, the intensity of its green response-light depends basically on its concentration in the cytoplasm. Since it is transfected in the heterologous system together with the glycine receptor subunit, their density in the cells are strongly correlated; thus, the presence of eGFP in the HEK239 cells, enables the experimenter to detect, first of all, if the transfection was successfully and, secondly, what are the cells in the plate

which probably have the higher concentration of ion channels on their surface. Coverslips were washed using fresh cell culture medium 5-16 hours after trasfection. Patch clamp recordings were made 12-48 hours after transfection.

5.6   Preparation of the pipettes

Patch pipettes for cell attached single channel recording and for outside-out recording were pulled from thick-walled borosilicate glass capillary tubes (GC150F; Harvard Apparatus, Edenbridge, UK). They were realized using a puller (P-97 Flaming/Brown Micropipette Puller Sutter instruments), a programmable electromechanical device which heats the capillary tubes and pulls, following a preset sequence of steps, producing tips with a precise and reliable shape (and, following, a controlled size of the hole and a controlled pipette-resistance).

Patch pipettes were then coated with a bubble of Sylgard (Silicone Elastomer, Dow Corning, Coventry, UK), about 100 um far from the tip. It allowed to decrease significantly the parasitic pipette-capacitance (namely, the capacitance between the intra-pipette saline solution and the extracellular solution bathing the cells). Finally, pipettes were fire-polished (MF-83 Microforge, Narishige, Tokyo, Japan) in order to smooth the borders of the pipette holes.

5.7   Solutions for patch clamp recordings

In the cell-attached single channel patch experiments, the extracellular solution (the solution used for bathing the cells) and the intrapipette solution had the same composition, but the last one contained also the glycine, being the solution surrounding the side of the cell membranes where the agonist binding

sites were located. The basic solution contained (mM): 102.7 NaCl, 20 Na gluconate, 4.7 KCl, 2 CaCl, 1.2 MgCl$_2$, 10 HEPES, 15 sucrose, 14 glucose, 20 TEACl (all products from Sigma-Aldrich). Solution pH was adjusted to 7.4 with NaOH; it's osmolarity was 320 mOsm. Milli-Q ultrapure water was used, and the solution was filtered before use.

5.8   Patch clamp experimental set-up

The basic elements of the set-up for cell-attached patch clamp experiments are:

- a platform with minimal mechanical interference. It's realized by an anti-vibration table(TMC Vibration Isolation Table, TMC, Peabody, MA, USA)
- a Faraday cage (home made)
- a microscope for visualization of the preparation and of the cell-patching procedure (Olympus IX70, Olympus Optical, Tokyo, Japan)
- a digital camera connected to the microscope
- a fluorescence system (X-Cite 120, Richardson, TX, USA)
- a micromanipulator to position the pipette (Burleigh PZ-301, Burleigh Instruments, New York, NY, USA)
- a patch-clamp amplifier (Axopatch 200B, Axon Instruments, USA)
- a monitor
- an oscilloscope (TDS 3034B, Tektronix, USA)
- a tape recorder (Biologic DTR1204, Biologic Instruments, Claix, France)
- an A/D converter (CED1401Power, Cambridge Electronic Design, UK)
- a PC (DELL).
- A perfusion system (see section 5.10 for details).

The inverted microscope and other experimental equipment associated directly with the electrophysiological recording process were mounted on an isolation table to eliminate vibration.

The hearted Faraday cage enclosed the set-up, to minimize noise from electrical interference. The front of the cage was open for access but could be closed, during recording, by a metallic mesh. All metallic objects inside the cage were also hearted to a single point that was connected to the amplifier hearth, to eliminate loops.

The inverted microscope was equipped with a 10x and a 40x objectives and connected to the digital camera. The fluorescence system was mounted on the microscope and could be switched into the optical path. This provided a broad spectrum of UV light used to excite green fluorescence protein expressed in the cytosol of the transfected cells. The emission spectrum of eGFP peaks in the visible range, at 510 nm. When using the UV source, a green bandpass filter was included in the objective path to exclude harmful UV light.

The amplifier was an Axopatch 200b, the same previously described (see section 2.2), equipped with an headstage Model CV-201 AU (Axon Instruments, USA), used in the capacitive-feedback configuration. The micropipette was mounted onto the headstage amplifier and filled, to minimise noise pickup during recording, with only enough intracellular solution to cover the dark silver chloride portion of the electrode wire The electrode holder included a side port for suction. Positive or negative pressure was applied from a 1 ml disposable syringe that was connected to the port with PTFE tubing. The headstage amplifier was firmly screwed onto a piezo-electric remote-controlled micromanipulator that was mounted on a coarse mechanical manipulator.

The output of the patch clamp amplifier was connected to an 8-pole Bessel filter (set to 3 kHz) and then to an oscilloscope for monitoring, during the experiments, cell-sealing and channel activities. At the same time, the output was connected to the input of the digitiser interface and then to the tape

recorder or directly to the personal computer, without any filtering stage after the one included in the Axopatch amplifier (a 4-pole Bessel filter), set to 10 kHz.
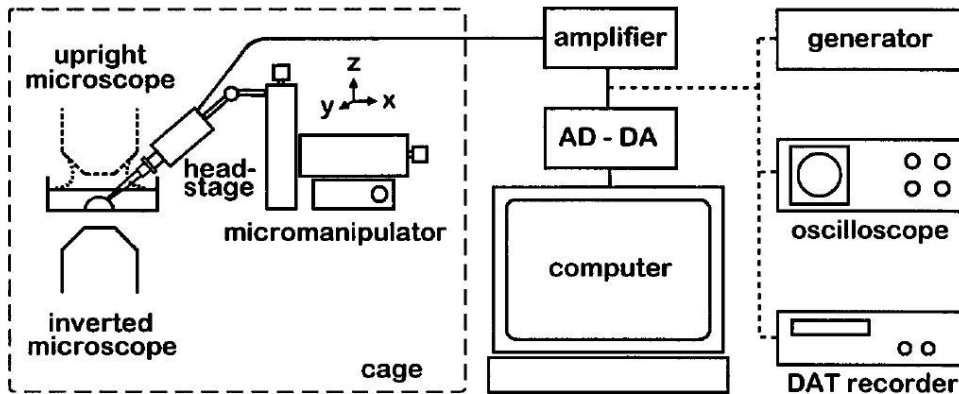
Figure 5.5   Patch clamp set up.

5.9   Cell attached experiments

One way to investigate the kinetics of the channel, and to estimate its rate constants for a postulated mechanism is to obtain steady state single channel records at a constant voltage applied and a constant glycine concentration. In order to understand how the channel electrical response depends on the agonist concentration, the steady state records should be obtained at several agonist concentrations. These experiments were conducted in cell-attached configuration, because it guaranteed a) the maximum seal stability, b) the most physiological conditions for the ion channels embedded in the membrane patch,

and c) lowest electric noise levels required for good kinetic rate constant estimation. In the first part of the experiments, the electrode tip was brought carefully onto the cell surface using initially coarse and then fine manipulation, while a 5 mV, 50 Hz square wave was applied, so that the contact between the tip and the cell and the following formation of the gigaseal were revealed by progressive reductions of the current output signal, monitored by the experimenter through the oscilloscope. Then a constant -100 mV command potential was kept in the pipette. As described before (section 5.3), this is the voltage applied between the electrodes, which differs from the real transmembrane potential, namely the potential between the two sides (intra and extra-cellular domains) of the ion channels. The overall transmembrane potential is given by $V_m = V_{cell} - V_{command}$ where $V_{command}$ is pipette potential, V_{cell} is resting membrane potential and V_m the effective transmembrane potential. Since the HEK293 have, in normal conditions, a ddp between -30 mV and -80 mV (from the inner to the outer side), the transmembrane potential in here described experiments was between −130 mV and −180 mV. The exact value couldn't be measured and differed from one patch to another. This causes a variability, in the values of single channel measured currents, largely greater than in case of excide patches (like outside-out configuration) and experiments conduct on artificial planar bilayers. In presence of channel activities, data were recorded on tape, filtered at 10 kHz (-3 dB) by the Axopatch Bessel filter. Selected recordings were replayed, digitised at 100 kHz and stored on computer hard disk using a continuous sampling program CONSAM (see www.ucl.ac.uk/Pharmacology/dcpr95.html). They were also digitally post-filtered (by an 8 pole Bessel filter, achieving a final cutoff frequency of 5 kHz) and decimated (final sampling frequency: 50 kHz). In figure 5.6 is reported an example of signal from single homomeric α_2 glycine receptor activity, 5 kHz filtered. In total, six values of glycine concentrations were used in patch experiments: 10 uM, 20 uM, 50 uM, 100 uM, 1 mM and 10 mM. No response was obtained using the lowest value (10 uM), although several attempts were

made (more than 60). Also in case of 20 uM, channel activity was registered just twice (but the recorded traces contained too few events to be used in statistical analysis).

10 second stretch

0.1 second stretch

111007c2.dat   50 µM glycine α2 GlyR
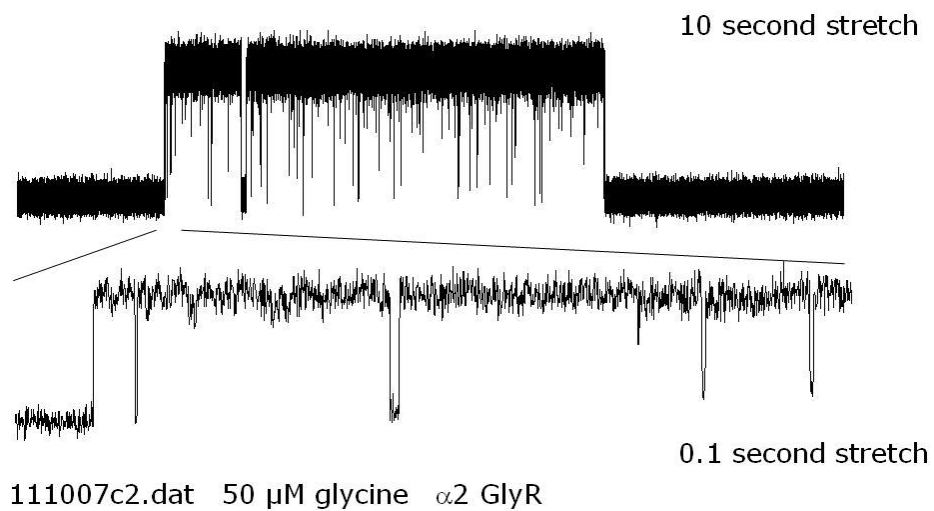
Figure 5.6   Example of single channel trace from homomeric α_2 glycine receptor

For everyone of the 20 selected records, amplitude histogram and stability plot were realised, in order to check the possible presence of unexpected events during recording, such as sudden voltage jumps, current leakages, anomalous conductive sublevels in channel activities. Amplitude histograms show the number of openings of the channel which has an amplitude that falls between the limits specified on the abscissa In our case, all present a single peak and are well approximated by a Gaussian-bell shape, confirming the presence of a

single conductance level in the channel activity[1]. Examples of these histograms and plots are reported below (figure 5.7). The mean value of the registered amplitude currents is I = 5.80 pA, with a standard deviation of σ = 0.73 pA, leading to a coefficient of variation (I/σ)% = 12.6%. These differences in single channel current amplitudes are mainly due, as described in section 5.3, to the uncertainty on the transmembrane voltage, typical of the cell-attached configuration.
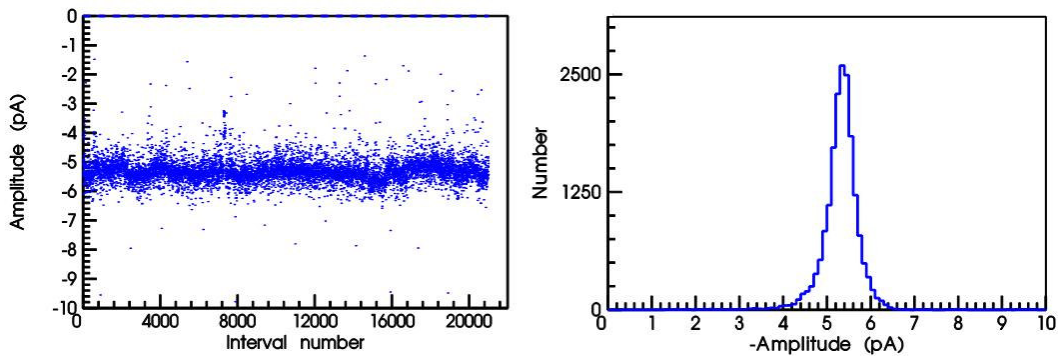
Figure 5.7   Examples of channel amplitude stability plot (left) and histogram (right).

[1]   Indeed, in some cases, there were sequences of openings with a smaller conductance inside bursts and clusters. In any case, they represented less than the 5% of the total amount of the openings. Moreover, they must be probably attributed to partial occlusions of the ion channel pores by some molecules in solution, since they were always characterised by a significant noise increase.

5.9.1 The measurement of durations

In order to characterise the kinetics of the channel, namely a plausible Markov model and the relative rate constants, it's indispensable to analyse the information contained in the durations of its opening and shutting events. It is common opinion that the conformational changes determining ion channel electrical switching occur in a time scale largely below the microsecond; thus, single ion channel current signal should look, in absence of noise and filter distortion, like a perfect rectangular wave. In practise, there are two main problems to be solved: firstly, transitions from one current level to another must be detected, then the duration of time between one transition and the next must be measured. The process leading from the experimental record to a sequence of the openings and shuttings with their durations is called idealization of the record, and obviously it aims to resemble, as close as possible, what would have been seen if the experiment had been free of noise and artefacts introduced by the filtering. With this purpose, several algorithms were developed (see, for example, Dempster, 1993), basically belonging to two different approaches: threshold crossing and time course fitting. In threshold crossing methods, a threshold value is fixed (usually is the 50% of the full amplitude of the channel signal), and the duration of an event is measured as the length of time for which the current stays above (or below) this threshold. Sometime, specially when the signal to noise ratio S/N is large, two thresholds are set (usually they are the 25% and the 75% of the full amplitude level). With two threshold set, an opening event is recognised when the current goes above the lower threshold, whilst a shutting event is indicated by the crossing of the higher threshold. Since the waveform is distorted by the filters, the time at which transitions occurs should be estimated by taking the data point on either side of the crossing of the threshold line (or threshold lines), and interpolating between them (on the basis of the filter step-response) to estimate the time at which a threshold is crossed. In general, threshold crossing methods are considerably

faster respect to time course fitting, and are totally automatic (no visual inspection of the data is needed, although it could bring to errors in some cases). It can be demonstrated that the duration of events needs to be above roughly 1.3 t_r (where t_r is the 10-90% risetime of the filter) before errors become negligible (Colquhoun and Sigworth, 1983).

In time course fitting, the theoretical time course of the current is computed on the basis of the step response of the recording system and fitted to the actual record. In practice, a calculated response, made from the convolution of the step responses corresponding to potential channel openings and shuttings, is superimposed on the observed current, and the time intervals and amplitudes are adjusted (by eyes or by a least square minimization) until a good fit is obtained. There are two major advantages in this method: it's particularly suitable for dealing with records that contain multiple conductances or subconductance states and allows better time resolutions than the ones obtained using threshold based methods. In fact, when a threshold method is incapable to fit events too brief to reach the threshold, a time course fitting approach could be able to detect them. For these reasons, this method is commonly used in many pharmacology and physiology research groups, where the first aim is to obtain the maximum available time resolution (in order to see also very fast components of the kinetics). In the case of time course, fittings of the shortest durations are basically decided subjectively by the experimenter, and are unlikely to be constant throughout an experiments, since the noise level could change. It is therefore highly desirable that a fixed resolution should be imposed on the data after analysis. In practice, it means that the experimenter should scroll all the record, checking the matching of the data with the superimposed convolution of the step responses (realised by a least square minimization method); at the end, he should decide the final time resolution, discarding all the shorter events. It is therefore understandable that this second approach of idealising the experimental data has a major drawback: it is not automatic (at least, no totally automatic programs were developed

102

successfully). It follows that a) this kind of analysis requires a great amount of time (and the presence of an operator); b) since the elaboration is not performed merely by a calculator, but an human operator takes the decisions about the fitting, inevitably he can introduce an arbitrariness in the process.

5.9.2 Apparent dwell time distributions

For the idealization of the records, a time fitting program SCAN was used (see www.ucl.ac.uk/Pharmacology/dcpr95.html). Two records of $\alpha2$ glycine receptor activations by 50 uM or 10 mM glycine were analysed and then used for estimating the rate constants.
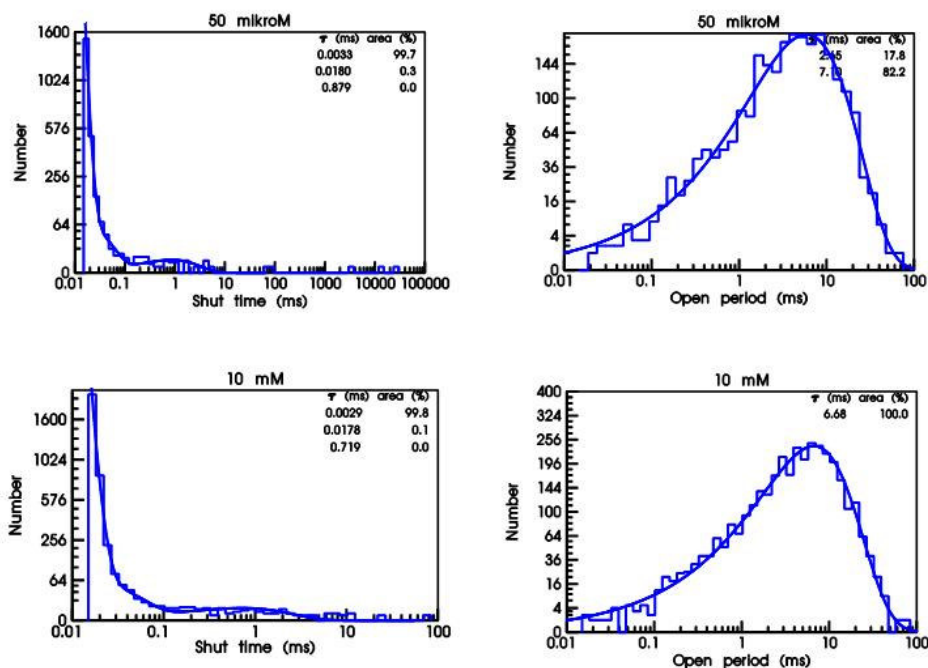
Figure 5.8   Single channel dwell time distributions, in correspondence of two different glycine concentrations (50 uM and 10 mM). Left: shut time distributions; right: open time distributions.

103

In both cases, data were filtered at 5 kHz, obtaining an signal to noise ratio greater than 19. In particular, 50 uM record was characterised by 30419 transitions, an average full amplitude of - 5.23 pA, a RMS of 240 fA; in the case of the 10 mM record, transitions were 26963, the average full amplitude was – 5.04 pA, the RMS 270 fA. In both cases, the final time resolution was imposed at 15 us. Figure 5.8 shows the open and shut time histograms of the two records[1]. The experimental histograms were fitted by mixtures of exponentials, using the EKDIST program (see www.ucl.ac.uk/Pharmacology/dcpr95.html).

[1] Reported histograms are displayed in the way suggested by McManus et al. (1987): the time axis is in log scale, to cover a wide range. It's not simply a log transformation of the conventional display, because this would have bins of variable width on the log scale, whereas the distribution of log(t) is shown by bins of constant width on the log scale. The distribution has the following form. If the length of an interval is denoted t, and we define $x = log(t)$, then we can find the p.d.f. of x, $f_x(x)$, as

$$f_x(x) = \frac{dP}{dx} = \frac{dP}{d\,log(t)} = \frac{dt}{d\,log(t)} \times \frac{dP}{dt} = t \times f(t) = \sum a_i\, \tau_i^{-1}\, exp(x - \tau_i^{-1}e^x)$$

where P is the cumulative probability distribution and the probability density function $f(t)$ is a multi-exponential function. In addition, a square root transformation of the frequency density was used, to keep the errors approximately constant throughout the plot. The function $f_x(x)$ is shaped as a composition of bell-shaped curves, whose peaks coincide with the time constants τ_i.

104

This is only an empirical fit of the distributions with no kinetic models taken into account. The estimation of the kinetic constant rates were then realised by HJCfit program (see www.ucl.ac.uk/Pharmacology/dcpr95.html), as it will be discussed later. Moreover, the histograms in figure 5.8 actually refer to the distributions of apparent open and shut times, namely the ones as appears from idealised data but without any compensation for the lost brief events. However, visual inspection of such histograms and their fits could provide preliminary information useful for understanding concentration dependent behaviour of the channel opening and for mechanism postulations.

The two files correspond to very different concentration values: the first one (50 uM) is close to the lower value of glycine concentration, able to evoke a receptor activity, whilst the second one (10 mM) is a saturating concentration. From the channel modelling theory discussed in Chapter 3, it follows that the channel activity in the lower concentration record (50 uM glycine) should be formed by bursts, namely the long shut periods should be caused by the unbindings of ligand molecules, which are not immediately followed by re-bindings because of the low glycine concentration in the solution surrounding the receptive sites of the channel. Moreover, it is usually supposed, for glycine receptors, the presence of more than one open state in the channel Markov model, where each open state corresponds to a different number of ligand molecules bound. In this case, for such a low concentration, conceivably the large part of the bursts should correspond to openings in not fully-bound conditions, that is the channel activates when not all its binding sites are occupied. A 10 mM glycine concentration, instead, is a saturating concentration, as results both from literature (Mangin et alii, 2003) and from our jump experiments (response evoked by a 10 mM concentration is basically the same evoked by a 1 mM concentration). In this case, we can assume that the channels receptive sites are basically always bound, in the sense that every unbinding is immediately followed by a re-binding, so that channels are in fully-bound conditions except for very short periods. Channel activity is then formed

105

by clusters, and the long shut intercluster periods are due to channel desensitizations. In the table below, time constant of the apparent open and shut times are reported, both for 50 uM and 10 mM glycine concentrations.

	50 uM		10 mM	
	tau (ms)	*area (%)*	*tau (ms)*	*area (%)*
Shut time components	0.0033	99.7%	0.0029	99.8%
	0.018	0.3%	0.0178	0.2%
Open time components	2.65	17.8%	-	-
	7.10	82.2%	6.68	100%

Table 5.1   Dwell time components from EKDIST empirical fitting.

Shut time histograms are basically identical in the two cases, and it is a surprising behaviour, compared to the ones of other glycine receptors (Burzomato et al., 2004; Beato et al., 2004) and, in general, of receptors belonging to the nicotinic superfamily (R. Lape, L. Sivilotti and D. Colquhoun, data not published). In all the other cases, in fact, even when the time constants don't change, their relative areas are strongly dependent on agonist concentration. In particular, for low concentrations, slower components are relevant. In the case of the $\alpha_1\beta$ glycine receptor, for example, in correspondence of the lowest concentration applied (10 uM), the sum of the areas belonging to slow components ($\tau > 0.1\text{ms}$) is greater than 35 %. This area progressively decreases when glycine concentration raises, becoming the 5.5 % in saturating conditions. In case of $\alpha 2$ GlyR, this concentration-dependent component is not evident. The only difference between the two records is in the apparent open time distributions, even if it's less definite than for other

receptors. There is a shift towards longer openings at the higher concentration: the area of the faster component, in fact, represent the 17.8% for the 50uM record, while can no longer be resolved in saturating conditions. In the case of the $\alpha_1\beta$ glycine receptor, fast component area is the 60% of the total for the lowest concentration, and disappears in saturating conditions. Overall, the dependence of this receptor from the ligand concentration appears to be less evident than in all the other in the nicotinic superfamily. This impression is also confirmed by the intraburst (intracluster) open probability, which is high (over the 98%) for all the concentrations tested between 20 uM and 10 mM.

5.9.3 Rate constants estimation

The estimation of the kinetic rate constant from data obtained in steady state conditions was realised using HJCfit software. This estimator basically maximises the likelihood of an entire sequence of apparent open and shut times, with the rate constant in a specified reaction mechanism as free parameters; it also corrects data with the exact method for missed brief events (Hawkes et al., 1990). Utilizing the transition matrices described in Chapter 3, the expression of the likelihood l, of a whole sequence of observed open and shut times, is

$$l = \Phi_{\mathscr{A}}\, G_{\mathscr{AF}}(t_{o1})G_{\mathscr{FA}}(t_{s1})G_{\mathscr{AF}}(t_{o2})G_{\mathscr{FA}}(t_{s2})...u_{\mathscr{F}} \tag{5.1}$$

In this expression, t_{o1}, t_{o2}… are the first, second apparent open times, t_{s1}, t_{s2}…the first, second apparent shut times; $\Phi_{\mathscr{A}}$ is the vector ($1 \times k_{\mathscr{A}}$) giving the probabilities that the first opening starts in each of the open states; u_F is an unitary $k_{\mathscr{F}} \times 1$ vector. Subset $\mathscr{A}$ includes the open states, $\mathscr{F}$ the shut states. Each transition matrix G is corrected for brief events, namely for keeping in

count the effects of the limited temporal resolution. It is interesting to observe that the equation product gives, at each stage, the joint density of the time intervals recorded thus far multiplied by a vector that specifies probabilities for which state the next interval starts with, conditional on the durations of those intervals. As a consequence, this likelihood expression takes into account not only the single intervals durations, but also all the information about correlations between intervals. Since it's impossible to know how many channels are present in the patch, nor if there was rundown during acquisition (namely, if there were channel deactivations), not all the shut periods can be included in the process. In particular, using the likelihood expression just defined, it's important to be sure that a sequence of consecutive openings derives from the just one channel. Since in bursts and clusters openings occur between short shut intervals, it is possible to analyse only intra-burst and intra-cluster periods, being quite sure that they belong to the activity of the same channel. In addiction, all the traces with signals from more channels open at the same time must be discarded. Practically, both for cluster and burst analysis, critical shut time lengths (t_{crit}) must be given as inputs, so that every burst (cluster) is contained between shut periods longer than t_{crit}. The overall (logarithmic) likelihhod is calculated as the sum of all the individual burst (or cluster) log-likelihoods, each defined as *L=log(l)*. HJCfit algorithm produces the likelihood maximisation following a heuristic procedure (a modified simplex algorithm), starting from a set of initial conditions given as inputs.

For fitting data with HJCfit, Markov chain reported in figure 5.9 was given as input: it was chosen in analogy with the one used for modelling the heteromeric $\alpha_1\beta$ glycine receptor (Burzomato et al., 2004). Respect to the Burzomato model, anyway, the branch corresponding to the monoliganded-opening condition (the path in the Markov chain leading to openings when only one receptive site is bound) was neglected, due to preliminary considerations about homomeric α_2 receptor's behaviour. In particular, the fact that channel activity was recorded only for relatively high concentrations ($\geq$20 uM), and the differences between

the dwell time histograms for different agonist concentrations were failrly slight, suggested a negligible contribute of the mono-liganded path to the channel kinetics. Also the di-liganded branch, which was considered in the fitting, revealed to have a very low occupancy probability, as will be discussed later.

$$R \underset{k_{-1}}{\overset{3k_{+1}}{\rightleftharpoons}} AR \underset{2k_{-2}}{\overset{2k_{+2}}{\rightleftharpoons}} A_2R \underset{3k_{-3}}{\overset{k_{+3}}{\rightleftharpoons}} A_3R$$
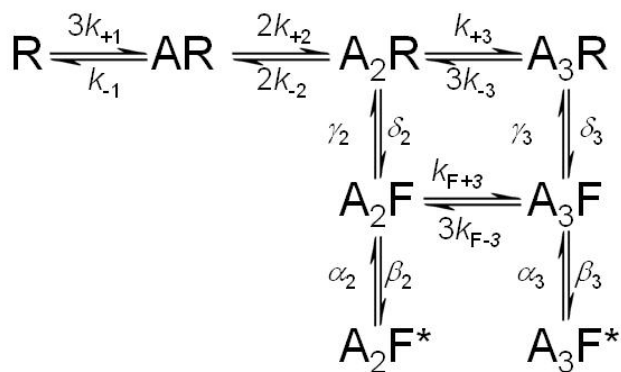
Figure 5.9   Markov model chain used for fitting data

Input files were the two ones used for EKDIST analysis, with the same resolution. Critical shut time values for bursts and clusters were fixed, respectively, at 0.5 ms and 0.8 ms, according to subsection 3.4.10. Fit was repeated using several different initial guesses, coming to the same results and showing that, presumably, the likelihood surface had a well defined maximum, every time reached, even if not all the rate constants were well estimated. The three binding sites were assumed equal and independent, by applying the following constraints to the values of the binding rate constants during the fitting: $k_{+1} = k_{+2} = k_{+3}$. In addition, δ_2 was constrained by microscopic reversibility[1]. Standard deviation of each parameter (each free rate constant)

was calculated starting from the likelihood covariance matrix (Colquhoun et al., 2003). Results from HJCfit are reported in the table 5.2.

Rate constant	Unit	Estimated value	CV%
α_3	s^{-1}	7874.99	4.86176
β_3	s^{-1}	265683	1.20675
δ_3	s^{-1}	6912.11	14.2798
γ_3	s^{-1}	151.300	13.1415
α_2	s^{-1}	751278	Not def
β_2	s^{-1}	118.283	Not def
γ_2	s^{-1}	3615.29	170.258
δ_2	s^{-1}	88.8864	constrained
k_{F+3}	$M^{-1}s^{-1}$	0.108807E+09	73.2908
$3k_{F-3}$	$M^{-1}s^{-1}$	74.3893	45.0865
$k_{+3} (= k_{+2} = k_{+1})$	$M^{-1}s^{-1}$	0.136561E+07	118.70
$k_{-1} (= k_{-2} = k_{-3})$	$M^{-1}s^{-1}$	578.277	140.66

Table 5.2   Estimated values and coefficient of variations of the rate constant fitted by HJCfit.

[1]   The principle of Microscopic reversibility states that in a reversible reaction the mechanism in one direction is exactly the reverse of the mechanism in the other direction. It follows that, in any cycle of a Markov chain, the product of the rate constants going one way around the cycle is the same as the product going the other way around.

As it can be seen from the coefficient of variation, not all the rates were well estimated by HJCfit. Firstly, the algorithm wasn't able to estimate accurately the binding and the un-binding rates $k_{+3} (= k_{+2} = k_{+1})$ and $k_{-1} (= k_{-2} = k_{-3})$. This is due to the fact that these rates are mainly involved in the interburst shut times, and these intervals weren't considered, as discussed before. Also the rates involving the di-liganded branch (connected to the two states A_2F and A_2F^*) weren't estimated in a satisfying way: γ_2, k_{F+3}, $3k_{F-3}$ had coefficient of variations close to the 50% or greater, while for α_2 and β_2 errors weren't estimated at all (it means that not enough intervals fell in A_2F^* to realises a statistic). The reason of these unfitness to estimate can be understood from the equilibrium occupancies of the states, namely from the probabilities of staying in each state of the model. These are reported in the table below.

State	Equilibrium occupancy (50 uM)	Equilibrium occupancy (10 mM)
A_3F^*	0.187489E-01	0.970518
A_3F	0.632544	0.287667E-01
A_2F^*	0.403628E-07	0.309645E-09
A_2F	0.256365E-03	0.196672E-05
R	0.249303	0.478135E-07
AR	0.883097E-01	0.338736E-05
A_2R	0.104272E-01	0.799927E-04
A_3R	0.410399E-03	0.629678E-03

Table 5.3   Equilibrium state occupancies.

It is clear, from these occupancies, that the states A_2F and A_2F^* have a very low probability to be occupied, even for low values of agonist concentration. The system, for a glycine concentration of 50 uM, remains in one of the two states composing the di-liganded branch one-three thousandth of the time spent in the fully-liganded branch. Even if these occupancies can't be absolutely right (since there isn't a correct information about the binding and the un-binding rates), this ratio suggests that the di-liganded opening condition is absent or, in every case, negligible. The model can be then simplified removing the states A_2F and A_2F^*, becoming the one drawn in figure 5.10.
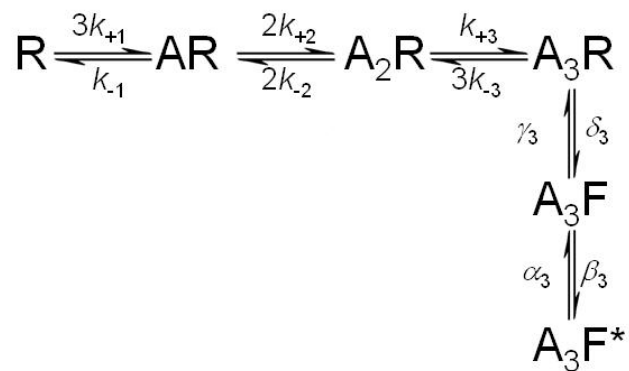
Figure 5.10   Markov model chain without mono- and di-liganded openings

Actually, in this model desensitisation states aren't present. The sojourns in the desensitised states generate the long shut intercluster periods when the channel is bound. They can't be etimated from steady-state experiments, since intercluster periods can't be included in the HJCfit analysis. In order to achieve information about these rates, jump experiments were conducted, as it will be

discussed in the following section. From the same experimental protocols, it was possible also obtain a better estimation of the binding rate.

5.10 Jump experiments

Analysis of single channel behaviour in steady state conditions can't give all the model rate constants, basically because it's not possible to gather the information relating the long inter-cluster and inter-burst shut periods from it. It is linked to the fact that the experimenter has no means to estimate the number of channels present in a patch. Only the minimal number could be deduced from the presence of double or triple openings. For example, the length of long desensitization periods which determine the inter-cluster channel inactivity can be underestimated in patches with more than one channel present. If clusters occur rarely no overlapping of them could happen but they would chop the desensitisation intervals and measured intervals would be apparently shorter than real ones. Ambiguity of information contained in measured desensitisation intervals does not allow reliable estimation of rate constants of desensitised states, thus, desensitised states are not represented in the kinetic schemes used for HJCfit fitting. Similar reasoning is valid for inter-burst intervals at low (bursting) concentrations. Steady state analysis of single channel activations at low concentrations can't usually estimate binding rates in an efficient way, because this could be done only taking into account the inter-burst shuttings. However, shut intervals between burst inside clusters contain information about binding/unbinding, thus, records at clustering concentrations can be used to estimate ligand association/dissociation rate constants. A difficulty in case of $\alpha 2$ GlyR is that there is no clear distinction between bursting and clustering information. The choice of t_{crit} becomes very subjective and especially could lead to under/over estimation of association rate constant. Luckily, an

113

independent measure of association rate constant can be done using concentration jump experiments. In such experiments short pulses of known agonist concentration (concentration jumps) must be applied to the solution wetting the extracellular domains of the ion channels, where receptive sites are placed. These experiments can't be conducted in cell-attached configuration, since it doesn't allow to change the drug concentration. The best choice is then to use an outside-out configuration, where the extracellular domains of the channel are placed on the side of the membrane patch in touch with the bathing solution, whose composition can be controlled through a perfusion system. The outside-out configuration is suitable for these experiments also because it entails membrane patches greater then the ones of the cell-attached configuration: it is then possible to get tens (or hundreds) of channels in the patches, without modifying substantially the procedures used for transfecting the cells and creating the pipettes, holding the ones seen in cell-attached single channel experiments. The drawback is that, as described in section 5.3, the kinetics of the ion channels could be influenced by the different configuration. The greatest challenge in jump experiments is to apply the short pulses of known agonist concentration to the membrane patches. Ideally, pulses of agonist should resemble a square-wave shape, with sharply defined, rapid on and off phases. This ensures that all the receptors are equally exposed to the agonist, to a first approximation. Moreover, it is important that the solution switch should remain quantitatively and qualitatively constant throughout a recording: that is, the waveform describing the temporal course of the ligand concentration of the flow wetting the membrane should be periodic, to assure reproducibility of the measurements. In order to obtain such a solution switch, a rapid agonist perfusion system was used; it represented the only new element respect to the set up already used for single channel steady state experiments. It was formed by a rapid agonist application system (embedding a theta tube), a set of syringes, each connected to a PTFE tube through a Teflon valve, a 4 input - 1 output joint. The theta tube is a glass pipette, with an hole having a

diameter of about 250 um, internally shared in two lumens by a septum. Two PTFE fine tubes were inserted in the pipette (one for each lumen) and fixed by a two-component epoxidic glue. The aim of the theta tube is to orient two laminar flows of different solutions, obtaining a straight, well defined interface between them, which can be directly observed when the salt concentrations of the two solutions are different. During the recording, the two flows corresponded instead to extracellular solutions having basically the same composition (having the composition described in 5.7), but just one of them including glycine. Theta tube was hold by the rapid agonist application system (LSS-3200; Burleigh, USA), a piezoelectric actuator that enabled rapid translation of the tube. It was assembled on a coarse manipulator and heavily damped to stop mechanical vibration being transmitted to other components. Sharp-profiled solution switches could be then obtained in this way: the pipette tip with the excided membrane patch was put under the stream of the solution without glycine, close to the theta tube end; the theta tube was then rapidly translated, so that the patch pipette tip entered in the flow of the glycine-containing solution. Similarly, the off phase was given by a fast re-positioning of the theta tube. One of the lumens of the theta tube was always connected to the solution without glycine, while the other was connected to the joint. The joint could receive solution from four syringes, three containing solutions with different glycine concentrations (100 uM, 500 uM, 10 mM), the forth filled with a normal extracellular solution, ten times diluted. All the syringes were hold in a vertical position, mounted on supports at the same height. The fluxes were then produced simply by the gravity, and syringe pistons were only used to fill the tubes avoiding air bubbles, during set up preparation, and to clean at the end of the experiments, inserting ethanol in all the tube network. The output solution of the joint could be manually switched by a knob.

115

An experimental acquisition was mainly composed by these steps:

1) Transfected cells on a coverslip are placed in the tub, under the microscope objective; a perfusion system composed by two magnetically-anchored tubes, placed in correspondence of opposite sites of the tub, fix a constant level of extracellular solution (bathing solution).

2) The theta tube is positioned with the tip inside the bathing solution and connected, by the joint, with syringe filled with the diluted solution. Since the other lumen is always filled with normal extracellular solution, it is possible to observe the interface between the two streams. A constant 60 mV ddp is imposed by the Axopatch amplifier.

3) The patch clamp pipette is positioned, inserting its tip in the not diluted solution flow. The piezoelectric actuator, driven by a specific software, winWCP (developed by Dr. John Dempster, of the University of Strathclyde in Glasgow, U.K.), switches the theta tube between two positions: in this way, the patch pipette tip is wet alternatively by the two solutions.

4) The relative position between the patch pipette and the theta tube is adjusted (and, eventually, also the amplitude of the piezoelectric oscillation), until the electrical response, caused by the different conductivity of the two solutions of the theta tube flows, assumes a square-wave shape.

5) The piezoelectric actuator is turned off (in the starting position).

6) The patch pipette is moved to the cells and an outside-out patch is realised. Basically, after sealed the cell surface like in cell-attached configuration, a strong positive intra-pipette pressure is created,

breaking the membrane patch under the tip. The patch pipette is then quickly raised, so that the attached membrane pieces fold back on themselves onto a patch covering the pipette.

7) The patch pipette is exposed to the theta tube flow, in the position previously chosen.

8) The first glycine concentration (10 mM) is set through the joint.

9) A protocol is applied to the actuator, imposing pulses 1.3 s long, repeated every 20 seconds.

10) Possible channel rundown is monitored, observing the peaks of the channel responses to the high concentration pulses in subsequent cycles.

11) Since the electrical response became roughly constant in amplitude, at least 10 cycles are recorded.

12) Step (11) is repeated for the other glycine concentrations (100 uM and 500 uM).

13) Another series of cycles with 10 mM glycine are realised, in order to check that the peak response is not decreased meanwhile.

14) The membrane patch is broken through an intra-pipette pressures, and the diluted solution is imposed through the theta tube.

15) The electrical wave shape is recorded. In fact, it corresponds to the glycine concentration pulse shape and is then used as input signal for analysing data.

In figure 5.11 examples of these recorded waveforms are shown. Macroscopic currents shown are averages of 6- 10 single sweeps.
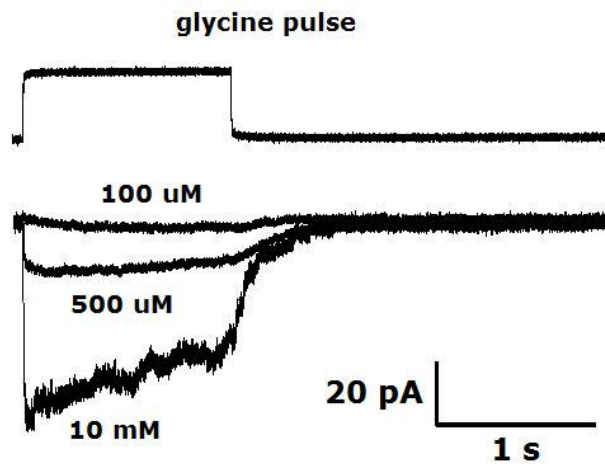
Figure 5.11 recorded waveforms from application of 1,2 s long concentration jumps. Three glycine concentrations were used: 100 uM, 500 uM, 10 mM.

5.10.1 Concentration jump current analysis

In the time course of the channel responses to the glycine pulses, three different phases can be observed. In the first phase, just after the application of the stimulus, there is a raising, due to the agonist bindings and the following openings, which lead to a peak. Larger is the glycine concentration applied, greater is the value of this peak and faster is the rise time. During the second phase, which starts after the peak, current declines until it reaches steady state. This decline of current happens despite the glycine is present in the solution. This phase is evident only for high glycine concentrations and it this is due to the desensitisation of the channels after the agonist binding. In particular, if we observe the saturation condition (10 mM) and assume that the activation

118

kinetics is extremely faster than the desensitization one, the peak corresponds to the all open channels condition, while the plateau represents the equilibrium: this means that the ratio between the plateau and the peak amplitudes is close to the overall open state probability of the receptors in equilibrium conditions. The third phase, after the end of the agonist pulse application, is a slow decaying due to the channel deactivation. Measurements of time course of all these phases are reported in the table 5.4. Concentration jump experiments were done on eight different patches. In four cases, the protocol just described was followed till its end, while in three cases, only the 10 mM and 500 uM concentration jumps were applied. In the last case, only the saturating concentration was applied before the patch was lost. Average values and coefficients of variation are reported, with regard to the peak amplitude, the 10-90% rise time, and the desensitisation and the deactivation constant times (these last two phases were fitted by a single exponential).

10 mM glycine concentration				
	10-90% rise time (ms)	**Desens. time Constant (ms)**	**Deact. time Constant (ms)**	**Amplitude (pA)**
Mean value	1.43	8.68	362	448
CV%	15	31	21	21
500 uM glycine concentration				
	10-90% rise time (ms)	**Desens. time Constant (ms)**	**Deact. time Constant (ms)**	**Amplitude (pA)**
Mean value	29	1575	393	276
CV%	24	37	26	28

100 uM glycine concentration				
	10-90% rise time (ms)	Desens. time Constant (ms)	Deact. time Constant (ms)	Amplitude (pA)
Mean value	2315	--	251	74
CV%	86	--	20	29

Table 5.4   Rise time and desensitisation and deactivation time constants from concentration jump experiments.

Hill equation was then fitted using the amplitude peak values, obtaining an EC_{50} of 355 uM (EC_{50} is the agonist concentration corresponding to a channel open probability of 0.5), and a Hill slope $n_H=1.29$. Hill curve is depicted in figure 5.12.
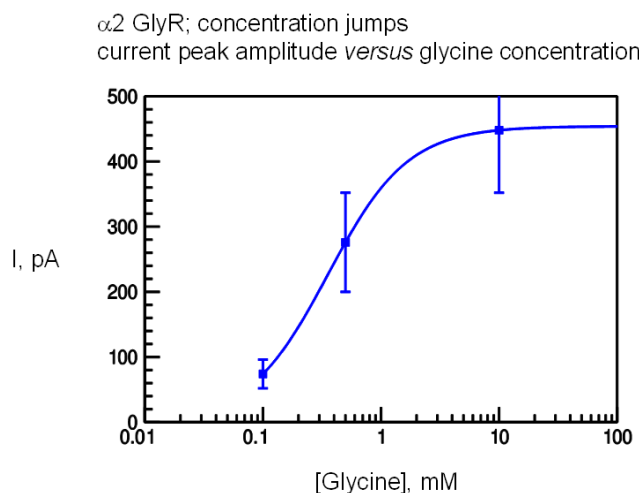

Figure 5.12   Hill equation fitted from amplitude peaks values in jumps experiments..

In agonist saturating concentration, if we assume that the binding process is largely faster than the deactivation one, we can achieve information concerning two different kinetics: agonist binding (from the first rising of the signal) and desensitisation (from the second part, till the plateau value). Instead, it is not straightforward to obtain useful information from the last part (the response after the end of the agonist application), because its kinetics is complex and depends on several rates, not only the dissociation one.

5.10.2   Rate constants estimation

The macroscopic currents obtained from concentration jumps were fitted using the software tool Channelab (Synaptosft Inc., Decatur, USA). Desensitisation and association rate constants were determined by least squares minimization fitting. Compared to the model used for single channel analysis, represented in figure 5.10, the one used in macroscopic current fittings included two desensitisation states D_1 and D_2, connected to the state A_3F^*. The number and the position of the desensitisation states were chosen in analogy with the heteromeric $\alpha_1\beta$ receptor (Beato et al., 2007). This model, shown in figure 5.13, was given as input to Channelab software. All the rate constants were fixed except the four rates relating to D_1 and D_2 or the binding rate $k_{+1} (= k_{+2} = k_{+3})$. All the fixed rates had the same values taken from single channel-steady state fitting by HJCfit. Fitting by Channelab was then conduced in two stages. Firstly, the saturating concentration trace was fitted, from the onset of the application up to the time when desensitisation reached the plateau (500 ms later). In this way, the rates for entry and exit into the desensitization states together with the association rate constant were estimated. Actually, since all the data points had the same weight in the fitting, and the initial rise time is greatly shorter than the

121

subsequent decay, this fit provided a good estimation only of the desensitization rates. Another fitting was then performed with k_{+1} the only free parameter. In this case, the traces of all the concentrations (10 mM, 500 uM and 100 uM) where fitted simultaneously and only the initial rise time was considered. Standard deviation of these rates are not available because just one acquisition set was used for fitting and the used software tool doesn't provide the an internal std estimation. The overall model, including the rates finally achieved, is reported in figure 5.13.
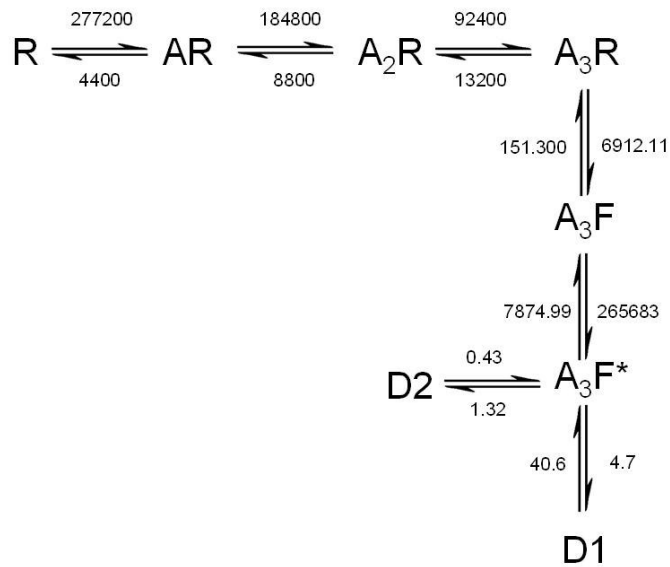
Figure 5.13   Overall model, including desensitizing states, with the estimated rate constants

122

6 Limits of using ligand gated ion channels as sensing elements

Let's start our final considerations from the Del Castillo-Katz model, which is a simple but significant example of ligand gated ion channel representation. It highlights that the activation of a ligand gated ion channel passes inevitably through two different stages: the binding between the receptor and one (or more) specific target molecules, and the opening of the selective pore, allowing ions to flow through. Observing the model, the presence of these two stages is reflected in the fact that the current-response of the receptor is influenced by two different ratios: the gating efficacy E and the dissociation rate constant K_{diss}. Channel efficacy is given by the ratio between opening and shutting constants ($E = \beta / \alpha$), and its value mainly depends on the energy barriers that the channel must exceed in the conformational changes leading from the shut to the open state and vice versa. It can be influenced by several factors: first of all voltage, but also temperature, pH, composition of the bilayer in which the channel is embedded. Dissociation constant K_{diss}, instead, is the ratio between the rate constants of the inverse and the direct binding reactions ($K_{diss} = K_I / K_D$). It depends, basically, on the strength of the chemical bond between the receptive site of the ligand gated ion channel and the agonist molecule, and it is then influenced by several variables (above all temperature and pH).
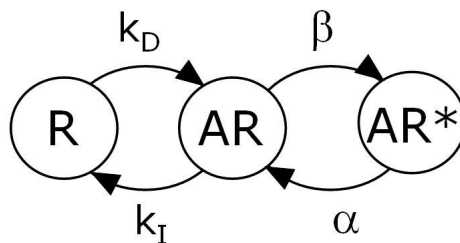
Figure 6.1   Del Castillo-Katz model.

In order to understand how E and K_{diss} influence the signal channel gating mechanism, the relation between agonist concentration [A] and open state probability, corresponding to the probability of being, in steady-state conditions, in the state AR*, must be considered. It can be drawn using the method described in section 3.4.3 or, in this simple case, solving the system

$$\begin{cases} \beta\, P_{AR} - \alpha\, P_{AR^*} = 0 \\[2mm] K_I\, P_{AR} - [A]\, K_D\, P_R = 0 \\[2mm] P_R + P_{AR} + P_{AR^*} = 1 \end{cases} \qquad (6.1)$$

In the system above, the first two equations are the differential equations describing the kinetics of the states R and AR*, where the derivatives were set to zero, since we are in equilibrium conditions. The third equations, instead, indicates that the probability of being in one of the states of the system must clearly be 1. From system 6.1 it follows that the probability of being in the unique open state of the system is

$$P_{open} = P_{AR^*} = \frac{[A]\, E}{K_{diss} + [A]\,(1 + E)}. \qquad (6.2)$$

In ligand saturating conditions, namely when $[A]$ tends to infinity, the asymptotic value of the open state probability is set by $E/(E+1) = \beta/(\beta+\alpha)$. This is a logical consequence, considering that, in saturating conditions, the receptive site of the ion channel is basically always bound: the state R has an occupancy probability close to zero and the three-states Del Castillo Katz model becomes a two-state model, formed by AR and AR*. Other information could be gotten from the slope of the function $P_{open} = P_{open}([A])$, which is expressed by (6.3).

124

$$\frac{dP_{open}}{d[A]} = \frac{E\,K_{diss}}{\left\{K_{diss} + [A]\,(1+E)\right\}^2} \qquad (6.3)$$

It is immediate to observe that, for very small concentrations, when *[A]* tends to zero, the slope of the curve tends to the value E/K_{diss}. It means that the two rate constants ratios have the same weight in influencing the relationship between open state probability and ligand concentration. A big efficacy E increases the slope, because give to the channel an high probability to move and remain in the open state whenever it reaches the bound condition. A small value of K_{diss} corresponds to a "sticky" chemical binding between ligand and receptor molecules. It means that, every time that the channel binds, it holds the agonist molecule for long time, making the channel opening easy.
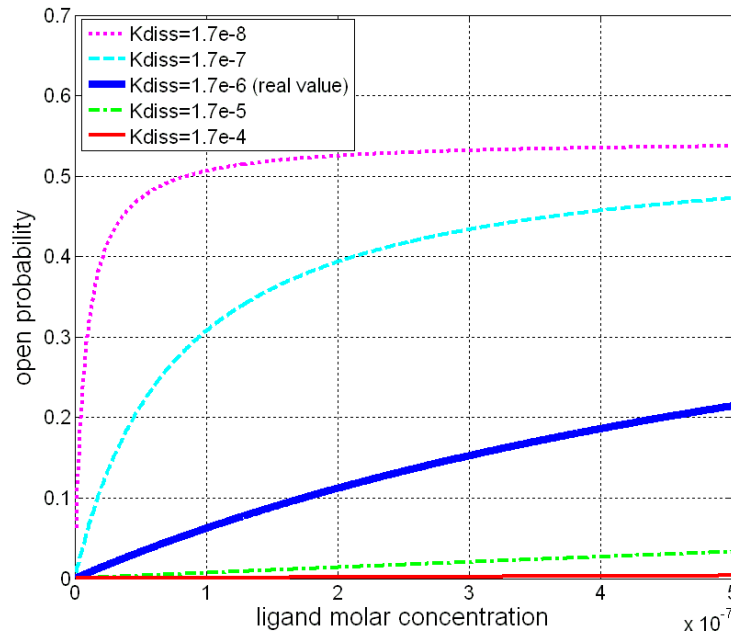
Figure 6.2   Example of the dependence of $P_{open}([A])$ on the dissociation constant. The other rates refer to an application of a Del Castillo-Katz model to a muscarinic receptor (Osterrieder, 1980) coupled with a G protein.

Finally, it can be observed that the function $P_{open} = P_{open}([A])$ is monotonically increasing, since it's derivative is always positive (because E and K_{diss} are, clearly, always positive); the slope, instead, is a monotonically decreasing function of the concentration, because [A] occurs only at the denominator. It could be than useful to understand how the parameters E and K_{diss} influence the passage from an high slope to a low slope condition. In particular, we can obtain an idea of it by extrapolating the concentration value $[A]^1$, corresponding to an unitary slope:

$$[A]^1 = \frac{\sqrt{E K_{diss}} - K_{diss}}{1 + E} \tag{6.4}$$

Since, in every case, the dissociation constant is several orders of magnitude lower than the efficacy ($E >> K_{diss}$), the expression above can be approximated:

$$[A]^1 \simeq \frac{\sqrt{E K_{diss}}}{1 + E} \tag{6.5}$$

So, for low values of K_{diss}, namely in case of "sticky" chemical bindings, the concentration value $[A]^1$ is low, increasing as the square root of the dissociation constant. When E increases (for values of E greater than 1), the concentration value $[A]^1$ moves left.

In order to use these kind of receptors for building chemical sensors, and, in particular, extracting the ligand concentration values from an estimation of the channel open probability, some considerations can be done. The first thing it could be important to achieve is a good lower limit of quantification (LLOQ). It is the lower value of concentration which could be measured with an acceptable relative error: in particular, it can be considered as the smaller concentration value whose measurement is characterized by a coefficient of variation lower

126

than 20% (FDA Guidance for Industry, 2001). Obviously, an high initial slope of the $P_{open}([A])$ curve could assure better LLOQ values. Best performance, in this sense, could be obtained with channels having large values of efficacy and small dissociation constants. On the other side, we could be interested in having a large assay range, defined as the difference between the upper limit of quantification (ULOQ) and LLOQ. The upper limit of quantification can be defined as the greater concentration value which can be estimated with a coefficient of variation lower than 15%: it depends, clearly, on the slope of the curve in proximity of the channel saturating conditions. In fact, since the slope of $P_{open}([A])$ steadily decreases when *[A]* increases, small variations in the probability estimations produce steadily increasing errors in the ligand concentration readout.
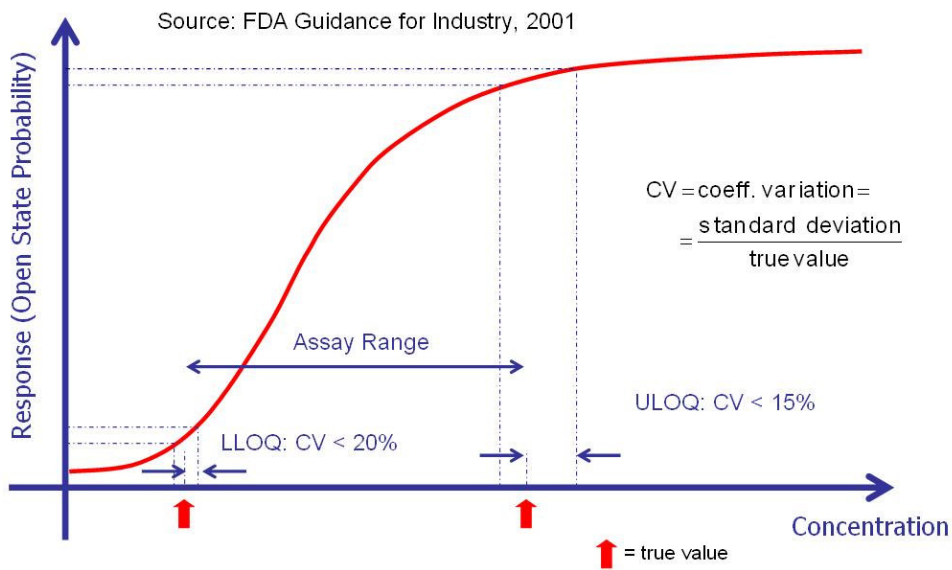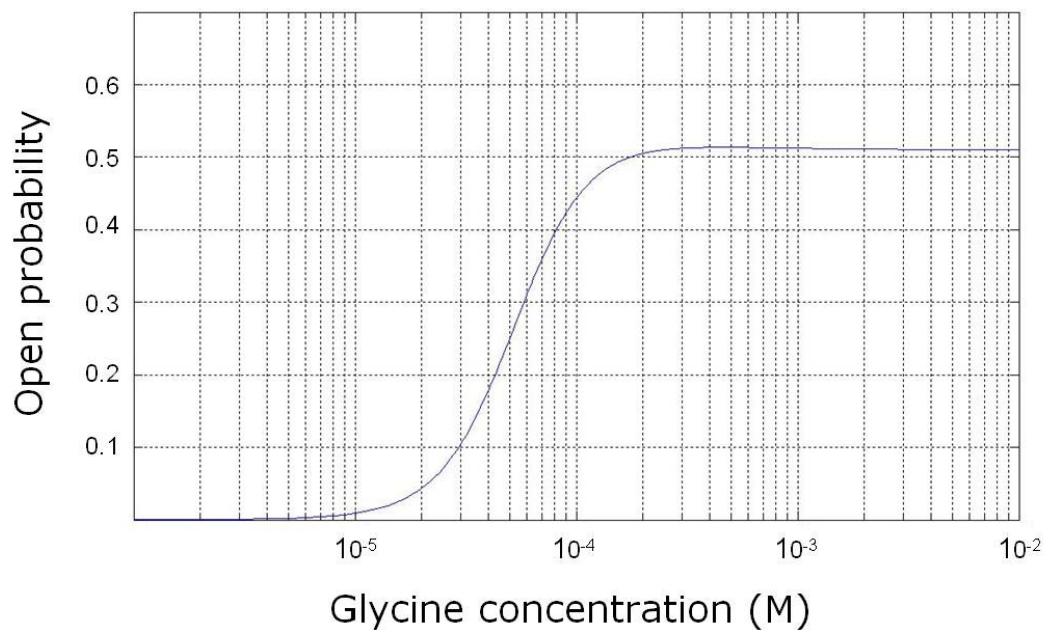

Figure 6.3   Concentration-response curve of a generic ligand gated ion channel.

From the analysis of the dependence of $[A]^1$ from the two parameters E and K_{diss}, it is possible to understand that a trade-off exists between the capability of obtaining a good LLOQ and a good ULOQ value. In particular, a value of E close to 1 represent an optimum for the ULOQ. Nevertheless E fixes also the asymptotic value which the open state probability can achieve: for these reason, and for its importance in guaranteeing a small LLOQ, it could be preferable to have a big efficacy value, able to allow P_{open} to reach values close to one for high agonist concentration values. The same trade-off problem affects the binding step: a "sticky" bound allows better values for the LLOQ, but leads $P_{open}([A])$ to quick saturation.

If we want to estimate the ligand concentration from the channel open state probability, following an approach like the one described in Chapter 4, another question to keep in consideration is the "quantity of information" that can be obtained from a record having a given temporal length. In fact, in this case, each sample of the record is basically considered as the value assumed by a binomial random variable having the open state probability as a parameter. The value of P_{open} is then determined on the basis of several observations, represented by the samples. It is then intuitive that, if we have a certain number of samples N_S, the overall information that they can give to the estimator depends on what's their level of correlation. If, for example, the kinetics of the channel presents a very long shut lifetime, and the N_S samples are taken, close together, all during the same shut period, they will bring no information. In order to bring the most information, they should have a temporal distance able to guarantee the independence of the observations. Therefore, if a channel has a complex kinetics, or has states with a very long mean lifetime, the acquisitions should become very long, in order to allow a satisfactory estimation. We could observe this limit in the Del Castillo-Katz model, when E or K_{diss} become too high: in particular, this means that the channel is too "sticky", so the number of binding events in a limited amount of time is inevitably too low for allowing a

statistical analysis. This is also, for example, the case of the homomeric α_2 glycine receptors described in Chapter 5, characterised by long inter-burst and inter-cluster periods. Another limit for this class of receptors is the relatively high ligand concentration that they need to become active. In fact, in the chapter dedicated to the single channel analysis, it was pointed out that homomeric α_2 glycine receptors can't be active for agonist concentrations smaller than tens of micromoles. Also in the case of the more functional heteromeric $\alpha_1\beta$ form, the overall open state probability gets to values close to the 1% only when the glycine concentration is larger than 10 uM. Similar (or even worst) lower limits of detection characterise all the receptors belonging to the nicotinic superfamily and, in general, are typical of the ligand gated ion channels regulated by extra-cellular agonist molecules. The reason of this behaviour can be understood thinking about their role in the cell membranes. In fact, these receptors are mainly located in the nerve cells, where turn neurotransmitter chemicals coming from the neighbouring cells in depolarizing electrical signals, allowing in this way the information transition between neurons. Neurotransmitter molecules are not homogeneously distributed in the extracellular fluid, because in this conditions, obviously, they could damage the correct propagation of the information stimuli, creating a cross-talking between cells. Chemical receptors, instead, thicken in correspondence of the synapses, specialized junctions where neurons are close together and parted by a gap, which is about 20 nm wide (synaptic cleft). Here, the presynaptic neurons secrete the agonist (neurotransmitter), inside specific vesicles: in this way, a relatively high concentration of target molecules can quickly spreads around the receptors facing into the synapse. The possible range of a sensor involving, as sensing element, such channels, goes basically from the tens of micromoles to, at the most, the millimolar concentration. An example of concentration response curve, referring to the $\alpha_1\beta$ heteromeric form of the glycine receptor, was drawn, using a Matlab routine, from the rate constants reported in two papers of the same group: Burzomato et al., 2004; Beato et al., 2007. From this last paper, in

particular, the rates referring to two desensitising states were considered, both connected with the tri-liganded opening; no information were inserted about other possible desensitizing states connected with mono- or di-liganded open states. The curve was drawn on the basis of the states occupancies of the three open states (the overall open probability is the sum of these three contributes) in function of the glycine concentration.

Figure 6.4   Concentration-response curve of the $\alpha_1\beta$ glycine receptor.

Basically, in this case, a measurable channel activity can be observed from a 10 uM concentration, and the saturation is reached around 200 uM. For very high glycine concentrations, it's possible to observe a slight reduction of the open probability, due to the desensitizing states.

The modelling of such a channel wase realised by an HJCfit fitting, following the procedures described in Chapter 5. HJCfit estimator is able to consider, for its fitting, a large amount of information concerning the lifetime of the sojourns in the states. A similar procedure could be used also for the readout of the ligand concentration, having, in this case, *[A]* as the unique parameter. However, this procedure could be very hard to realise in an automatic way. Firstly, it could be necessary to consider very complex models, characterised by several time constants, with very fast kinetic components. A great temporal resolution could be needed, and this is not reachable, at present, in BLMs obtained in an automatic way, because of the relatively large dimensions of the membranes, necessary for inserting complex ion channels through vesicles fusion (see section 2.8). Moreover, the idealisation of the record in an automatic way is a greatly challenging and unsafe process (as observed by D. Colquhoun, 1995). Probably, the way described in Chapter 4, even if it doesn't use all the possible information, could be more suitable, eventually tailoring it to the characteristics of the used ligand gated ion channels. In the case of channels of the nicotinic superfamily, for example, it could be useful to consider only the parts of the records corresponding to single channel bursts, extracting their open probability simply from the amplitude histograms. In particular, this could be realised extracting the parts of record containing bursts and clusters of a single ion channel by a threshold-based procedure. The open probability during the single burst and cluster could be then easily extracted from the subtended area of the signal, if the used filter approximates the Gaussian one.

Conclusions

In this thesis, several aspects were described and analysed, concerning the use of ligand gated ion channels as constitutive elements of chemical sensors. The attempt to use such natural nanomachines is a consequence of several considerations. Firstly, the increasing interest for chemical and biological assays, especially in the diagnostic field. Here the most widespread used ELISA assays show, in most applications, heavy limits in terms of performance, costs, reliability, time and ease to use. Moreover, the current developments, both in nanotechnologies and in genetic engineering, could allow the use of "tailored" ion channels, embedded in artificial systems and potentially able to detect single molecule bindings: consequently, they could bring to a strong reduction of the lower limits of detection, respect to the state of art sensors. Actually, in my experiments I tested the behaviour of natural ion channels, not engineerized for the proposed applications; anyway, my impression is that the use of LGICs as sensing elements has, at present, several practical limits, as discussed in Chapter 6. The kinetic behaviour of the principle neural ligand gated ion channels, for example, doesn't allow to quantify concentrations under the micromolar range. Moreover, in touch with complex mixtures, their current response show alterations, even if the receptive sites have a great affinity for the target molecules, probably due to partial occlusion of the conductive pores. Also from the point of view of the artificial bilayer creations and the insertion of channels, many practical problems must be overcome. In particular, there is a clash between two different requirements: stability of the artificial membranes and capability to insert the receptors. In order to have resistant membranes, more stable than the suspended bilayers usually adopted in the biological laboratories, it appears to be mandatory to decrease the dimensions of the substrate's pores, or to support the bilayer as mentioned in section 2.5. On the other side, these contrivances don't permit the efficacious insertion of complex

channels like the LGICs. An "hybrid" strategy, studied by several research groups and consisting in the creation of supported bilayers on nanoporous substrates, could be promising; however, the investigations made so far require time to be fully proven. In conclusion, it seems difficult that LGIC-based sensors, could compete with state-of-the-art techniques commercially available in the near future.

However, new perspectives are very recently coming worldwide into the scene due to the availability of artificial pores in the nanometer size. These pores are competing natural ion channels from both the stability and the functionality point of view avoiding the high complexity in handling artificial lipid bilayers. Therefore, in this scenario, the work done in this thesis regarding single molecule stochastic analysis will be extremely fruitful to understand the perspectives of these novel technologies.

Appendix A

EIGENVALUES AND EIGENVECTORS OF A MATRIX

Given an $n \times n$ matrix M, a nonzero $n \times 1$ column vector $\bar{x}$ is said to be an eigenvctor of M if there is a scalar λ such that

$$M\bar{x} = \lambda \bar{x}. \tag{A.1}$$

In this case, λ is the eigenvalue corresponding to $\bar{x}$. Such an eigenvector is not unique: it can be multiplied by any nonzero scalar; equation remains satisfied. The above equation can be equally written as

$$(M - \lambda I)\bar{x} = 0 \tag{A.2}$$

where I is the $n \times n$ identity matrix. Any square matrix, when is multiplied by a nonzero vector, can be yield a zero result only if it is singular, namely, its determinant is zero. Thus the eigenvectors of M can be found solving the equation

$$|M - \lambda I| = 0 \tag{A.3}$$

The set of equations $M\bar{x}_i = \lambda I$, $i = 1,2,...,n$ can be written in a single matrix equation

$$MX = X\Lambda \tag{A.4}$$

134

where X is a matrix having the eigenvalues of M as columns, Λ is an $n \times n$ diagonal matrix whose diagonal elements are the eigenvalues of M.

In case of reversible Markov processes (like the ones used for modelling ion channels), the eigenvalues are all real and distinct and X is also real and invertible; Postmultiplying the elements of (A.4) for X^{-1} we obtain

$$X\Lambda X^{-1} = MXX^{-1} = MI = M \tag{A.5}$$

So, M matrix can be expressed starting from its eigenvectors and eigenvalues. This property can be useful, for example, to calculate the powers of the matrix. In fact

$$
\begin{aligned}
M^2 &= X\Lambda X^{-1} X\Lambda X^{-1} = X\Lambda\Lambda X^{-1} = X\Lambda^2 X^{-1} \\
M^3 &= X\Lambda X^{-1} X\Lambda X^{-1} X\Lambda X^{-1} = X\Lambda^3 X^{-1} \\
&\ldots \\
M^r &= X\Lambda^r X^{-1}
\end{aligned}
\tag{A.6}
$$

where Λ^r is simply another diagonal matrix having the powers of the eigenvalues (λ_i^r, $i = 1, 2, ..., n$) as diagonal elements.

It is also possible to express M^r, and, in general, every function of M, using its spectral matrices. In fact, considering X^{-1} as a set of n columns y_i, $i = 1, 2, ..., n$, the product $X\Lambda^r X^{-1}$ can be written as

$$
X\Lambda^r X^{-1} = \begin{bmatrix} x_1 & x_2 & x_n \end{bmatrix}
\begin{bmatrix}
\lambda_1^r & 0 & \ldots & 0 \\
0 & \lambda_2^r & & \\
\ldots & & \ldots & \ldots \\
0 & & & \lambda_n^r
\end{bmatrix}
\begin{bmatrix}
y_1 \\
y_2 \\
\ldots \\
y_n
\end{bmatrix}
= \sum_{i=1}^{n} x_i y_i \lambda_i
\tag{A.7}
$$

where the elements x_i y_i are $n \times n$ matrices, called *spectral matrices* of the matrix M:

$$A_i = x_i y_i, \quad i = 1,2,...,n \tag{A.8}$$

Equation A can be than written as a composition of the eigenvalues and the spectral matrices of M:

$$M^r = \sum_{i=1}^{n} A_i \lambda_i^r \tag{A.9}$$

But this important result can be extended. Spectral matrices can be used for calculating any function of the matrix M, as:

$$f(M) = \sum_{i=1}^{n} f(\lambda_i) A_i \tag{A.10}$$

This result, due to J. J. Sylvester, give us a practical way to calculate $exp(Qt)$, allowing the p.d.fs of the time distributions of the ion channels to be expressed as a mixture of scalar exponential components:

$$exp(Qt) = \sum_{i=1}^{n} exp(\lambda_i t) A_i \tag{A.11}$$

Appendix B

IMPEDIMETRIC ANALYSIS OF THE WARNER INSTRUMENTS PLANAR LIPID BILAYER WORKSTATION.

INTRODUCTION

The subject of this appendix is an impedimetric analysis of the system for the creation of artificial lipid bilayers realized by Warner Instruments. In particular, the device under analysis is the cup and chamber system included in the Planar Lipid Bilayer Workstation.

The study involves:

- the definition of an electrical model of the system;
- the estimation of the main model's parameters;
- the comparison of the estimated values with the values resulting from experimental data.

Experimental data were produced using an LCR Meter (Agilent 4284A Precision LCR Meter, USA), acquiring the real and the imaginary part of the system impedance simultaneously at various frequency in the range between 20 Hz and 1 MHz. Starting from these data values, fitting, plotting and parameter's calculation were realized using the software tool LEVM (Solartron Analytical, UK).

ELECTRICAL MODEL

The Warner system is formed by a chamber in black delrin in which a cylindrical delrin cup is inserted. On the surface of the cup, whose wall is 1 mm thick, there is a concavity: in its thinnest part, where the wall is only 250 um thick, there is the hole which the bilayers are realized across.
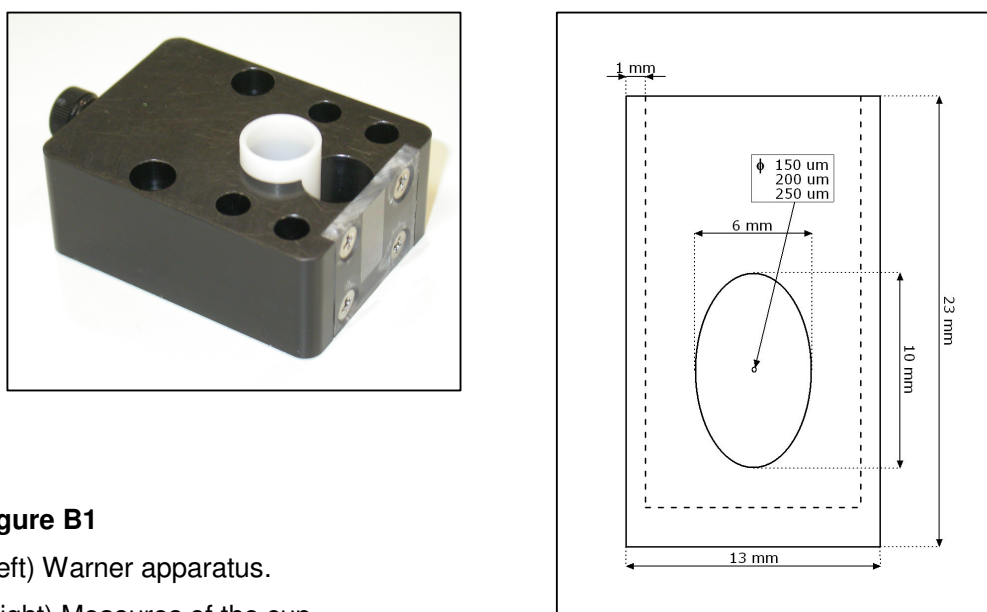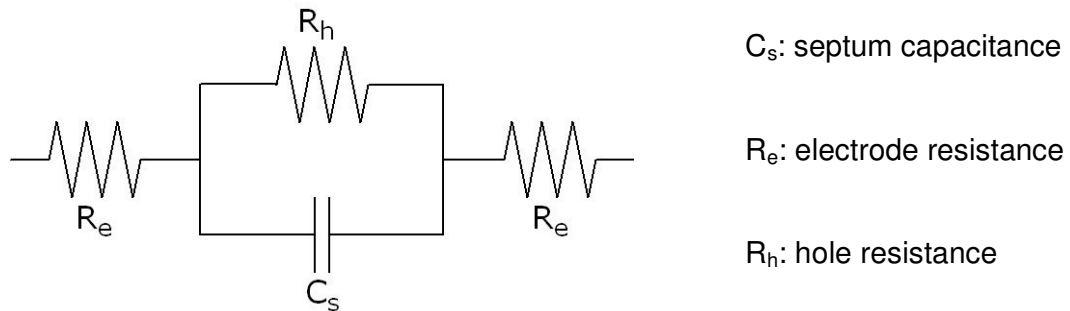

Figure B1

(Left) Warner apparatus.

(Right) Measures of the cup.

The impedance acquisitions are made by the LCR Meter, using four-terminal configuration and auto-balancing bridge method. The electrical connections are obtained linking the BNC cables on a metal board with two Ag/AgCl cylindrical electrodes. The two compartments of the Warner system are filled by electrolytic solution and communicate through the hole (in absence of formed membranes). The Ag/AgCl electrodes are immersed in solution, one for compartment.

The DUT, between the electrodes, can be modelled using this scheme (for low frequencies):

R_h

C_s: septum capacitance

R_e: electrode resistance

R_e

R_h: hole resistance

C_s

Figure B2
system electrical model

This scheme, composed by a resistance ($2R_e$) with in series the parallel between a resistance and a capacitance (R_h and C_s) can be plotted on a Nyquist diagram, where the the x-axis is the real part of the total impedance and the y-axis is the imaginary part changed in sign. The qualitative graph is the following one, where the arrow indicates the direction of the increasing frequencies.
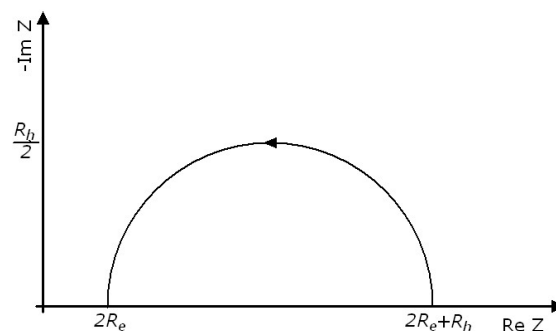
Figure B3   Expected shape of the Nyquist diagram of the system

The two resistance values can be easily obtained from the graph, by the points where the plot crosses the x-axis. The value of the septum capacitance can be obtained noting that the trajectory described by the system is a semicircumference. The overall impedance of the system, Z, is given by:

$$Z = 2R_e + \frac{R_h}{1 + j\omega C_s R_h} \qquad\qquad (B.1)$$

so, at the characteristic angular frequency $\omega_C = \dfrac{1}{C_s R_h}$, we have:

$$Z(\omega_C) = 2R_e + \frac{R_h}{1+j}$$
$$Re\{Z(\omega_C)\} = 2R_e + \frac{R_h}{2}, \quad -Im\{Z(\omega_C)\} = \frac{R_h}{2}. \qquad (B.2)$$

The characteristic angular frequency corresponds to the maximum, in the y-axis, of the lobe; the value of Cs can be obtained from: $C_s = 1/\omega_C R_h$.

CALCULATION OF THE MODEL PARAMETERS

Septum Capacitance (C$_s$)

As previously shown, the system for bilayer creation is formed by two compartments solution-filled divided by a septum. In the Warner system, a delrin cup is embedded in a chamber, in a specially shaped hole. The cup is not hermetically sealed in the chamber, so a thin solution layer envelops it.

When the frequencies are not too high (as in our case, where they are lower than 1 MHz), the electrolytic solution behaves like a metal, while the cylindrical delrin cup is a dielectric, being the conductivity of the delrin quite low (ε_r=3.7). Therefore, the cuvette filled and surrounded by electrolytic solution behaves like a cylindrical capacitor. In our case, neglecting the presence of the concavity and of the hole, the value of the capacitance can be obtained by:

$$C_s = \frac{2\pi\varepsilon_o\varepsilon_r\, h}{\ln(\frac{d_{ext}}{d_{int}})} = \frac{2\pi * 8.85 * 10^{-12} * 3.7 * 15 * 10^{-3}}{\ln(\frac{13 * 10^{-3}}{11 * 10^{-3}})} = 18.5\,pF \qquad\qquad (B.3)$$

where h=15 mm is the cuvette's height, d_{ext}=13 mm and d_{int}= 11 mm are its external and internal diameters. Further simulations made using FemLab showed that the presence of the concavity introduces a contribution of 5 pF. Consequently, the overall septum capacitance becomes:

$C_s = 18.5 + 5 = 23.5\,pF$

Hole Resistance (R_h)

As shown in figure B1, Warner produces cup having holes with three different sizes. In proximity of the hole, the wells are in every case 250 um thick. Calling σ the conductivity of the solution, A the hole's area, l the hole thickness, R_h is given by:

$$R_h = \frac{1}{\sigma}\frac{l}{A}. \qquad\qquad (B.4)$$

In the experiments afterwards presented, the cup had a 150 um-diameter hole and the solution, the same for both the compartments, was 0.1M of KCl in

distilled water. For this solution and this salt concentration, the conductivity is $\sigma_{KCl} = 1.264$ $\Omega^{-1}m^{-1}$, at a temperature of $24^oC^{[1]}$. Then, the estimate hole resistance is:

$$R_h = \frac{1}{s_{KCl}} \frac{l}{A} = \frac{1}{1.264} \frac{250 * 10^{-6}}{\pi * (\frac{150 * 10^{-6}}{2})^2} = 11.2 \, KW \tag{B.5}$$

[1] The conductivity value was gotten from tables.

Electrode Resistance (R_e)

This term depicts, at frequencies upper then some tens of Hz, the behaviour of the interface between the electrode and the electrolytic solution, where the ion charge accumulates and redox occurs. At lower frequencies, the electrode-solution interface couldn't be represented only by an omhic resistance, becoming the impedance expression given by the parallel of a capacitance (double layer capacitance) and the charge transfer resistance.

In every case it's hard to estimate the electrode resistance R_e, because it's expression $R_e = RT/nFi_0$ shows that it depends on the exchange current i_0. The exchange current is the current that flows from electrode to solution (or from solution to electrode) at the equilibrium (without ddp applied) and in most cases is unknown. However, the impossibility in calculating R_e is not a big matter, because the electrode resistance actually moves the lobe in the x-axis but doesn't modify its shape.

PARAMETERS VALUES FROM EXPERIMENTAL DATA

The following results refer to three impedimetric acquisitions made on the Warner system by the LCR Meter. The values of the real and the imaginary parts of the impedance were measured in correspondence of about fifty frequency values between 20 Hz and 1 MHz.

In all the experiments, the same setup was used:

- the cup had a 150 um diameter hole
- the solution was 0.1M of KCl
- the Ag/AgCl electrodes were prepared inserting the silver electrodes in bleach for about fifteen minutes
- the applied voltage, during the acquisitions, was 100 mV
- final Z(f) values were obtained averaging thirty measurements
- during the acquisition, DUT was placed in a Faraday cage.

The first experimental acquisition was done on the 12th of January 2005, without measuring the effective conductance of the KCl solution (the conductivity value was got from tables). The others two acquisitions were performed on 4th of November 2005, using two different cup-chamber systems: the first one is a system used for several months for bilayer experiments, the second is new.

Nyquist diagrams of the three experiments were made using Matlab and the parameters values were calculate using LEVM, fitting the data with a complex nonlinear square method.
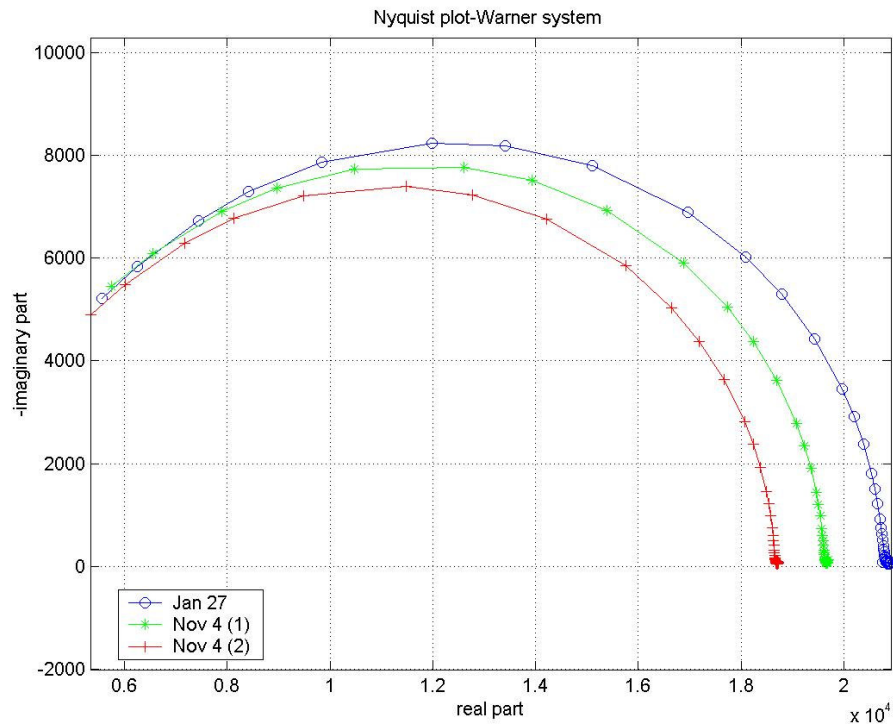
Figure B4   Nyquist diagram of the experimental acquisitions

The following table shows the calculated parameters R_h, C_s, $2R_e$, resulting from the LEVM fitting.

	R_h [kOhm]	C_s [pF]	$2R_e$ [kOhm]
27th Jan	16.65	33.52	4.15
4th Nov (old system)	15.72	29.85	3.90
4th Nov (new system)	14.85	34.11	3.81

Table B1   Calculated values

COMPARISON BETWEEN VALUED AND FITTED VALUES

In order to understand how the proposed model can predict the behaviour of the system, the percentage errors in the valuation of R_h and C_s is presented for all the experiments:

	$\Delta R_h\%$	$\Delta C_s\%$
27th Jan	48.7	42.6
4th Nov (old system)	40.3	27.0
4th Nov (new system)	32.6	45.1

Table B2   Mean percentage errors

Instead the percentage displacements between the values calculated in different experiments, referred to the smallest values, are:

$$\frac{R_{h,MAX} - R_{h,MIN}}{R_{h,MIN}} * 100 = \frac{16.65 - 14.85}{14.85} * 100 = 12.12\%$$

$$\frac{C_{s,MAX} - C_{s,MIN}}{C_{s,MIN}} * 100 = \frac{34.11 - 29.85}{29.85} * 100 = 14.27\%$$

(B.6)

Bibliography

Andersen O. S., Koeppe R. E., Roux B. (2005). "Gramicidin channels" IEEE Transactions on Nanobioscience, vol. 4, n. 1.

Akagi H. and Miledi R. (1988). "Heterogeneity of glycine receptors and their messenger RNAs in rat brain and spinal cord". Science 242, Issue 4876, 270-273.

Bayley H. and Cremer P.S. (2001). "Stochastic sensors inspired by biology", Nature 413.

Beato M., Burzomato V., and Sivilotti L. G. (2007) "The kinetics of inhibition of rat recombinant heteromeric $\alpha1\beta$ glycine receptors by the low-affinity antagonist SR-95531" *J Physiol* 580.1:171–179.

Beato M., Groot-Kormelink P. J., Colquhoun D., and Sivilotti L. G. (2004). "The activation mechanism of α1 homomeric glycine receptors". J. Neurosci. 24, 895–906.

Beato M., Groot-Kormelink P. J., Colquhoun D., and Sivilotti L. G. (2002). "Openings of the rat recombinant α1 homomeric glycine receptor as a function of the number of agonist molecules bound". J. Gen. Physiol. 119: 443–466.

Brejc K., van Dijk V. J., Klaassen R. V., Schuurmans M., van der Oost J., Smit A. B. and Sixma T.K.. (2001). "Crystal structure of an ACh-binding protein reveals the ligand-binding domain of nicotinic receptors". Nature 411: 269–276.

Burzomato V., Groot-Kormelink P. J., Sivilotti L. G., Beato M. (2003). "Stoichiometry of Recombinant Heteromeric Glycine Receptors Revealed by a Pore-Lining Region Point Mutation" Recept. Channels 9:353-361.

Burzomato V., Beato M., Groot-Kormelink P. J., Colquhoun D., and Sivilotti L. G. (2004) "Single-Channel Behavior of Heteromeric α1β Glycine Receptors: An

Attempt to Detect a Conformational Change before the Channel Opens". J. Gen. Physiol. 96:395-437.

Cascio, M. (2004). "Structure and Function of the Glycine Receptor and Related Nicotinicoid Receptors" J. Biol. Chem. 279 : 19383–19386.

Celie P., van Rossum-Fikkert S., van Dijk W., Brejc K., Smit A., Sixma T. (2004). "Nicotine and carbamylcholine binding to nicotinic acetylcholine receptors as studied in AChBP crystal structures". Neuron 41: 907–914.

Cohen F. S. (1986). "Fusion of liposomes to planar bilayers". In *Ion Channel Reconstitution*, (ed. C. Miller), pp. 131-139. New York: Plenum.

Cohen, F. S., Niles, W. D., and Akabas, M. H. (1989). "Fusion of phospholipid vesicles with a planar membrane depends on the membrane permeability of the solute used to create the osmotic pressure". *J Gen. Physiol*. 93: 201-210.

Cole, K. S. (1949). "Dynamic electrical characteristics of the squid axon membrane" Arch. Sc. Physiol. *3,* 253.

Colquhoun D and Sigworth F. L. (1995). "Fitting and statistical analysis of single canne records". In *Single Channel Recording, 2nd ed.* (Eds: Sakmann, B., Neher, E.) Plenum Press, New York.

Colquhoun D., Hawkes A.G. (1982). "On the stochastic properties of bursts of single ion channel openings and of clusters of bursts". Philos Trans R Soc Lond (Biol) 300:1–59.

Colquhoun D., Hatton J. C. and Hawkes A. G. (2003). "The quality of maximum likelihood estimates of ion channel rate constants". J Physiol 547.3:699-728.

Del Castillo J. and Katz, B. (1957). "Interaction at end-plate receptors between different choline derivatives". Philos Trans R Soc Lond (Biol) 146:369–381.

J. Dempster. (1993). *Computer Analysis of Electrophysiological Signals*. Academic Press.

Finkelstein A. and Andersen O. S. (1981). "The gramicidin a channel: A review of its permeability characteristics with special reference to the single-file aspect of transport". J. Mem. Biol, 59:155-171.

Finkelstein A., Zimmerberg J. and Cohen, F. S. (1986). "Osmotic swelling of vesicles: its role in the fusion of vesicles in planar phospholipid bilayer membranes and its possible role in exocytosis". *A. Rev. Physiol*. 48:163-174.

Graham J. and Gerard R. (1946) "Membrane potentials and excitation of impaled single muscle fibers", J. Cell. Comp. Physiol 28:99-117.

Gritsch V., Nollert P., Jähnig F. and Sackmann E. (1998). "Impedance spectroscopy of porin and gramicidin pores reconstituted into supported lipid bilayers on indium–tin oxide electrodes". *Langmuir* 14: 3118–3125.

Groot-Kormelink P. J., Beato M., Finotti C., Harvey R. J., Sivilotti L. G. (2002). "Achieving optimal expression for single channel recording: a plasmid ratio approach to the expression of α1 glycine receptors in HEK293 cells". J Neurosci Methods 113:207–214.

Hawkes A. G., Jalali A., Colquhoun D. (1990). "The distributions of the apparent open times and shut times in a single channel record when brief events can not be detected". Philos Trans R Soc Lond A.*332:511–538.*

Hanke W. (1986). "Incorporation of ion channels by fusion". In *Ion Channel Reconstitution*, (ed. C. Miller), pp. 141-153. New York: Plenum.

Hille, B. (2001) *Ion channels of excitable membranes* , 3rd ed., Sinauer Associates.

Hladky S. B., Haydon D. A. (1972). "Ion transfer across lipid membranes in the presence of gramicidin A. I. Studies of the unit conductance channel". Biochim Biophys Acta. 274(2):294-312.

Hodgkin L. and Huxley A. F. (1952). "Currents carried by sodium and potassium ions through the membrane of the giant axon of loligo" J. Physiol. II6:449-472.

Imagawa, T., Smith, J. S., Coronado, R., and Campbell, K. P. (1987). "Purified ryanodine receptor from skeletal muscle sarcoplasmic reticulum is the Ca2+-permeable pore of the Ca release canne". *J. Biol. Chem.* 262: 16636-16643.

Jones M. V., Westbrook G.L. (1995). "Desensitized states prolong GABA channel responses to brief agonist pulses". Neuron 15:181–191.

Koper I. (2007). "Insulating tethered bilayer lipid membranes to study membrane proteins". Mol. BioSyst.3:651–657.

Kuhse J. , Laube B., Magalei D., Betz H. (1993). "Assembly of the inhibitory glycine receptor: identification of amino acid sequence motifs governing subunit stoichiometry". Neuron 11:1049–1056.

Labarca P., Coronado R., and Miller C. (1980). "Thermodynamic and kinetic studies of the gating behaviour of a K+-selective channel from the sarcoplasmic reticulum membrane". *J. Gen.Physiol.* 76:397-424.

Lai, F. A., Erickson H. P., Rousseau E., Liu Q.Y. and Meissner G. (1988). "Purification and reconstitution of the Ca release channel from skeletal muscle". *Nature* 331: 315-319.

Lang H., Duschl C., Grätzel M. and Vogel H. (1992). "Self-assembly of thiolipid molecular layers on gold surfaces: optical and electrochemical characterization". *Thin Solid Films* 210/211: 818–821.

Latorre, R. (1986). "The large calcium-activated potassium channel". In *Ion Channel Reconstitution*, (ed. C. Miller). New York: Plenum.

Legendre P., Muller E., Badiu C. I., Meier J., Vannier C., and Triller A. (2002). "Desensitization of Homomeric α1 Glycine Receptor Increases with Receptor Density" *Mol Pharmacol* 62:817–827.

Malosio M.L. , Marqueze-Pouey B., Kuhse J. and Betz H. (1991). "Widespread expression of glycine receptor subunit mRNAs in the adult and developing rat brain". *EMBO J* 10: 2401–2409.

Mangin J. M., Baloul M., Prado de Carvalho L., Rogister L., Rigo M. and Legendre P. (2003). "Kinetic properties of the α2 homo-oligomeric glycine receptor impairs a proper synaptic functioning" J Physiol553.2:369–386.

Marty A., and Finkelstein A. (1975). "Pores Formed in Lipid Bilayer Membranes by Nystatin "TIIE J. Gen. Physiol. 65:515-526.

Martynski T. and Tien H.T. (1991). "Spontaneous assembly of bilayer membranes on a solid surface". *Bioelectrochem. Bioenerg.* 25:317–324.

McManus O. B., Blatz A. L., Magleby K. L. (1987). "Sampling, log binning, fitting, and plotting durations of open and shut intervals from single channels and the effects of noise". Pflugers Arch. 410 (4-5):530-53.

Miller C. & Racker E. (1976). "Calcium-induced fusion of fragmented sarcoplasmic reticulum with artificial planar bilayers". *J. Memb. Biol.* 30: 283-300.

Miller C. (1978). "Voltage-gated cation conductance channel from fragmented sarcoplasmic reticulum: Steady-state electrical properties". *J. Memb. Biol.* 40:1-23.

Miyazawa A. , Fujiyoshi Y., Unwin N. (2003). "Structure and gating mechanism of the acetylcholine receptor pore". Nature 424: 949–955.

Moczydlowsky E., Garber S. H. and Miller, C. (1984). "Batrachotoxin-activated Na+ channels"in planar lipid bilayers. Competition of tetrodotoxin block by Na+". *J. Gen. Physiol.* 84:665-686.

Molleman A. (2003). *Patch Clamping: An Introductory Guide to Patch Clamp Electrophysiology*., Wiley and Sons ed., UK.

Monod J. L. , Wyman J. J. and Changeux J. P. (1965). "On the nature of allosteric transitions: a plausible model". J. Mol. Biol. 12:88-118.

Montal M., and Mueller P. (1972). "Formation of bimolecular membranes from lipid monolayers and a study of their electrical properties". Proc. Natl. Acad. Sci. U.S.A. 69:3561-3566.

Montal M., Anholt R. and Labarca, P. (1986). "The reconstituted acetylcholine receptor". In *Ion Channel Reconstitution*, (ed. C. Miller), pp. 157-204. New York, London: Plenum.

Neher R., and Sakmann B. (1976). "Single-channel currents recorded from membrane of denervated frog muscle fibers". Nature 260:779–802.

Osterrieder W., Noma A. and Trautwein W. (1980). "On the kinetics of the Potassium Channel Activated by Acetylcholine in the S-A node of the Rabbit Heart". Pflugers. Arch. 386:101-109.

Rostovtseva T. K., Aguilella V. M., Vodyanoy I., Bezrukov S. M., Parsegian V. A., "Membrane surface-charge titration probed by Gramicidin A channel conductance". Biophys. J. 75:1783-1792.

Sine S. M., Claudio T., and Sigworth F. J. (1990). "Activation of Torpedo acetylcholine receptors expressed in mouse fibroblasts: single channel current kinetics reveal distinct agonist binding affinities". J. Gen. Physiol. 96:395–437.

Singer S. J. and Nicolson G. L. (1972). "The fluid mosaic model of the structure of cell
membranes". *Science* 175:720-31.

Steinem C., Janshoff A., Galla H.J. and Sieber M. (1997). "Impedance analysis of ion transport through gramicidin channels incorporated in solid supported lipid bilayers". *Biolectrochem. Bioenerg.* 42: 213–220.

Tien H.T. and Salamon Z. (1989). "Formation of self-assembled lipid bilayers on solid substrates". *Bioelectrochem. Bioenerg.* 22: 211–217.

Tien H. T., *Bilayer lipid membranes (BLM), Theory and practice* (1974). Ed. Marcel Dekker Inc. New York.

Trojanowics M. (2003). "Analytical applications of planar bilayer lipid membranes", in *Planar Lipid Bilayers and their Applications*, Elsevier Science.

Unwin N. (2003). "Structure and action of the nicotinic acetylcholine receptor explored by electron microscopy". FEBS Lett. 555: 91–95.

U.S. Department of Health and Human Service, Food and Drug Administration, CDER, CVM (2001). ""Guidance for Industry-Bioanalytical Method Validation".

Wang D. S., Mangin J. M., Moonen G., Rigo J. M., and Legendre P. (2006). "Mechanisms for Picrotoxinin and Picrotin Blocks of α2 Homomeric Glycine Receptors" J. Biol. Chem., 281,7:3841-3855.

White S. H. (1986). "The physical nature of planar bilayer membranes". In *Ion Channel Reconstitution*, (ed. C. Miller), pp. 3-35. New York, London: Plenum.

Woodbury D. J. & Miller C. (1990). "Nystatin-induced liposome fusion. A versatile approach to ion channel reconstitution into planar bilayers". *Biophys. J.* 58:833-839.

Woodbury D. (1998). "Nystatin/Ergosterol method for reconstituting ion channels into planar lipid bilayers", in *Methods in enzymology*, vol. 294, Academic Press.

Woodbury D. J. and Hall, J. E. (1988). "Role of channels in the fusion of vesicles with a planar bilayer". *Biophys. J.* 54:1053-1063.